2-9-2011

Biofuel Cell Anode for NAD-Dependent Enzymes

Ovalles Rosalba Rincón

Follow this and additional works at: https://digitalrepository.unm.edu/cbe_etds

Recommended Citation

Rincón, Ovalles Rosalba. "Biofuel Cell Anode for NAD-Dependent Enzymes." (2011). https://digitalrepository.unm.edu/cbe_etds/7

Rosalba Adriana Rincón
Candidate

Chemical and Nuclear Engineering
Department

This dissertation is approved, and it is acceptable in quality
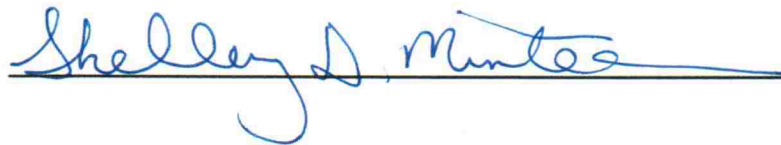and form for publication:
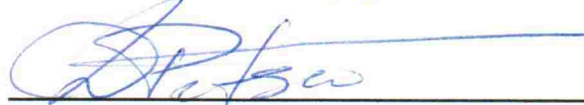
Approved by the Dissertation Committee:

_____, Chairperson

_____

_____

_____

_____

_____

_____

_____

BIOFUEL CELL ANODE FOR NAD$^+$-DEPENDENT ENZYMES

BY

ROSALBA ADRIANA RINCÓN OVALLES

B.S. Chemical Engineering, Univesidad Simón Bolívar, Venezuela,
2006.

Submitted in Partial Fulfillment of the
Requirements for the Degree of

**Doctor of Philosophy
Engineering**

The University of New Mexico
Albuquerque, New Mexico

December, 2010

iii

DEDICATION

Dedico este trabajo a la memoria de mi papá, Luis Antonio Rincón Küper,

quien siempre me inspiró a dar lo mejor de mí.

ACKNOWLEDGEMENTS

First of all, I would like to thank God for the strength he has given me, and my family for their love and support. This work would have not been possible without them. I would like to thank my mom Rosalba, a strong professional woman, for being a role model for me to follow. I would to thank my dad for all the love and encouragement he gave me. I would also like to thank my sister for her unconditional love. I would like to thank my friends Brenda and Ana María who have become family, and made Albuquerque a place that I can call home. I would also like to thank Iván, for all his love, patience and support during the last months of my dissertation work.

I would like to thank my advisor Plamen Atanassov for his guidance, for believing in me and teaching me so much over the past five years. Without his encouraging words I could have not come this far. I would also like to thank professors Shelley Minteer, Scott Calabrese Barton and Michael Cooney for their academic support and contributions to this work. I would also like Carolin Lau for sharing her expertise in the laboratory and always making things look easier. I would like to thank Margarite Arechederra for our collaborative work and Piyush Kar for his contribution with the computational part of this work. I would like to thank Kristen Garcia for all of her help performing experiments. I would like to also thank all of the wonderful students in the laboratory who have supported me and helped in several ways Bayo Falase (who solved all my computer problems), Jared Roy, Claudia Narváez and Pablo de la Iglesia.

BIOFUEL CELL ANODE FOR NAD$^+$-DEPENDENT ENZYMES

BY

ROSALBA ADRIANA RINCÓN OVALLES

ABSTRACT OF DISSERTATION

Submitted in Partial Fulfillment of the
Requirements for the Degree of

**Doctor of Philosophy
Engineering**

The University of New Mexico
Albuquerque, New Mexico

December, 2010

BIOFUEL CELL ANODE FOR NAD⁺-DEPENDENT ENZYMES

by

Rosalba Adriana Rincón Ovalles

B.S., Chemical Engineering, Universidad Simón Bolívar, 2006

Ph.D., Engineering, University of New Mexico, 2010

ABSTRACT

Enzymatic biofuel cells are a very attractive young technology based on utilization of natural, renewable and plentiful resources that offer an alternative energy source. Most fuel cells run on hydrogen; but it is extremely expensive and difficult to obtain, which is why research has moved to target fuels that are already available in nature, avoiding high costs of production, both economically and environmentally. Several biofuels with very high energy densities are available to us in abundance, but the challenges to make use of them are plenty. These biofuels contain several carbon-to-carbon bonds which make their oxidation processes significantly more complex than those of hydrogen. Examples of these biofuels are sugars and alcohols. If we refer back to nature, we have learned that enzymes play a very important role in oxidizing these types of fuels to obtain energy. If we could mimic such processes in a fuel cell, we would be able to harvest the energy of the fuels and convert it into electrical power. There are several advantages to using enzymes as catalysts for biofuel cells including their availability, easiness to produce in large quantities and selectivity.

The main pitfall when mimicking nature's pathways to oxidize biofuels by enzymatic action is that they usually require multiple oxidation steps. The full energy potential of

biofuels can only be attained if all of the reaction steps are completed achieving the complete oxidation to CO_2. This must be achieved by including all individual enzymes that catalyze each step of the oxidation of biofuels. Several of the necessary enzymes for those oxidation steps depend on the diffusive cofactor NAD^+/NADH which by itself presents a great challenge. The optimal performance of a biofuel cell requires continuous operation and oxidation of the fuel which can only be achieved if the enzymes' cofactors are constantly regenerated. NADH oxidation has been a practical challenge in biotechnology over decades, since it requires very large overpotentials. In this work, we evaluated the utilization of standardized fuel cell apparatus built for cross-lab analysis by preparing poly-(MG) electrocatalysts for NADH oxidation onto different electrode materials. These electrocatalysts have been studied and characterized both electrochemically and structurally in order to develop NAD^+-dependent enzyme anodes. Immobilization of enzymes also represents an important design aspect. One immobilization technique is chosen in this research; based on the combination of porous chitosan scaffolds and multi-walled carbon nanotubes that stabilizes enzymes while enabling mass transport of fuels and providing electrical conductivity.

This research ultimately introduces a common technology platform for NADH re-oxidation in a flow through electrode format that can sustain single- or multi-enzyme anodes into biofuel cell technology. Future directions and optimization of the design are discussed.

Table of Contents

Table of Contents

Table of Contents

List of Figures

List of Figures

List of Figures

List of Figures

List of Figures

List of Tables

List of Appendices

A novel approach for building bioinorganic interfaces was tested. Biologically derived silica with single-walled carbon nanotubes were combined to create a conductive matrix for immobilization of glucose oxidase for bioanode applications. This strategy allowed for direct electron transfer during glucose oxidation. The synthesized materials were characterized by means of X-ray photoelectron spectroscopy and Scanning Electron Microscopy.

An alternative method to electrochemically synthesized poly-(MG) and poly-(MB) was studied. Chemical polymerization of poly-azines was achieved by different methods and the resulting polymers were characterized towards NADH oxidation. Structural analyses were also performed by XPS in order to better understand the resulting structures and compare them to those of the electrochemical synthesized polymers. Amperometric investigations were used to compare the catalytic activity of chemically and electrochemically synthesized polymers as electrocatalysts for the oxidation of NADH.

Electropolymerization of MG on nanostructured materials based on single-walled carbon nanotubes (SWNTs) was explored. The creation of smart catalytic materials that are in

intimate proximity to the enzymes is of great interest. For NAD$^+$-dependent enzymes the incorporation of poly-(MG) catalyst becomes a necessity so exploration of its deposition at the nano-scale is highly desirable. "Bucky paper" novel materials based on SWNTs was used as the electrode material due to its characteristics of high conductivity and nano-sized features. The resulting materials were analyzed by SEM and electrochemical techniques.

Chapter 1. Introduction

Interest in energy harvesting devices based on alternative fuels has exponentially increased over the last decades. Several factors have pushed the search for alternative energies in the U.S. and worldwide, including the limited availability of fossil fuels and the environmental consequences of their extraction and use. Consequently, it has made sense for government agencies to invest in research that enables the development of clean, efficient, and renewable energy technologies.

Biofuel cell history dates to the early 1910s with the demonstration of a half cell using microorganisms, when M.C. Potter observed electricity production by *E. coli*.[1] However, it was not until the early 1960s[2-4] that the expansion of fuel cell research was triggered by the U.S. space program. This program led the development of microbial fuel cells as a waste disposal system that would also generate power for space flights. In addition, in the late 1960s, research in biofuel cell using enzyme systems began, with the initial goal of supplying power for an implantable artificial heart.

Researchers have increasingly drawn their attention to biological fuel cells in recent years, seeing that conventional fuel cell technologies are reaching mass-market introduction (Figure 1-1). Reasons for this shift in interest are based on conditions of operation that cannot be met by conventional fuel cells; namely low-temperature operation (20-40 °C) activity near neutral pH and, selective catalytic activity. Even though the research in biofuel cells has not been extensive; the work on biosensors based on biocatalytically modified electrodes over the past decades, provides a solid foundation for biofuel cell development. Both technologies involve many of the same technical

requirements such as chemical and mechanical stability, selectivity, and cost of materials.[5]

The main difference between both technologies is that biosensors are usually energy-consuming devices, while biofuel cells are energy-producing devices. Biofuel cells must be able to generate maximum power, meaning both high current and high voltage. In this perspective, biofuel cells are designed with materials and structures that can minimize overpotentials due to kinetics, mass transport limitations and ohmic resistance for maximum current densities. For biofuel cells to be used in any practical application (e.g. implantable devices, portable energy sources), operating lifetimes must range between months and years. Long-term stability is required. These design constraints can be achieved by immobilization of the biocatalytic species in porous materials. In this way, the biofuel cell research path has taken an independent route to that of biosensors.

Development of self-sustaining biofuel cells requires an understanding of the fundamentals, comprising electron and proton transfer kinetics between biocatalytic species and the electrode surface, novel electrode design for enhanced stability and the lifetime of biocatalytic species, theoretical modeling of mass transport in biofuel cells, and optimization of current and power production for high efficiency. With such an understanding, biological fuel cells then become a promising alternative for conventional energy harvesting devices.
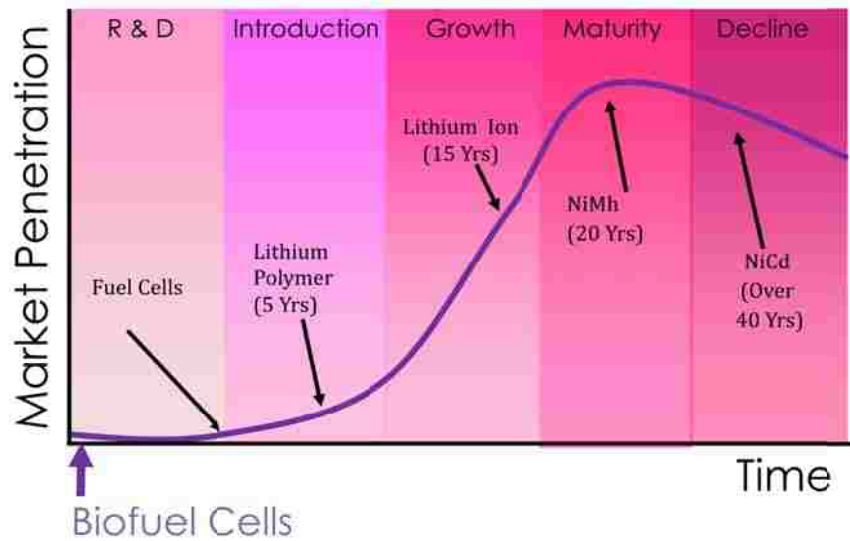
Figure 1-1 The stage of biofuel cells today

1.1. Biofuel Cell Principles

Biofuel cells represent a unique type of fuel cell that uses organic fuels such as ethanol or glucose. The basics of a biofuel cell are the same as a conventional fuel cell; fuel is oxidized at the anode, releasing electrons that travel through an external circuit to produce power, and protons that travel through a membrane to the cathode where oxygen or other oxidants are reduced. Nevertheless, the distinctive biological aspect is that they employ enzymes or microbes as catalysts to promote the reactions at the anode or cathode, unlike the chemical catalysts (e.g. platinum) used in conventional fuel cells. In general, biofuel cells are classified according to the location of the catalytic enzymes. If the enzymes are located inside living cells, the system is considered to be microbial. Fuel cells with the enzymes extracted and separated from living cells are considered enzymatic.[5] Microbial biofuel cells exhibit unique features such as long-term stability and fuel efficiency, but are limited by low power densities due to resistance to mass transport

across cell membranes. Enzymatic biofuel cells also possess various limitations, but they usually offer higher current and power densities that make them applicable in micro- and miniscale technologies. These limitations are mainly due to incomplete oxidation of biofuels by single-enzymes systems and the difficulties in achieving long-term stability of enzymes for prolonged operation of biofuel cells.

Enzymes are excellent catalysts that work by lowering the activation energy for their specific reactions. They are highly selective, meaning that catalysis is substrate specific; an attribute unique to biofuel cells. Figure 1-2 shows a schematic for an enzymatic biofuel cell that oxidizes methanol by a cascade of three enzymes. An oxido-reductase enzyme in the cathode is used to reduce the oxygen from air to water. An ion exchange membrane separating the anode from the cathode is also shown in the figure. Due to the enzyme selectivity, the reactions of the cathode and anode do not interfere with each other, negating the need to design for crossover prevention. This allows for a simpler and possibly cheaper fuel cell.

Traditional fuel cells run on hydrogen with the use of platinum or other metal catalysts. Oxidation of fuel at the anode becomes more complex with the addition of carbon atoms. The presence of these carbon atoms can result in carbon dioxide poisoning of the metal catalysts. Fortunately, enzymes are immune to this phenomenon. Enzymes do not suffer from carbon dioxide contamination; and advantage of these biological systems. Enzymes are also naturally abundant, green (sustainable) and cheap to produce, which is not necessarily the case for metallic catalysts. Overall, there are a number of

advantages to enzymatic biofuel cells that make them a very attractive and promising technology.
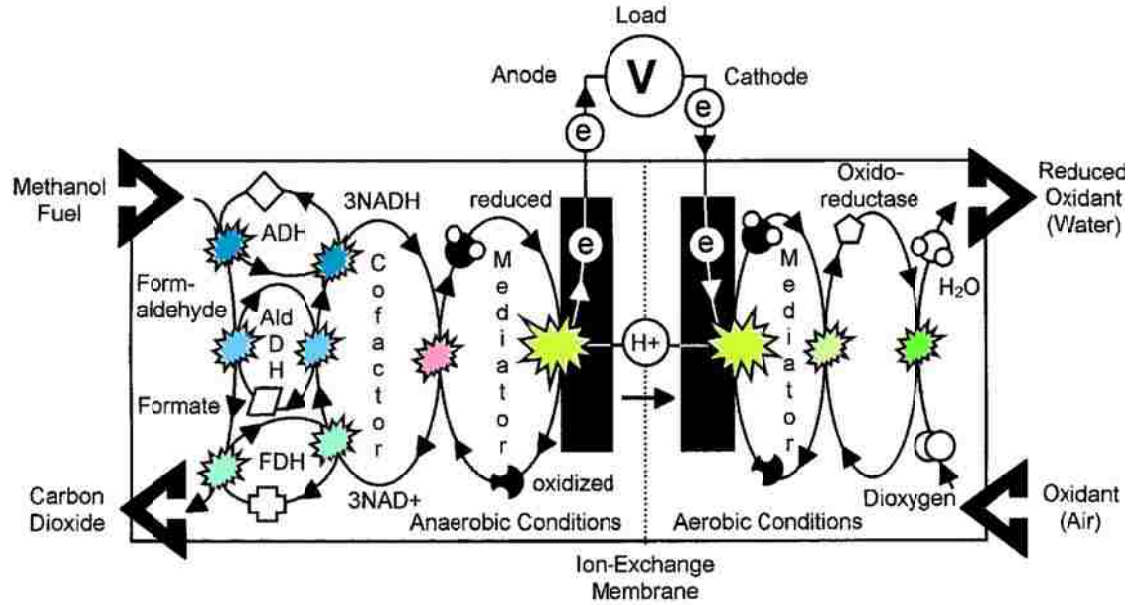
Figure 1-2 Schematic of an enzymatic biofuel cell, from S. Wilkinson, Univ. South Florida.

1.1.1. *Fuel cell performance and thermodynamic considerations*

When building a power source device, the goal is to obtain the best performance, which is given by the highest power outputs as possible. In the case of fuel cells, the power (P) is given by the product of the voltage of the cell (E_{cell}) by the current (i):

$$P = i \cdot E_{cell} \qquad \text{(Eq. 1-1)}$$

The voltage of the fuel cell is given by the difference between the potential of the cathode (E_c) and the potential of the anode (E_a):

$$E_{cell} = E_c - E_a \qquad \text{(Eq. 1-2)}$$

The operating potentials of the anode and cathode are usually measured electrochemically relative to a standard reference electrode. The maximum *operating*

5

voltage of the fuel cell is determined by measuring the open circuit voltage (E_{0cell}, voltage at zero current) or by taking the difference of the open circuit potentials of the cathode and anode (E_{0c} and E_{0a}, potential at zero current).

The maximum *theoretical* cell voltage is known as the thermodynamic (reversible) open circuit voltage (OCV) or electromotive force (EMF) and it can be calculated from Eq. 1-3 with thermodynamic data of Gibbs free energy of formation for the anodic and cathodic species, with n being the number of electrons transferred and F the Faraday constant (96,485 C/mol).

$$E = \frac{-\Delta G_f}{nF} \qquad \text{(Eq. 1-3)}$$

If we consider a biofuel cell that fully oxidizes glucose in the anode and uses oxygen in the cathode, the reactions will be:

Anode: $C_6H_{12}O_6 + 6\ H_2O \longrightarrow 6\ CO_2 + 24\ H^+ + 24e^-$

Cathode: $6\ O_2 + 24\ H^+ + 24e^- \longrightarrow 12H_2O$

Overall: $C_6H_{12}O_6 + 6\ O_2 \longrightarrow 6\ CO_2 + 6\ H_2O$ $\qquad$ (Eq. 1-4)
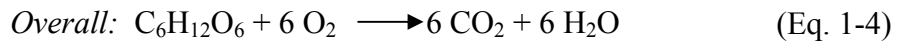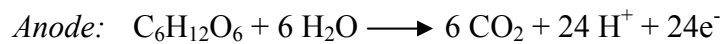
With the values of Gibbs free energy for the species in Eq. 1-4 and $n = 24$, the maximum theoretical cell voltage is found to be 1.24 V.

The principal method used to evaluate fuel cell performance is the construction polarization and power curves. Figure 1-3 shows a typical polarization curve (in blue) for a fuel cell indicating the maximum theoretical cell voltage (thermodynamic OCV) as well as the maximum operating cell voltage (E_{0cell}). A power curve (in red) can be constructed, by multiplying the current density (i) with the measured cell voltage (E_{cell}) as depicted in Eq. 1-1. Deviation from the thermodynamic OCV is usually known as overpotential or overvoltage.
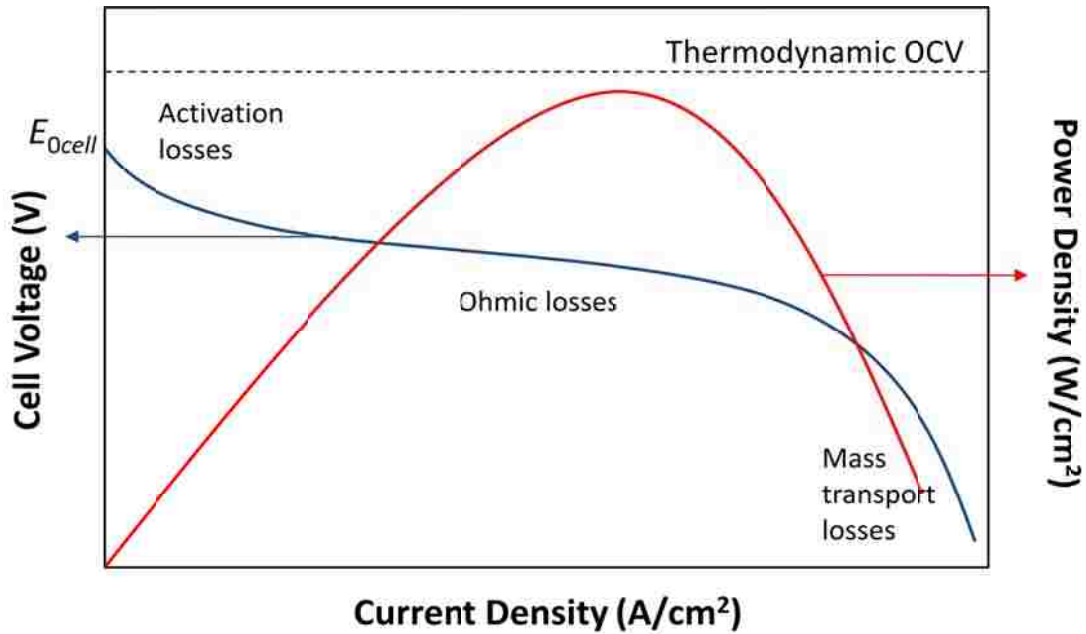
Figure 1-3 General schematic of the performance of a fuel cell showing the regions where activation, ohmic and mass transport losses occur

The overvoltage causes loss in the fuel cell performance. There are three types of overvoltage (η) in an electrochemical cell and they occur at different current density regimes as indicated in Figure 1-3. In the region of low current densities, *activation* or *kinetic* (η_{act}) losses are observed. They occur due to the chemical reactions that transfer electrons to and from the electrode occurring at slow rates. Voltage generated is lost in driving such reactions. The Tafel equation describes the voltage drop due to activation limitations:

$$\eta_{act} = \beta ln \left(\frac{i}{i_0} \right)$$

(Eq. 1-5)

Where i_0 is usually called exchange current density and is considered as the current density at which the overvoltage begins to move from zero. The constant β (Tafel slope) is higher for an electrochemical reaction that is slow, making the drop in voltage higher for slower reactions. It is defined by Eq. 1-6:

7

$$\beta = \frac{RT}{n\alpha F} \qquad \text{(Eq. 1-6)}$$

With R being the ideal gas constant, T is the temperature, n is the number of electrons, α is called the charge transfer coefficient, and F is the Faraday constant.

At intermediate current densities, *ohmic* or *resistive* overvoltage is observed (η_{iR}). The voltage drop is caused by resistance to the flow of electrons through the electrode materials, as well as the resistance to flow of the ions through the electrolyte. It is proportional to the current density; therefore it is identified as the linear area of the curve. It is defined by Eq. 1-6:

$$\eta_{iR} = iR \qquad \text{(Eq. 1-7)}$$

In the region of high current densities, the main contributor to electrode polarization is the *mass transport* or *concentration* overvoltage (η_{conc}). This arises from a failure to transport enough fuel to the electrode surface resulting in a change of concentration of the reactants. The concentration overvoltage is defined by the Nernst equation as:

$$\eta_{conc} = \frac{RT}{nF} ln\left(\frac{i_{lim} - i}{i_{lim}}\right) \qquad \text{(Eq. 1-8)}$$

Where the limiting current i_{lim} is defined as:

$$i_{lim} = nFD\left(\frac{C^0}{\delta}\right) \qquad \text{(Eq. 1-9)}$$

In Eq. 1-9 D is the diffusion coefficient of the reagent, δ is the Nernst diffusion layer, and C^0 is the bulk concentration of the reagent.

The total overvoltage across the fuel cell is defined by Eq. 1-10:

$$\eta_{total} = \eta_{act} + \eta_{iR} + \eta_{conc} \qquad \text{(Eq. 1-10)}$$

In the case of enzymatic biofuel cells, the *operating* cell voltage will depend on the enzymes used in both the anode and the cathode along with the mechanisms of electron transfer between the enzymes and electrode surface.

There are two types of mechanisms in which the electron transfer between the active site of the enzyme and the electrode surface can occur. *Direct* electron transfer (DET) occurs when the active site of the enzyme is close enough to the electrode surface so there is direct electrical communication between the enzyme and the electrode to transfer the electrons. *Mediated* electron transfer (MET) consists of using a redox couple as a mediator to shuttle the electrons between the active site of the enzyme and the electrode surface. The use of mediator is necessary in many cases and usually results in losses of cell voltage compared to the non-mediated system.

Figure 1-4 shows a potential vs. current diagram with individual polarization curves for the cathode and anode of an enzymatic fuel cell. This figure indicates the position of the thermodynamic potentials for oxygen reduction and glucose oxidation. The difference of these values results in the *theoretical* maximum cell voltage of 1.24 V for glucose oxidation. However, the values of redox potentials of the enzymes that could be used for the cathodic and anodic reactions are usually a little different. Cathodic enzymes have active sites with redox potentials that are very close to the thermodynamic potential of oxygen reduction. Furthermore, there are several reports indicating that DET is possible with enzymes such as laccase and bilirrubin oxidase.[2-33]
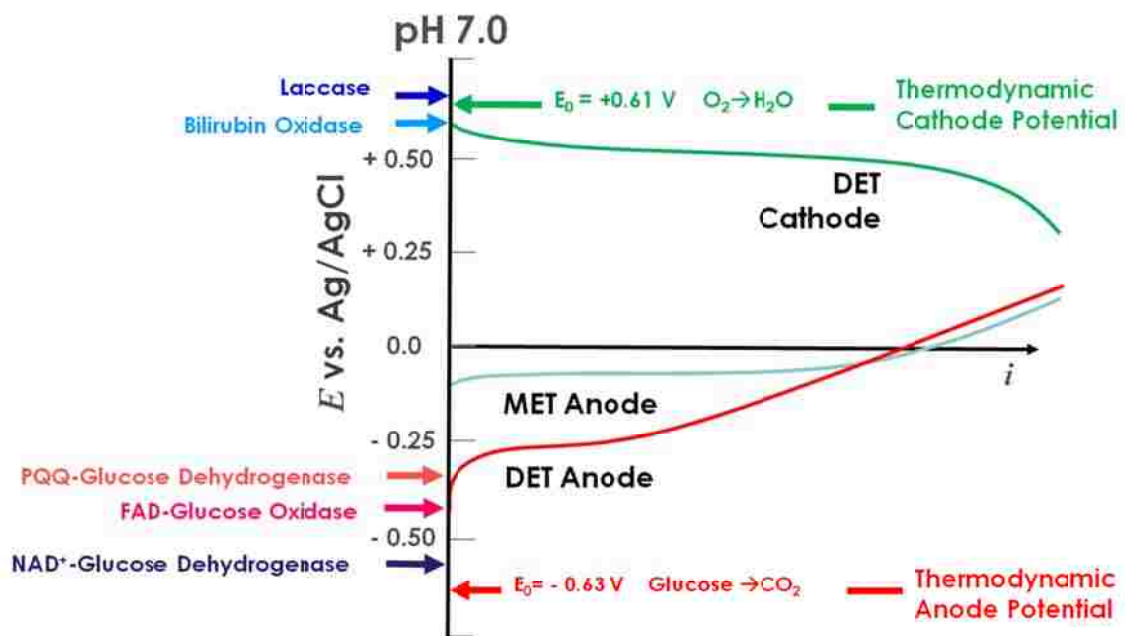
Figure 1-4 Cathode and anode polarization curves diagram showing the standard redox potentials for different enzymes

A wider range of enzymes can be explored for the anode of a biofuel cell, since a variety of fuels could be used. Considering again the oxidation of glucose, multitude of enzymes are able to catalyze the first-step of glucose oxidation. These enzymes are based on different cofactors (nicotinamide adenine dinucleotide, NAD^+; flavin adenine dinucleotide, FAD; or pyrroloquinoline quinone, PQQ) that have different redox potentials. On Figure 1-4 it can be seen that NAD^+-dependent enzymes have the lowest redox potential, and has a thermodynamic potential close to that of glucose oxidation. Since one would like to work at the lowest anode potential in order to obtain the maximum cell voltage, the use of NAD^+-dependent enzymes is highly desirable. Figure 1-5 shows the NAD^+-dependent that were studied in the research: malate dehydrogenase

(MDH) as a part of the Krebs cycle, and alcohol dehydrogenase (ADH) as part of alcohols oxidation.
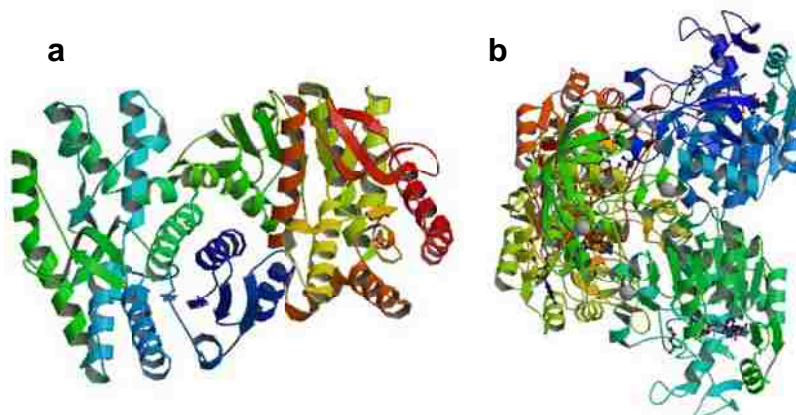
Figure 1-5 Structures of: a) malate dehydrogenase open conformation and b) alcohol dehydrogenase.

1.2. Enzymatic anode design considerations

The challenges in every new technology are numerous; enzymatic biofuel cells are not an exception. Despite the advantages of enzymes that were mentioned before one of the major obstacles in enzymatic biofuel cell design is given by the partial oxidation of fuels by single enzymes. This particular challenge is compartmentalized within the anode design of the fuel cell and it means that there is a need to use multi-enzymes systems with consecutive-step reactions in order to fully oxidize complex fuels like alcohols and sugars while simultaneously, being able to obtain the largest energy densities as possible. Enzymes, by nature, perform such complex oxidation processes by using the product of one enzyme reaction as the reactant for the next one to ultimately converting sugar to energy in the form of ATP, while releasing carbon dioxide and water. There are different pathways for such enzymatic breakdowns of sugars and alcohols that are known in nature. The details as well as other design aspects are discussed in the next sections.

1.2.1. *Multienzyme cascade reactions*

Figure 1-2 shows an example[2] of full oxidation of a biofuel running on a cascade of three enzymes: alcohol dehydrogenase, aldehyde dehydrogenase and formate dehydrogenase; allowing for the complete oxidation of methanol to carbon dioxide. Glucose, a more complex potential biofuel, holds the highest volumetric energy density as shown in a comparative graph in Figure 1-6.
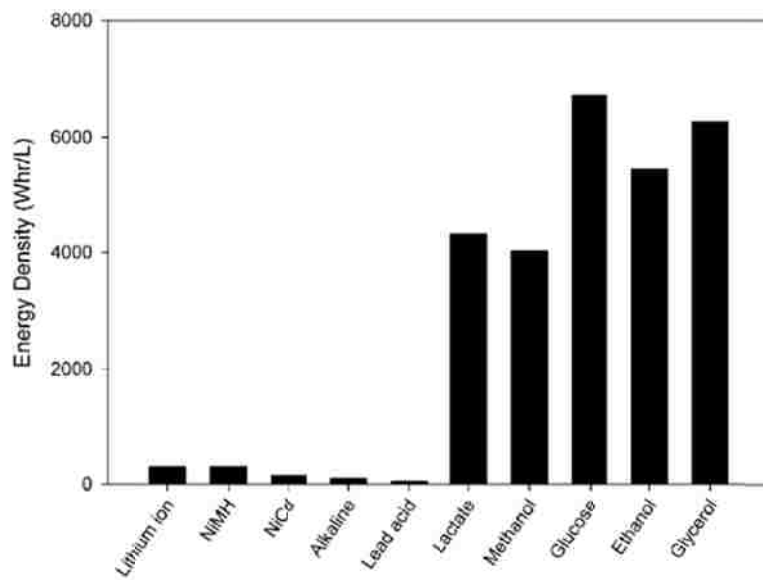
Figure 1-6 Theoretical energy densities of common batteries and biofuels for biofuel cells[2]

In order to completely glucose and obtain the maximum energy density as depicted in Figure 1-7, one needs to mimic the mechanisms that animals do during cellular respiration to obtain ATP. There are a few pathways that comprise this mechanism including glycolysis and the Krebs cycle.
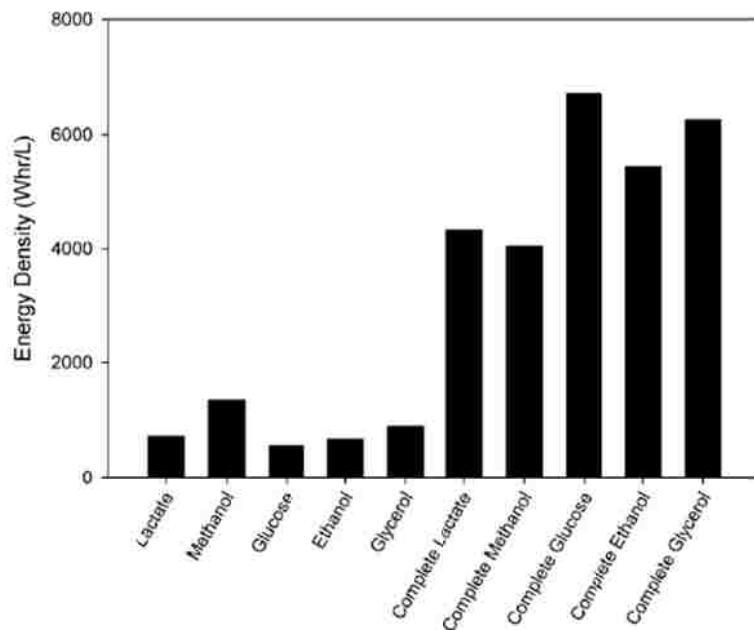
Figure 1-7 Comparison of volumetric energy densities of single-step (2 electrodes) and complete oxidation of different biofuels for biofuel cells[2]

Glycolysis is a metabolic pathway that occurs under anaerobic conditions in which glucose is converted to pyruvate while releasing energy, following this reaction:

$$C_6H_{12}O_6 + 2NAD^+ + 2P_i + 2ADP \longrightarrow 2C_3H_4O_3 + 2NADH + 2ATP + 2H^+ + 2H_2O$$

The glycolysis pathway occurs in a series of 10 consecutive reactions catalyzed by enzymes. If oxygen is present, pyruvate then undergoes a sequence of reactions and is converted to acetyl-CoA. The atom carbon that is oxidized during this process is converted to CO_2 and NADH is also released. Following this reaction, acetyl-CoA enters the Krebs cycle where a sequence of reactions leads to the full oxidation of glucose to CO_2 while generating energy in the form of ATP. The Krebs cycle can be summarized in this reaction:

$$\text{Acetyl-CoA} + 3NAD^+ + FAD + ADP + Pi \longrightarrow \text{CoA-SH} + 3NADH + 3H^+ + FADH_2$$
$$+ ATP + 2CO_2$$

13
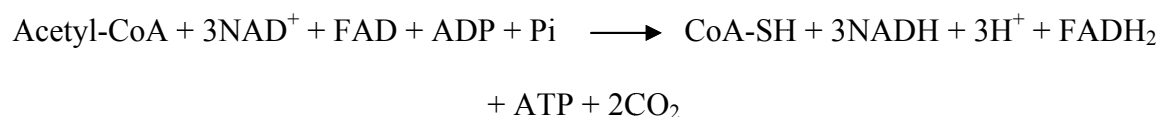
Figure 1-8 shows a schematic of the glucose oxidation emphasizing on the sequence of reactions that take place during the Krebs cycle.
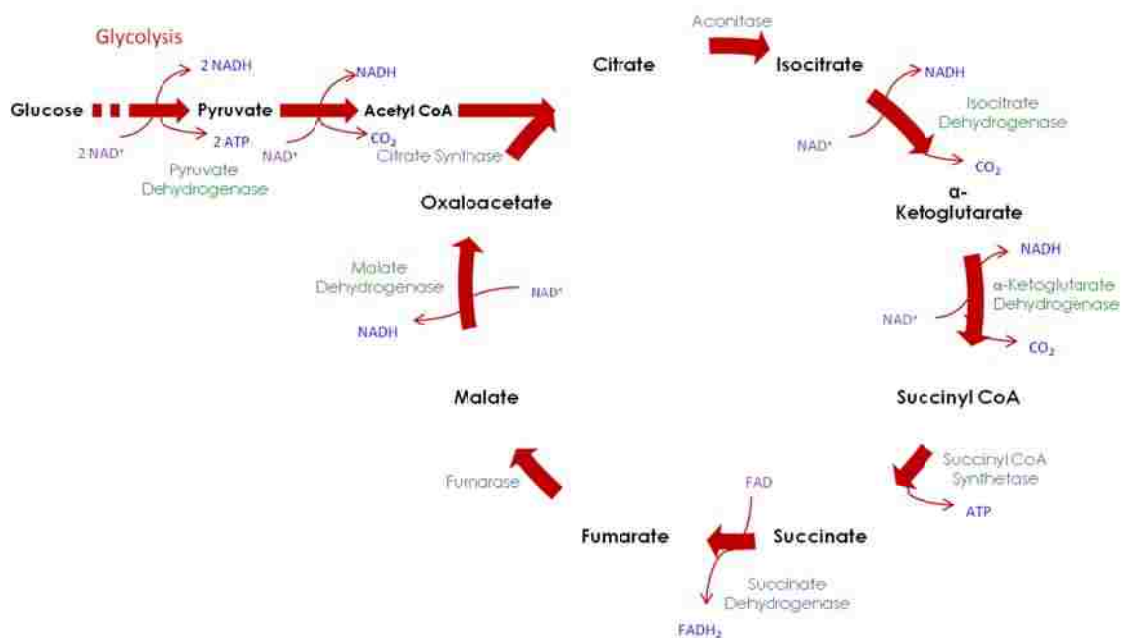
Figure 1-8 Schematic of glucose oxidation with general diagram of the Krebs cycle

An enzyme cascade that mimics the Krebs cycle in order to fully oxidize pyruvate and ethanol has been reported by Minteer et al.[6, 7] Complete oxidation using enzymes shows that the power density of the fuel cell can be enhanced by the utilization of multi-enzyme systems. Complete oxidation of glucose will require the mimicking of both the glycolytic pathways and the Krebs cycle on the anode of the biofuel cell. Both processes have their own constraints and obstacles to overcome.

Three enzymes in the Krebs cycle depend on the NAD^+/NADH (nicotine adenine dinucleotide) cofactor that play a role in glucose oxidation. Table 1-1 shows a list of NAD^+-dependent enzymes (including the ones from Krebs cycle) that are involved in oxidation of glucose and other biofuels for biofuel cells.

Table 1-1 Commercially available NAD(P)$^+$-dependent dehydrogenase enzymes[8]

Enzyme	Substrate	Product	Coenzyme
Alcohol dehydrogenase	Ethanol	Acetaldehyde	NAD, NADP
Acetaldehyde dehydrogenase	Acetaldehyde	Acetate	NAD, NADP
Glucose dehydrogenase	Glucose	D-Glucono-δ-lactone	NAD
Phosphogluconic dehydrogenase	Phosphogluconate	Ribulose-5-phosphate	NAD, NADP
Glycerol dehydrogenase	Glycerol	Dihydroxyacetone	NAD
Glycerophosphate dehydrogenase	Dihydroxyacetone phosphate	Glycerophosphate	NAD
Sorbitol dehydrogenase	Sorbitol	Fructose	NAD
Lactic dehydrogenase	Lactate	Pyruvate	NAD
Mannitol dehydrogenase	Mannitol	Fructose	NAD
Galactose dehydrogenase	Galactose	Galactonate	NAD
Cyclic alcohol dehydrogenase	Cyclic alcohol	Cyclic ketones	NADP
Formate dehydrogenase	Formate	Carbon dioxide	NAD
Pyruvate dehydrogenase	Pyruvate	Acetyl-CoA	NAD, CoA

The following section will discuss the main obstacle associated with the design of enzymatic biofuel cells based on these types of enzymes.

1.2.2. NADH re-oxidation issue

Dehydrogenase enzymes play an essential role in the breakdown of sugars and oxidation of alcohols. There are over 300 dehydrogenases that are known to be dependent on the nicotinamide adenine dinucleotide cofactor (NAD$^+$/NADH), comprising the largest group of redox enzymes known today.[9] Despite of their abundance in nature, their utilization for biosensor and biofuel cell applications is limited. Unlike other redox enzymes (e.g. oxidases) dehydrogenases' activity relies on the presence of a soluble cofactor (NAD$^+$/NADH),[9] that must be introduced in the device configuration. Once the cofactor is present and the dehydrogenase enzyme catalyzes the oxidation reaction of its specific substrate, the cofactor NAD$^+$ is reduced to NADH by the following reaction:
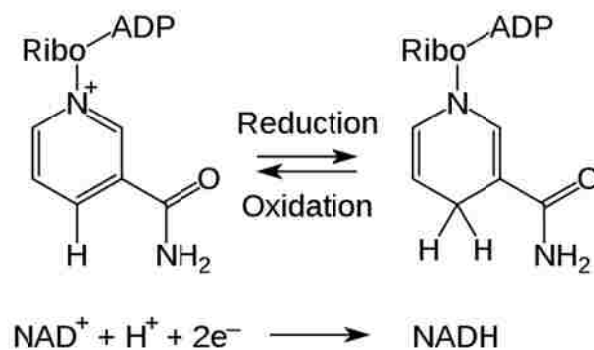
Figure 1-9 Redox reaction of the NAD$^+$/NADH cofactor

The electrochemistry of this cofactor in both oxidized (NAD$^+$) and reduced (NADH) form is irreversible and conveys additional complexities in the design of devices for biotechnology. Electrochemical reduction of NAD$^+$ requires specific conditions in order to reduce and avoid adsorption effects that are reported to be caused by the adenine moiety of the cofactor.[10-14] On the other hand, direct electrochemical oxidation of NADH has shown to be irreversible and it can be inhibited by the presence of adsorbed NAD$^+$.[15]

The mechanism for electrochemical oxidation of NADH has been proposed in a number of studies[15-21] as an electrochemical-chemical-electrochemical (ECE) mechanism characterized by the following reaction scheme:

$$\text{NADH} \xrightarrow{-e^-} \text{NADH} \cdot^+ \xleftrightarrow{-H^+} \text{NAD} \cdot \xrightarrow{-e^-} \text{NAD}^+ \qquad \text{(Eq. 1-11)}$$

The high overpotential of the direct electrochemical oxidation of NADH described in Eq. 1-11 is caused by the very high potential of the NADH$\cdot^+$/NADH redox couple[22] (first step in the reaction), resulting in an initial rate-limiting electron transfer step. It has also been suggested that the intermediate radicals that result from the first and second step of

this reaction might participate in other reaction routes for electrochemical oxidation of NADH.[19, 20]

To summarize, direct electrochemical reactions of the NAD^+/NADH cofactors at metallic or carbon electrodes are highly irreversible, occur at large overpotentials and can be affected by side reactions and fouling (adsorption) of cofactor related products.[9] The development of biotechnology devices based on NAD^+-dependent dehydrogenases cannot rely on direct electrochemical reactions of the oxidized or reduced form of the cofactor. Many years of research have been especially devoted by numerous scientists in finding suitable methods for the electrochemical oxidation of NADH.

As previously stated, in an enzyme-catalyzed reaction involving the NAD^+/NADH cofactor, NAD^+ is reduced to NADH while the substrate is oxidized. If used in a biofuel cell, NAD^+ that is reduced to NADH, must be re-oxidized to NAD^+ in order to perpetuate the reaction cycle and continue to oxidize the fuel. However, direct oxidation of NADH at ordinary electrodes like gold or glassy carbon requires high overpotentials exceeding 1 V.[23-25] By overcoming this high overpotential, one could possibly use any NAD^+-dependent enzyme in a biofuel cell anode and create cascades of enzymes that could achieve deep oxidation of complex fuels, giving us a wide variety of these biofuels to choose from. Hence, finding ways of re-oxidizing the NADH active site is a crucial task that will broaden the opportunities for enzymatic biofuel cells.

1.2.3. *Mediators for electrochemical oxidation of NADH*

The use of mediators for chemically modified electrodes (CMEs) to reduce the overpotential of NADH oxidation and improve its kinetics started in the late 1970s and

has been extensively reported on since then and summarized in several reviews.[9, 26-37] An appropriate mediator must meet very specific demands. It must:

i) Substantially decrease the overpotential of NADH oxidation while preserving good reaction rates that approach diffusion-controlled regimes. In the particular case of biofuel cells, the $E°'$ (formal redox potential) value of the mediator should approach that of the enzyme cofactor NAD$^+$/NADH so that the energy loses are minimized.[24, 38]

ii) Possess high chemical and electrochemical stability in the presence of NADH, as well as long term stability (weeks-months)[36] so that the immobilization of the mediator must be irreversible.

iii) Be selective for NADH oxidation and yield enzymatically active NAD$^+$; while maintaining high reaction rates of the mediator modified system. This includes maximizing electron transfer rates between the electrode and mediator (k_s), fast charge-transfer rates within the mediator, and fast reaction rates between NADH and the mediator (k_{obs}).[36]

The first researchers to report a significant decrease in the overpotential of electrochemical oxidation of NADH on CMEs were Kuwana and Tse.[39] They achieved this by activating glassy carbon electrodes with cyanuric chloride and then modifying them with immobilized primary amines containing *o*-quinone derivatives, dopamine, or 3,4-dihydroxybenzylamine, forming a monolayer film on the electrode. These electrodes showed a decrease in overpotential of about 0.4 V. This report was followed by many others that investigated similar structures for the mediation of electrochemical oxidation of NADH, all containing a basic catalytic functionality that can be characterized by being *ortho-* or *para*-quinone,[39-46] phenothiazine and phenoxazine derivatives that contain

positively charged *para*-phenylenediimine structures.[26, 47-51] Figure 1-10 shows a group of these basic functionalities. It has also been reported that organic two-e⁻ acceptors (also proton acceptors) are more efficient in decreasing the overpotential of NADH electrochemical oxidation than one-e⁻ acceptors.[9]
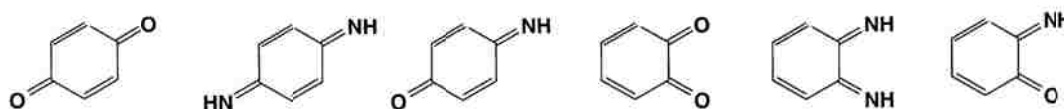
Figure 1-10 Basic catalytic functionalities of many organic 2-e- proton acceptors efficient for catalytic NADH oxidation.[36]

Formerly, the mediator was typically immobilized by physical adsorption[42, 46-59] or covalent binding[40, 43, 60] onto the surface of the electrodes to create the CMEs, which limited their long-term stability due to leaking or desorption of the mediator from the electrode surface.[61] Physical attachment of the mediator to the electrode also limits the operational mode of the device; CMEs with adsorbed mediators could only work in quiescent conditions (biobattery)[62] and not under a flow through regime (biofuel cell) where desorption will be more likely. This issue was targeted by scientists[63-91] by depositing films of mediators such as azine monomers through electrochemical polymerization on the surface of electrodes, resulting in a polymeric form of the azine with improved stability and reaction rates that is then considered an electrocatalyst. This method has proven to be the most reliable strategy for immobilization concerning the stability issue.[92]

There have been numerous reports on electrochemical polymerization of different monomers for applications in biosensors[64, 66, 70-72, 76, 84, 93-115] and biofuel cells.[88, 116-121] Karyakin et al. reported that methylene blue can be successfully electropolymerized in

solutions with weak acidity and that basic media is actually optimal for the polymer growth.[65] They later reported the main advantage of electropolymerized methylene blue as a catalyst for NADH oxidation to be its improved long-term stability compared to its monomeric form.[66] The work of Karyakin's group continued over the years, investigating different azine monomers that could be electropolymerized in search of the best one for NADH oxidation.[70, 71] In 1999, they reported that poly-(methylene green) (poly-(MG)) was the best catalyst among the ones they studied.[71] More recently, Dai et al. have reported that a poly-(MG) modified electrode can oxidize NADH by a simultaneous two-electron reaction and reduce the overpotential of NADH oxidation by about 0.65 V.[108]

1.2.4. *Electropolymerization of azines*

From the point of view of applications, the electrochemical polymerization of cheap, simple aromatics benzoid or nonbenzoid and heterocyclic compounds is of extreme interest. The reaction is usually an oxidative polymerization, although reductive polymerization is also possible. Chemical polymerization can also be used in certain cases (e.g. the oxidation of pyrrole or aniline by $Fe(ClO_4)_3$ in acid media leads to the respective polymer), but electropolymerization is preferred if the resulting polymer is intended for use as a polymer film electrode, thin-layer sensor, in microtechnology, etc. Due to the potential control during the synthesis, it is necessary for producing a good-quality material and form the polymer film at the desired location for practical applications.

In general, the electropolymerization process consists of polymerizing a monomer by an electrochemical technique. Electropolymerization can be achieved by potentiostatic (constant potential), galvanostatic (constant current) or cyclic voltammetry (multi-scan)

methods resulting in well-adhered polymer films. Polypyrrole, the most studied conducting polymer, was one of the first structures achieved by electropolymerization, method that proved to be the most effective for its synthesis.[122]

In an electrochemical polymerization, the monomer, dissolved in an appropriate solvent containing the desired anionic doping salt, is oxidized at the surface of an electrode by application of an anodic potential (oxidation). The choice of the solvent and electrolyte is of particular importance in electrochemistry since both solvent and electrolyte should be stable at the oxidation potential of the monomer and provide an ionically conductive medium. In the case of pyrrole, that has a relatively low oxidation potential, electropolymerization can be carried out in aqueous electrolytes that are not possible for thiophene or benzene.[122]

The mechanism and the kinetics of electropolymerization have been widely studied, especially in the cases of polyaniline and polypyrrole; by addressing two aspects: the chemical reaction and kinetics of the growth on a conducting surface. A general scheme cannot be provided since there is a great chemical diversity of the compounds studied. Nevertheless, it has been showed that the first step is the formation of cation radicals. The following step of this highly reactive species depends on the experimental conditions (i.e. composition of the growing solution, temperature, potential or the rate of the potential change, galvanostatic current density, electrode material, etc.). In favorable cases, the next step is a dimerization reaction and then stepwise chain growth proceeds via the association of free radical ions (RR route) or the association of a cation radical with a neutral monomer (RS route).[123] Parallel dimerization reactions leading to different products or to a polymer with a disordered structure may occur.

Inactive ions present in the solution may play a key role in the stabilization of the radical ions. Potential cycling is usually more efficient than potentiostatic method since it allows a partial reduction of the oligomer helping the polymerization reaction. This might be the case if the RS route is preferred and the monomer carries a charge (e.g. a protonated aniline molecule). A relatively high concentration of cation radicals should be maintained in the vicinity of the electrode. The cation radicals and the dimers can diffuse away from the electrode, hence intensive stirring of the solution usually decreases the yield of the polymer produced.

Usually the oxidation of the monomer is an irreversible process and takes place at higher positive potentials than that of the reversible redox reaction of the polymer. However, in the case of azines, reversible redox reactions of the monomers occur at less positive potentials and this redox activity can be retained in the polymer; this means that the polymerization reaction that takes place at higher potentials does not substantially alter the redox behavior of the monomer. The catalytic activity towards the oxidation of biological molecules like NADH of azine dyes like methylene blue is then preserved in its polymeric form.

The kinetics of electropolymerization also depends on the factors previously mentioned, though the role of the electrode material and the properties of its surface are more pronounced. The specific interactions and the wetting may determine the nucleation and the dimensionality of the growth process. The resulting film morphology is highly dependent on the composition of the solution, particularly on the type of counterions present in it, and the plasticizing ability of the solvent molecules. If the conditions are not

carefully optimized, a mixed material containing electrochemically active and conducting as well as inactive and insulating parts can be deposited on the electrode surface.[124]

Polymer-modified electrodes that are prepared by electropolymerization of monomers with mediating properties towards NADH oxidation are then very attractive since the synthesis is irreversible and enhances the long-term stability of the electrode while retaining the catalytic properties of the monomer in many cases. A diversity of reports on electropolymerization of *o*-quinone derivatives,[29, 93, 125-132] and phenothiazine and phenoxazine derivatives[61, 65-68, 70-74, 76-78, 85, 91, 133-140] with different levels of success for practical applications, can be found in the literature. Electropolymerization of azine derivatives has mainly been reported on gold[68, 70] and platinum,[141] glassy carbon electrodes,[66, 71, 73, 77, 79, 88, 108, 124, 139, 142-144] and other carbonaceous electrode materials (Toray paper,[6, 7, 145] graphite[140] and screen printed carbon[76, 80, 81]).

Svoboda et al. have studied the morphology of poly-(MG) films grown on platinum electrodes and observed that a conformal coating of the electropolymerized film is deposited on the two-dimensional structure of the electrode.[141]

1.3. Enzyme immobilization techniques

Another practical challenge that is encountered in the design of an enzymatic biofuel cell is given by the fact that enzymes are not used to staying put. On the contrary, in nature they are freely floating and very active; but to be able to work in a fuel cell they have to stay in a specific place and remain active and stable over time. The process of holding an enzyme in place is called immobilization. This procedure can provide the enzyme with enhanced chemical, thermal and mechanical stability due to the improvement in resistance to several denaturation factors like extreme pH and temperature, high ionic

strength, etc.[146, 147] Furthermore, by holding the enzyme in place it can be separated from the products of the reaction allowing for the enzyme to be reused, continuous operation of the enzymatic processes and controlled product formation.[148] All of these aspects are requirements for an operational and efficient enzymatic biofuel cell.

There are several techniques that can be used for immobilizing enzymes to specific supports that can be chosen depending on the enzyme, the surface to be immobilized on, and the desired applications. These techniques must in general satisfy certain conditions: the binding process should not cause loss of enzymatic activity, and the active site of the enzyme should remain unaffected. Among the types of immobilization techniques that have been developed we can find:

- Physical adsorption: This technique is based on the physical adsorption of the enzyme on the surface of water-insoluble supports. Even though this method is easy, cheap and causes little or no conformational damage to the enzyme, it is disadvantageous because it results in a weak binding since the enzyme can easily leak from the carrier or support.

- Covalent binding: This procedure is based on the formation of covalent bonds between the enzyme and the supporting matrix. There are several functional groups that might participate in this type of binding, including: amino group, thiol group, hydroxyl group, carboxyl group, phenolic group, among others. This technique requires more complicated and less mild conditions that may result in structural conformational changes, resulting in some loss of activity. Nonetheless,

leakage of enzyme is very unlikely due to the strong binding provided by this method.

- Ionic binding: This method relies on the ionic binding of the enzyme to water-insoluble supports that contain ion-exchange residues. The conditions for this procedure are much milder than the ones in covalent binding, usually resulting in immobilized enzymes with high activity. Leakage of the enzyme can occur under extreme conditions of ionic strength and pH. Polysaccharides and synthetic polymers that contain ion-exchange centers are usually used as carriers.[149]

- Cross-linking: Immobilization of enzymes can also be achieved by intermolecular cross-linking of the enzyme to another protein molecule or to functional groups on a support matrix. This method is usually combined with another one like adsorption in order to increase the stability and prevent leakage of the enzyme. The most popular cross-linker used for this technique is glutaraldehyde. The conditions of this procedure are somehow harsh and they can result in conformational changes by decreasing freedom of the active center to move and change configuration, and thus decrease the enzymatic activity.

- Entrapment: This method is based on the localization of the enzyme within the lattice of a polymer lattice or membrane[149]. The process generally retains the enzyme while allowing the substrate to penetrate and react. During this type of immobilization the enzyme does not attach to the support surface, which makes this method very applicable, contrasting with covalent binding where there is linkage between the enzyme and the carrier. However, the conditions during the process can also be severe and it can cause loss in activity of the enzyme.

The immobilization support should also be chosen in such a way that it ensures the highest possible retention of the enzyme activity, stability and durability.[148] An ideal enzyme support should possess high affinity to proteins and non toxicity; it should also be easy to prepare in different forms and be inexpensive.

1.3.1. *Enzyme entrapment in chitosan scaffolds*

Chitosan is a linear polysaccharide that is derived from chitin[150] and is produced industrially by deacetylation of chitin. It is the most important chitin derivative, in terms of its applications.[151] Chitin is commonly found in the exoskeleton of crustaceans, in certain insects and microorganisms, which makes it widely available. It has become a broadly-used biopolymer in biomaterials research thanks to its inexpensiveness and being the second most abundant biomass.[152] Figure 1-11 shows the basic chemical structure of chitosan.
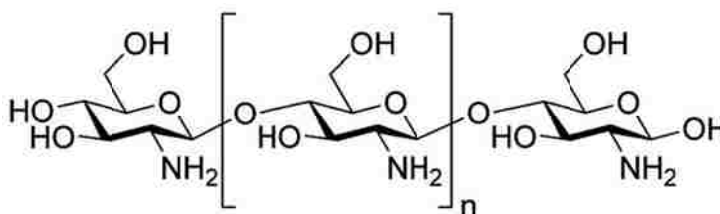
Figure 1-11 Structure of chitosan

When the degree of deacetylation of chitin reaches 50%, the amino groups along the polymer backbone become protonated and therefore chitosan acquires a polyelectrolyte behavior and becomes soluble in aqueous acidic media.[151, 153] Although the solubility of chitosan depends on several parameters such as the degree of deacetylation, the ionic concentration, the pH, the nature of the acid used for protonation, and the distribution of acetyl groups along the polymer chain; its pK_a value ranges between 6.1 and 7.0,[154]

which means chitosan is generally soluble at pH below 6. At basic pH, the free amino groups are no longer protonated ant the polymer becomes insoluble.[143]

Since it is soluble in various aqueous solutions and can adopt a semirigid shape, it can be largely used in various applications in different forms (solutions, beads, gels, films, fibers, sponges). In addition, chitosan is also known to for its diverse properties like being non-toxic, biocompatible, biodegradable and chemically inert. All of these characteristics make this material very versatile for biomedical and biotechnology applications. There are several reports of the use of chitosan in tissue engineering[155-167] and other biomedical applications[168-175]; and for protein and enzyme immobilization for biosensing[151, 154, 176-206] and biofuel cell applications.[142-144, 207-216] A common approach that has been used for enzyme immobilization or biomolecule entrapment within chitosan films is the use of dip-coating or drop-casting techniques.[142, 151, 154, 174, 176, 177, 179, 180, 192, 217] Other approaches have used freeze-gelation and freeze-drying techniques to produce macroporous chitosan scaffolds with highly interconnected pores for biomedical applications including slow drug release and support matrices for tissue growth.[155, 156, 158-167, 169, 173] More recently, chitosan has been used to decorate CNTs as a solubility dispersing agent and to create new composite nanomaterials with combined properties.[175, 183-191, 194-197, 199, 201-203, 205, 209, 213, 218-222] The resulting CNTs-chitosan films result in a very attractive material for biosensor and biofuel cell applications since chitosan provides an immobilization matrix for biomolecules and the CNTs offer conductive properties that are desired in any electrochemical technology.

A novel method that combines the addition of CNTs to chitosan matrices and uses freeze-drying as the fabrication method has been developed by Lau et al. , resulting in

macroporous and highly conductive chitosan-CNTs composite scaffolds as an advanced material to build electrodes for biocatalysis applications.[215] Chitosan scaffolds are produced by a thermally induced phase separation (TIPS) process in which the water present in the chitosan aqueous solution is frozen into ice crystals that are surrounded by thin layers of the precipitated polymer. This process is followed by a freeze-drying step that allows for the frozen crystals to sublimate under vacuum conditions yielding a highly macroporous scaffold structure; the final pore structure is determined by the shape of the sublimated ice crystals. There are several parameters that can affect the final structure of the scaffold, these include: pH, freezing rate, orientation of thermal gradient, and chitosan concentration.[143, 144, 215] The presence of carboxyl and amine side groups along the polymer backbone of chitosan allows for functional modifications that can change the polymer properties (e.g. hydrophobicity) for enhanced enzyme immobilization. The addition of alkyl chains along the hydrophilic backbone of chitosan gives the polymer an amphiphilic character creating internal forces that tend to fold the polymer chain and create regions exhibiting micellar behavior.[223, 224] Such regions seem to provide good enzyme retention and enhanced lifetimes without loss of activity exhibiting overall an ideal chemical microenvironment for enzymes.[143] Furthermore, the porosity of the resulting scaffolds allows for mass transport of the enzymatic substrates in flow-through regimes for biosensor and biofuel cell applications. The addition of CNTs into chitosan scaffolds also holds the promise of facilitating electron transfer in certain systems due to the provided conductivity that could either shorten the diffusion distance (i.e. mediated electron transfer systems); or eliminate the use of mediators (i.e. direct electron transfer systems).

1.4. Biofuel cell applications

The range of possible applications of biofuel cells can be classified in two main areas: ex-vivo applications and in-vivo applications. Evidently, the latter comprises the novelty and principal attraction of biofuel cells. In-vivo applications include microscale cells implanted in human or animal tissue or larger cells or larger cells implanted in blood vessels; such as pacemakers, glucose sensors for diabetics or small valves for bladder control; all of which can potentially be fueled by blood-borne glucose which would be available without limit, providing long-term power supply. Pacemakers nowadays are powered by lithium-iodine batteries with an operating power output of $\sim 1\mu W$ and lifetimes of over 10 years.[5] The benefit of an implantable biofuel cell compared to such a battery is given by high power density (currently ranges between hundreds of $\mu W/cm^2$ and a few mW/cm^2) and possibly infinite energy density from the available physiological fuel. Moreover, biocatalysts are suitable for implantable power since they can efficiently catalyze reactions at physiological temperature and pH, and for the most part generating reaction products that are tolerable to the host organism. However, biological compatibility of the immune system with foreign materials as well as implantation of the devices, have not yet received much attention in the context of biofuel cells design.

Ex-vivo applications are even more diverse. At a large scale, power can potentially be recovered from waste water with simultaneous remediation by microbial fuel cells. Smaller scale applications are usually targeted with enzymatic fuel cells devices that allow for miniaturization, and their greatest potential lies in the replacement of battery packs for consumer electronic devices like laptop computers or cell phones. The exploitation of ambient fuels (e.g. carbohydrates derived from plants or from effluent of

human or animal processes) is very attractive for such small devices applications. In this category of applications, biofuel cells must compete with conventional fuel cell technologies that are better understood and characterized. Hence, biofuel cells must take advantage of the natural biocatalytic properties that cannot be reproduced by conventional catalysts (i.e. activity at low temperatures and neutral pH, selectivity, low-cost production).

Lastly, cost is always crucial when commercializing a new technology like fuel cells. In conventional fuel cells, the major costs associated with these systems are related with the materials, the separator inside the fuel cells, and primarily catalyst materials. It can be expected that the cost of separator materials will decrease as their production increases and competitive materials emerge. Nonetheless, the costs of conventional catalysts like noble metals, especially platinum, are expected to increase due to increased production and demand. This is when the employment of alternative catalysts comes to play; including biotacatalysts that are available in nature (e.g. enzymes) and can be produced in large quantities through low-cost well established processes that are at the same time environmental friendly.

The work of this dissertation is presented in several chapters, the next two chapters describing the problem statement, objectives and methodology. The following chapters describe studies performed on the evaluation of stackable modular cell (Chapter 4), development and evaluation of electrocatalyst for NADH oxidation in 2-D electrodes (Chapter 5), their incorporation into 3-D electrodes for flow-through anodes with immobilized NAD^+-dependent enzymes (Chapter 6), combination with a biocathode for building a fully enzymatic biofuel cell (Chapter 7), and initial MATLAB simulation

studies for optimizing biofuel cell parameter (Chapter 8). The last chapter presents the conclusions of this work as well as some considerations for future work. Additionally, the appendices show some publications that represent contributions of the author to other aspects of enzymatic biofuel cells that are not part of dissertation topic.

Chapter 2. Problem Statement and Objectives

2.1. Problem statement

The development of the young technology of enzymatic biofuel cells has been very limited by several factors, one of the main factors being the inability of fully oxidizing complex biofuels. The use of multi-enzyme systems could be very efficient in achieving complete oxidation of fuels like glucose. However, before building an anode based on such a system, the obstacles inherent to the enzyme-catalyzed reactions must be overcome. A number of enzymes that are of interest for biofuel cell applications depend on the NAD^+/NADH cofactor. The issues regarding NADH re-oxidation have been described in the previous chapter. As a consequence, the practical implementation of this group of enzymes is restricted by the regeneration of their active site; thus a great deal of attention has been given to finding ways of re-oxidizing NADH. Despite the effort of many researchers and the many reports that have been published, there is still little progress in the use of NAD^+-dependent enzymes in fully enzymatic biofuel cells.

The first reports on electrodes that were able to decrease the overpotential of NADH oxidation are focused on CMEs, in which *mediators* are used to overcome the energy barrier of the reaction. As new techniques were implemented (e.g. electropolymerization), those *mediators* (e.g. azine monomers) were transformed into *electrocatalysts* (poly-azines) with enhanced performance and stability. Several reports on different catalysts are found in the literature of electropolymerization to build poly-azines for NADH oxidation since the early 90s.

The ability of these catalysts to oxidize NADH has been attributed to the presence of certain chemical moieties that are originally present in the monomer form (mediator). The resulting structures from electropolymerization of the monomers are not completely understood.

2.2.   Hypothesis

This research is focused in studying some of the electrocatalysts for NADH oxidation and providing a scientific understanding of their structures. Poly-(methylene green) (poly-(MG)) and of poly-(methylene blue) (poly-(MB)) are of particular interest, because of their ability to oxidize NADH at low potentials. The fabrication method of these polymers can be adapted to provide the means of modifying different electrode supports depending on the specific application which is highly desirable.

If we achieve an understanding of these polymers, their structures and their properties; we will be able to provide a basis for design of successful catalysts-modified materials for NADH oxidation. Moreover, these materials will have the capability of being integrated into enzymatic anodes for biofuel cells with improved geometries (i.e. 3-D electrodes for flow-through systems) for optimal performance.

2.3.   Objectives and specific aims

The scientific objectives of this work mainly involve the study and understanding of the nature of the electrocatalyst materials by performing structure-to-property studies, characterizing them and proposing a mechanism for their formation and structures. In addition, the following task will be to incorporate the electrocatalysts for NADH oxidation into the design of a 3-D anode that can house NAD^+-dependent enzymes for the

ultimate goal of integrating it in a fully enzymatic biofuel cell. Thus, the main focus of this work is on the material building at different length-scales. At the nano-scale we can create a good electrical contact between the enzyme and the catalyst for NADH oxidation by utilization of CNTs into the enzyme immobilization matrices. The immobilization of enzymes by entrapment into CNTs-chitosan scaffolds provides a conductive and stable matrix that can retain their stability and activity supporting long lifetime. Their porosity is also advantageous to support both efficient mass transport and high loading densities. And finally, it will be necessary to incorporate these chitosan scaffolds onto a carbonaceous electrode material that will act as a house and mechanical support for the bioanode. The plan of research is detailed in the following specific aims.

- Understand the mechanism of electropolymerization of poly-azines by depositing it on different electrode materials via cyclic voltammetry (glassy carbon, carbon nanotubes, Toray paper, and reticulated vitreous carbon).

- Identify possible bond formations when creating the polymers and establish a hypothetical structure of the poly-azines by using characterization tools like angle-resolved X-ray photoelectron spectroscopy (XPS), nuclear magnetic resonance (NMR) as well as studying their morphologies with high-resolution scanning electron microscopy (SEM).

- Demonstrate the catalytic capabilities of poly-(MG)-modified electrodes for NADH oxidation in neutral media through electrochemical characterization performing cyclic voltammetry and chronoamperometry experiments.This also includes testing the poly-(MG)-modified electrode in the presence of a NAD^+-enzyme in solution to determine if it can successfully oxidize its substrate.

- Evaluate the catalytic performance of poly-(MG)-modified electrodes at different pH solutions via cyclic voltammetry experiments, in order to determine the optimal conditions for operation in fuel cells.

- Evaluate immobilization of enzymes into chitosan and CNTs-chitosan porous scaffolds prepared by freeze-drying process and demonstrate that the addition of CNTs enhances the catalytic activity of the enzymes in two-dimensional (glassy carbon) electrodes. This can be done electrochemically by testing the electrodes with the different scaffolds via chronoamperometry that can yield the necessary information to examine Michaelis-Menten type of behavior of the enzymes.

- Study the electropolymerization of poly-(MG) catalysts onto the three-dimensional porous surface of RVC and its catalytic performance. Electropolymerization will be performed by varying the amount of deposition cycles to determine the best conditions for obtaining the highest catalytic activity of the electrocatalyst.

- Incorporate enzymes through immobilization into a poly-(MG)-modified RVC in order to get a flow through electrode system that can be tested for enzymatic activity. Anodic polarization curves will be built to describe the performance of the electrode.

- Combine the anode based on a NAD^+-dependent enzyme built for a flow through system with an enzymatic cathode to obtain a fully enzymatic biofuel cell and test its performance. Performance will be tested by determining the operating voltage of the cell and obtaining its polarization and power curves.

- Use of theoretical models developed in MATLAB for catalytic oxidation at enzymatic bioanodes based on poly-(MG)-modified electrodes to predict their performance. Comparison with the experimental data will be made to demonstrate the

validity of the model. This technique will provide with the means for optimizing the

electrode design based on the materials' parameters.

Chapter 3. Experimental Methodology

3.1. Electrochemical characterization techniques

A standard three-electrode electrochemical cell setup is typically used when analyzing processes that occur at individual electrodes (e.g. anode). The cell consists of a *working electrode* (WE) which is the electrode system of interest, coupled with a *reference electrode* (RE) of known potential that approaches ideal non-polarizability; and a the third electrode known as *counter electrode* (CE) passes all the current needed to balance the current observed at the WE. The CE must be chosen so that its electrochemical properties do not affect the behavior of the electrode of interest (WE).[225]

3.1.1. Cyclic voltammetry

Cyclic voltammetry (CV) is the most used technique for obtaining general information about an electrochemical process. It is usually the first experiment performed in electroanalytical studies, because it quickly provides information about the thermodynamics of redox reactions and kinetics of electron transfer reactions.[226] It consists of linearly scanning the potential of a working electrode, using a triangular potential waveform. It can be performed during single or multiple cycles. The potential is applied at a given scan rate and the resulting current is measured. Figure 3-1 shows a typical cyclic voltammogram for a reversible redox couple. The cathodic peak E_{pc} and anodic peak E_{ca} are observed providing information of the potentials at which reduction and oxidation reactions occur.
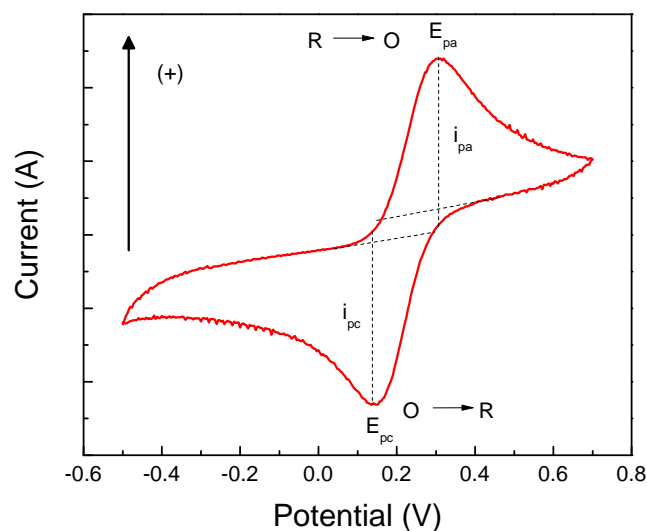
Figure 3-1 Cyclic voltammogram for a reversible redox couple

From this information the *formal* redox potential ($E^{0'}$) for a reversible couple can be calculated as shown in Eq. 3-1.

$$E^{0'} = \frac{E_{pa} + E_{pc}}{2} \qquad \text{(Eq. 3-1)}$$

In this work, CV technique will be used for both analyzing electrode systems and also for synthesis of poly-azines by electrodeposition.

3.1.2. *Chronoamperometry*

Chronoamperometry is a controlled-potential technique that involves stepping the potential of the working electrode and maintaining it at a constant value with respect to a reference electrode, while the current response due to a faradaic process (caused by the potential step) is monitored over a period of time. Figure 3-2a shows the waveform of an applied potential step for a chronoamperometric measurement. In this type of experiment the electroactive species must be inactive at the initial potential E_1, but undergo a faradaic process (oxidation or reduction) at a diffusion-limited rate at E_2.
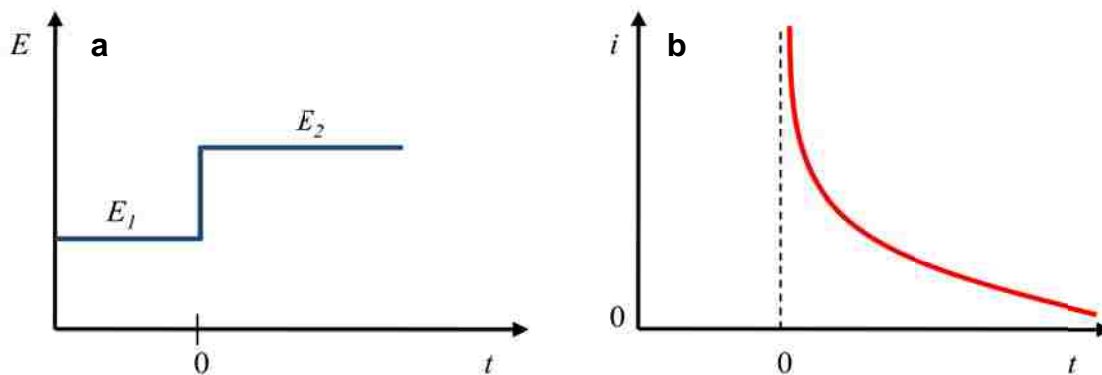
Figure 3-2 a) Waveform for a step potential experiment b) Current flow *vs.* time

Amperometric methods are very commonly used in sensors and biosensors since they provide a quantitative technique for detection devices. Amperometric sensors or biosensors function by the production of a current (measured by chronoamperometry) at a specific potential. The current that is produced by a redox process is associated with the selective recognition of an analyte of interest, and it is also proportional to the quantity of the analyte present. A typical way of studying enzyme-catalyzed electrodes in biosensors is by performing chronoamperometry measurements over a period of time in which consecutive additions of the enzyme substrate are made. Such additions should result in an increase of the anodic or cathodic current depending on the process that the enzyme catalyzes. Figure 3-3 shows what a typical chronoamperometry looks like for an oxidative process with increase of the anodic current.
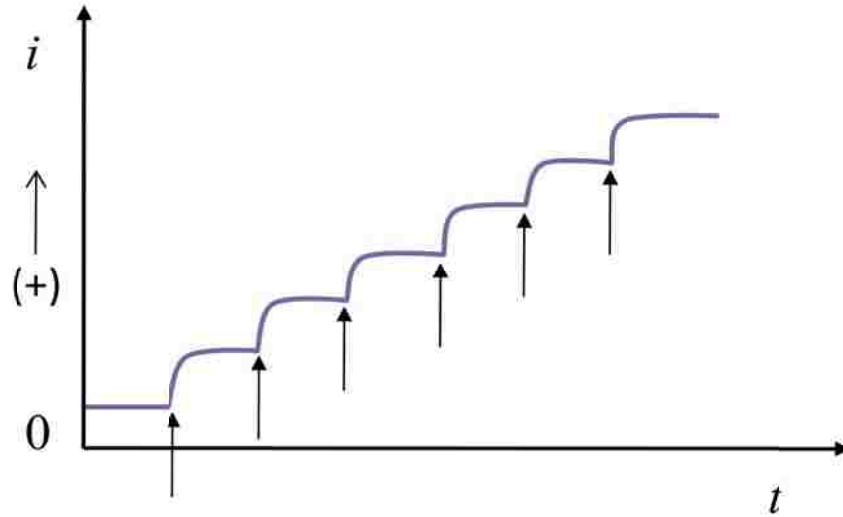
Figure 3-3 Chronoamperometry depicting an oxidation process with consecutive additions of substrate

3.1.3. *Polarization and power curves*

Polarization curves have already been described in section 1.1.1. as an important tool for characterizing the fuel cell performance (Figure 1-3), as well for describing and understanding the processes in both the anode and cathode (Figure 1-4). Polarization curves can be built several ways, and there are two basic methods that have been used for this research: i) chronoamperometry (3.1.2) by measuring steady-state currents at different applied potentials; and ii) chronopotentiometry which is a controlled-current method by which potential responses to an applied current are measured over time. Through both methods we can generate a point-by-point curve that shows the dependence of current with potential for the anode, cathode and fuel cell. The fuel cell power curve is then found through Eq. 3-1 and usually graphed in the same plot as the fuel cell polarization curve.

3.2. Scanning electron microscopy (SEM)

High-Resolution SEM is a useful technique for making visual direct observations at the nano-scale of the morphology of the materials that will be synthesized. This technique is based on probing a sample using an accelerated beam of electrons, under vacuum conditions. SEM detects electrons that are scattered off of the sample surface at different angles from a beam accelerated at 2-20 keV. The beam current absorbed by the sample can be detected and used to create images of the distribution of sample current. This technique requires very small amounts of a sample, in comparison to other characterization methods.

SEM will allow us to observe the morphology and features of poly-(MG) on different materials. It will also be used to observe the morphology of chitosan composite materials on RVC. This tool will give us ideas about uniformity of poly-(MG), as well as the homogeny of integration of CNTs into chitosan scaffolds and their incorporation with RVC. Two SEMs were used in this work: Hitachi S-5200 which provides resolution up to ~5 nm and very small samples; and Quanta 3-D FEG which allows for observation of bigger samples like planar glassy carbon and RVC materials.

3.3. X-ray photoelectron spectroscopy (XPS)

XPS is quantitative spectroscopic technique that measures the elemental composition within a material and provides information about the chemical state of the elements detected. It uses an x-ray source to irradiate the sample surface and induce the emission of photoelectrons whose energies (eV) are characteristic of the elements within the sample.

For this work, a Kratos Axis Ultra XPS was employed. It possesses a monochromatic Al KR (1486.6 eV) source running at 300 W. This instrument is useful for complex materials such as poly-azines, because small shifts from the expected emission energy for a pure element indicate chemical bonding with other elements. The probing depth depends upon the mass of the sample and the incident angle of the beam, usually ranging between 3-10 nm. Angle-resolved XPS is an essential technique for compositional analysis and can be used for studying the complex composition of poly-azines and help elucidate their structures.

Chapter 4. Standardized Characterization of Electrocatalytic Electrodes

This research is part of a collaborative effort across four independent laboratories in different universities for designing and building enzymatic fuel cells. This has raised the need for a standardized testing platform as well as standardized protocols to allow exchange of results and comparative analysis. The work presented in this chapter describes the assessment of such standardized experimental platform and protocols using the material processing and electrochemical characterization of poly-(MG)-modified glassy carbon (GC) electrodes as a model system. The apparatus used is a modular stack cell with defined geometry and dimensions designed at the University of Hawaii in 2008. The configuration of the stack cell is flexible and can be modified for different electrochemical studies, and its use will result in controlled conditions of experimental parameters, avoiding uncertainties that can often cause inconsistent results. Some of these parameters include electrolyte concentration and its volume in the cell, and positioning of each electrode in the cell.

This chapter presents the results obtained at the University of New Mexico as part of standardized test protocols to support the cross-lab comparison of materials and electrochemical measurements to characterize poly-(MG)-modified electrodes for NADH oxidation at neutral pH and low overpotential. The modular stack cell is completely reusable, and can be easily assembled, disassembled, and cleaned.

Glassy carbon (GC) electrode characterization and modification was chosen as model experiments. It was first characterized using a redox couple (ferri-/ferrocyanide) to

determine its electrochemical accessible surface area and then it was modified with poly-(MG) by electropolymerization via cyclic voltammetry (CV).[227] The last experiment tested the poly-(MG)-modified GC for its ability to oxidize NADH. Poly-(MG) was chosen because it has already been reported in the literature that it works as a catalyst for NADH oxidation in NAD^+-dependent enzymes in biofuel cells.[228, 229] These experiments were analyzed across labs to assess reproducibility of experiments, and the variations in the results are all summarized in a collaborative report published in 2008.[124]

4.1. Experimental

Potassium ferricyanide ($K_3Fe(CN)_6$) of analytical grade and purity of 99% (Sigma Cat. 393517), analytical grade methylene green (Fluka Cat. 66870), β-nicotin adenine dinucleotide reduced form (β-NADH) of 98% purity (Sigma Cat. N8129), analytical grade potassium nitrate (KNO_3, EMD Cat. PX1520-1), sodium phosphate monobasic (NaH_2PO_4, EMD Cat. SX0710-1) and sodium phosphate dibasic (Na_2HPO_4, EMD Cat. SX0720-1) were used without further purification. Ag/AgCl/3.0 M KCl was used as reference electrode (CH Instruments Inc. Cat. CHI111) and all potential values are given against this reference. Glassy carbon (GC) electrodes (CH Instruments Inc., Cat. CHI104) were used as working electrodes. The GC electrode possesses a polished glassy carbon disk of 3 mm diameter and prior to use, it was polished with alumina (BAS Polishing kit, Al_2O_3, 1 μm) to a mirror finish. The counter electrode was platinum gauze of thickness 0.127 mm and purity 99.9% (Alfa-Aesar Cat. 10282).

4.1.1. Modular stack cell

The modular stack cell is comprised of three stacking modules: the reaction chamber with reference electrode inlet and solution filling ports, a working electrode plate with inlet for

the GC electrode, and a counter electrode plate to house the counter electrode (Figure 4-1). All modules were manufactured from polycarbonate and the material faces were polished in order to provide sufficient sealing. Custom gasket seals of 0.1 mm thickness were fabricated from Pt. cured silicon rubber.
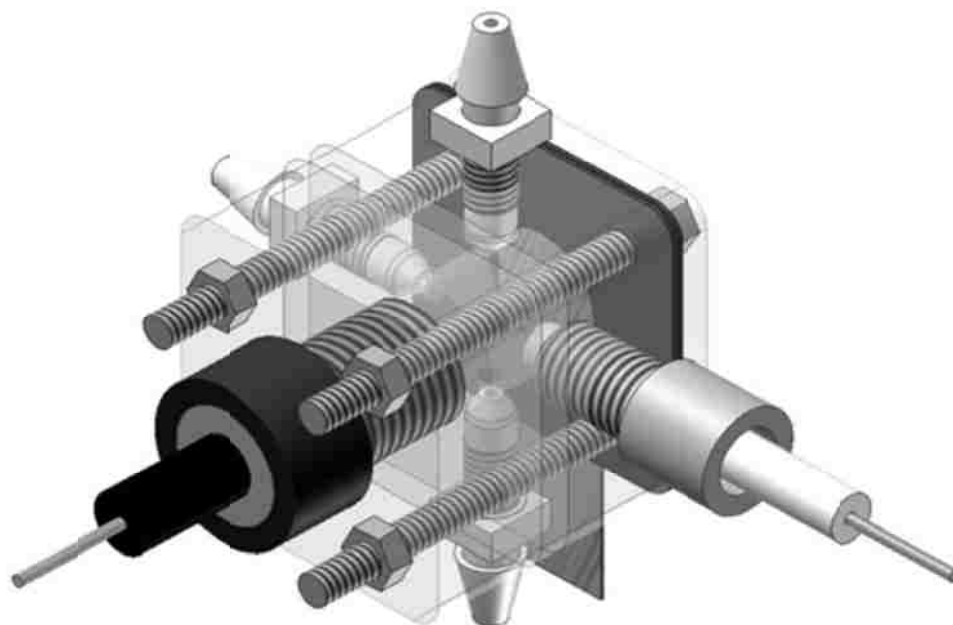
Figure 4-1 3-D drawing of the modular stack cell[124]

The stack cell was used in standard three-electrode configuration and operated in batch mode. The GC and Pt electrode surfaces were oriented concentrically and parallel to each other. To provide enough over sizing of the Pt counter electrode surface area relative to the GC electrode, Pt gauze was used. The reference electrode was centered between the working and the counter electrodes and oriented from side to side to avoid insulation by bubble retention. Figure 4-2 shows in detail how each component of the stack cell was assembled for the three-electrode configuration. The electrolyte volume in the stack cells chamber was 1.786 mL with the volume taken up by that portion of the reference electrode that protruded into the chamber neglected.
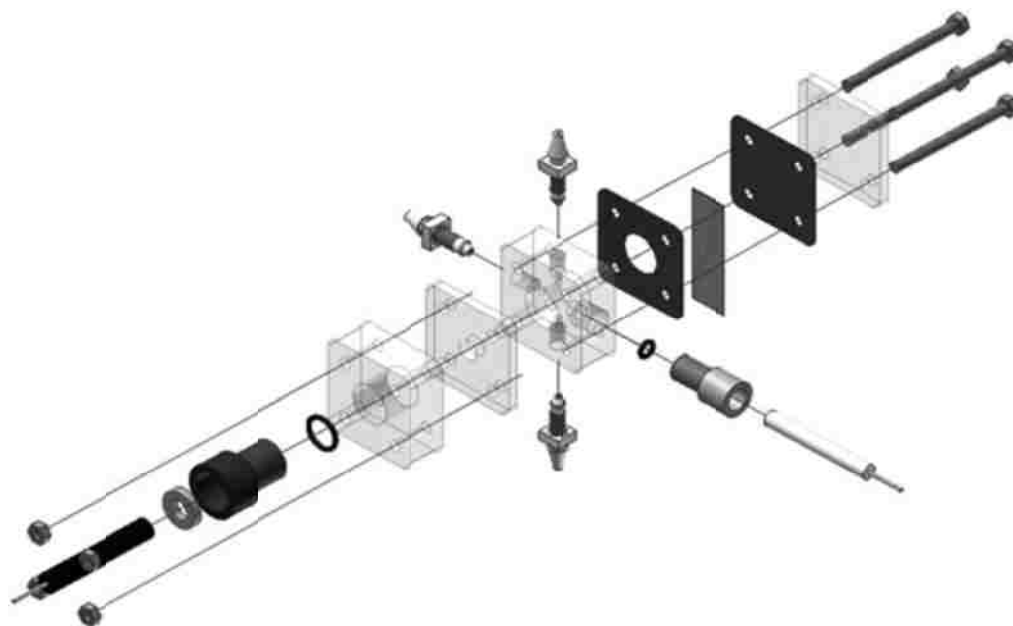
Figure 4-2 Exploded 3-D drawing of the modular stack cell showing the configuration of individual components[124]

The components of the stack cell were cleaned through rinsing and sonication in ultra pure water before each experiment.

4.1.2. Electrode testing with redox couple

The stack cell was filled with a freshly prepared and de-aerated (bubbled with N_2 gas for 25 minutes) solution of 1 mM $K_3Fe(CN)_6$, 0.1 M KNO_3, and pH 7.0 0.1 M phosphate buffer (PBS). Cyclic voltammetry was then performed and recorded for five cycles, between -0.5 V and 0.7 V (vs. Ag/AgCl) with a scan rate of 50 mV/s.

4.1.3. Poly-(methylene green) deposition

Fresh methylene green solution was prepared (0.5 mM MG, 0.1 M KNO_3, and 50 mM PBS pH 7.0) and de-aerated for 25 minutes before used to fill the stack cell chamber. CV was performed for 10 cycles from -0.5 V to 1.3 V (vs. Ag/AgCl) at a scan rate of 50 mV/s in order to electropolymerize methylene green onto the surface of the GC electrode.

The GC electrode was then rinsed ultra pure water in order to remove any residual methylene green solution, any water drops remaining on the tip of the electrode were blown off with a stream of N_2 gas.

4.1.4. NADH oxidation by poly-(MG)-modified electrode

The final experiment tested the catalytic ability of the poly-(MG) film deposited on the GC electrode. Cyclic voltammetry technique was chosen in this case because it has been frequently used in the literature to test mediator modified electrodes for NADH oxidation.[70, 71, 227, 229] Choosing approaches from the literature seemed to be a reasonable basis for the standardization purposes of this work. Other techniques for catalytic characterization of poly-(MG)-modified electrodes like steady-state chronoamperometry and rotating disk electrode experiments are explored in the following chapters.

NADH solution was freshly prepared in PBS (0.1 M, pH 7.0) to a final concentration of 1 mM and then immediately transferred to the reaction chamber of the stack cell and left to rest for 20 min for its temperature to reach room temperature and to allow wetting of the electrodes. An aliquot of the stock solution was set aside, at room temperature, as a reference sample. CV was applied for 5 cycles from -0.5 V to 0.5 V (vs. Ag/AgCl) at a scan rate of 50 mV/s. Upon completion, the solution was retrieved from the stack cell, and its absorbance was measured at 340 nm by UV-vis spectrophotometer, and compared to the reference sample. The amount of NADH oxidized at the electrode surface was estimated by calculating the difference between the concentration of reference sample and the concentration of the remaining solution in the chamber, using Beers law with an extinction coefficient $\varepsilon = 6300$ $M^{-1}cm^{-1}$.

4.2. Results and discussion

4.2.1. GC electrode quality test

The first experiment was performed to verify the proper operation of the three electrodes in the modular stack cell. The electrochemistry of ferri-/ferrocyanide redox couple is well defined and it is known to be very reversible. It follows the reaction:

$$Fe(CN)_6^{3-} + e^- \longleftrightarrow Fe(CN)_6^{4-}$$
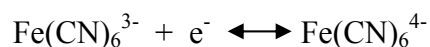
Figure 4-3 presents five consecutive CV cycles in the presence of the redox couple indicating the position of the anodic and cathodic peaks. The values of formal redox potential ($E^{0'}$), peak separation (ΔE), anodic and cathodic peak currents (i_{pa}, i_{pc}) and their ratio i_{pc}/i_{pa}. Table 4-1 summarizes these values.
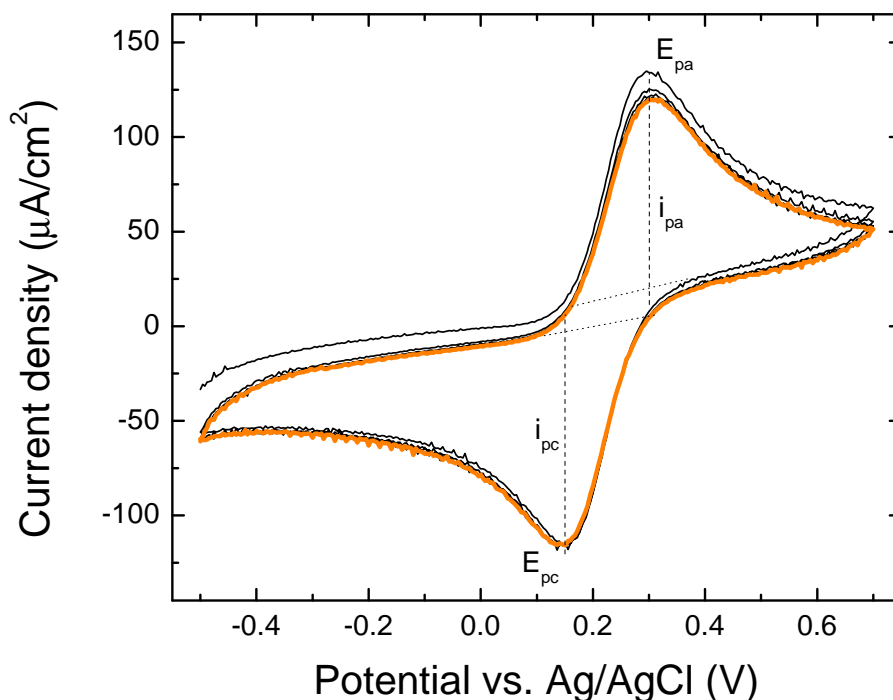
Figure 4-3 Electrode testing: CV cycling of electrodes in 1 mM ferricyanide solution; scan rate 50 mV/s, cycles 1 to 5. Current reported by geometrical surface area (0.07 cm^2)

Table 4-1 Electrochemical parameters obtained from CV in ferri-/ferrocyanide

$E^{0'}$ (V)	ΔE (V)	i_{pa} (μA/cm^2)	i_{pc} (μA/cm^2)	i_{pc}/i_{pa}
0.224	0.152	119.7	115.7	0.97

The values of formal redox potential, reduction and oxidation peak current and their ratios helped verify the standardization conditions and reproducibility when comparing to the results obtained by the other labs. The formal redox potential specifically describes the thermodynamics of the system and the peak currents provide information about the kinetics.

This experiment was also used to check the surface quality of the GC electrode. Since the specified polishing of the electrode does not actually provide very effective and reproducible control of the true surface area of the electrode, this experiment measures its electrochemical accessible surface area for the given reaction. The ratio of cathodic to anodic peak currents (i_{pc}/i_{pa}) provides information about the reversibility of the reaction, which should be unrelated to the active surface area of the electrode. A completely reversible reaction has a ratio of cathodic to anodic peak currents of unity. The result obtained (Table 4-1) indicates that the expected reversible reaction was achieved.

By comparing the results with the other labs it was possible to verify the proper behavior of the GC electrode, in terms of correct redox potential of ferri-/ferrocyanide reaction, as well as the general operation of the three-electrode cell. This indicates that the modular stack cell was properly constructed thanks to the protocols that were developed.

4.2.2. Poly-(MG) deposition

Figure 4-4 shows a typical cyclic voltammograms for the electrochemical polymerization of methylene green onto the GC electrode for 10 cycles, performed in the modular stack cell. The three important regions are indicated on the graph. The first region corresponds to the adsorption of positively charged methylene green MG^+ onto the electrode surface. According to the literature[227] the positively charged methylene green s then reduced in a two-electron, single-proton reaction. This reduced form undergoes then an anodic process defined in the second region, where it is oxidized and then desorbed. Another anodic process begins at potential values above 0.9 V vs. Ag/AgCl defines the third region where the oxidation processes that complete the poly-(MG) development occur and it is referred to as the polymerization shoulder.
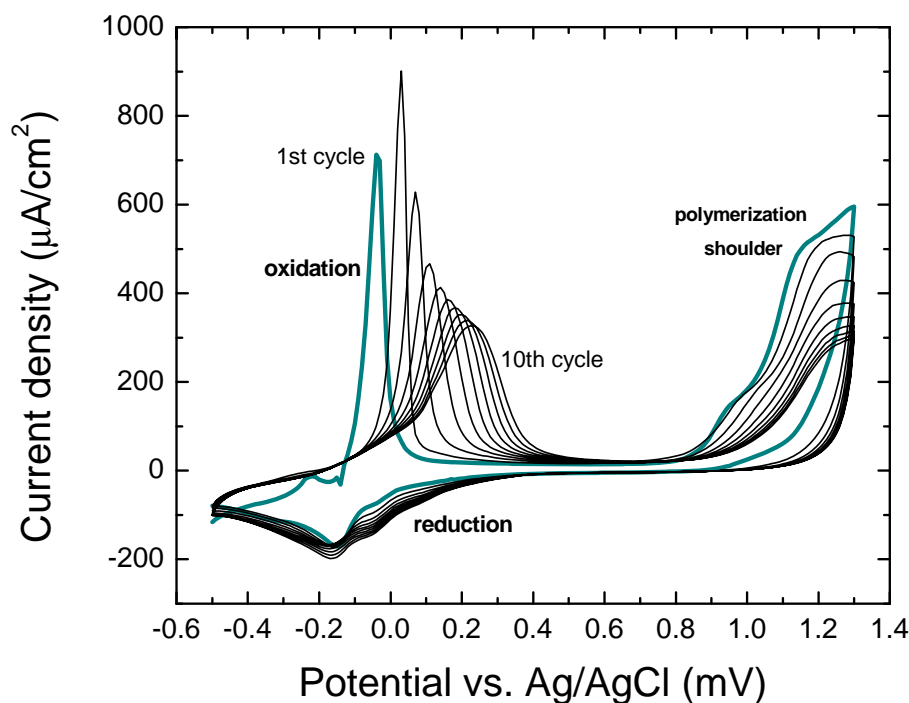
Figure 4-4 CV deposition of methylene green on GC electrode for 10 cycles; scan rate 50 mV/s

The parameters of cathodic (E_{pc}, i_{pc}) and anodic (E_{pa}, i_{pa}) peak potentials and currents, the peak current ratio (i_{pc}/i_{pa}), and the potential and current (i_{inf}) associated with the inflection point of the polymerization shoulder; were determined in order to characterize key aspects associated with the electropolymerization of MG. The inflection point was determined as the maximum value of the first derivative of the current. All of the parameters were obtained from the last deposition cycle and are summarized on Table 4-2.

Table 4-2 Electrochemical parameters obtained from electropolymerization of MG

E_{pc} (V)	E_{pa} (V)	i_{pc} ($\mu A/cm^2$)	i_{pa} ($\mu A/cm^2$)	i_{pc}/i_{pa}	i_{inf} ($\mu A/cm^2$)
-0.17	0.23	197.9	326.7	0.61	266.3

All of these parameters were also compared to those obtained by the other labs. Different statistical criteria were applied to again demonstrate good reproducibility of the results of this experiment across labs.[124]

4.2.3. Oxidation of NADH by poly-(MG)

The last experiment was conducted to evaluate the ability of the poly-(MG)-modified GC electrode prepared in the modular stack cell towards NADH oxidation. The oxidation of NADH by poly-(MG) and other poly-azines has been extensively studied.[69-71, 85, 228] When in contact with the oxidized poly-(MG) film, NADH reacts with it and forms a complex that subsequently decomposes the NADH to NAD^+ and reduces the poly-(MG^+) to its reduced form poly-(MGH). The oxidized form of the polymer is then regenerated when the reduced poly-(MGH) is electrochemically reoxidized to poly-(MG^+).   Figure 4-5 shows five consecutive CV cycles applied to the poly-(MG)-modified electrode in the

presence of 1 mM NADH solution. This voltammograms illustrates the anodic oxidations of poly-(MGH) to poly-(MG$^+$) and the cathodic reduction of the oxidized poly-(MG$^+$) to poly-(MGH). Four inflection points (E_{ip1}, E_{ip2}, E_{ip3}, E_{ip4}) that were used for comparison across labs, are indicated in Figure 4-5. Table 4-3 summarizes the potential values of the four inflection points.
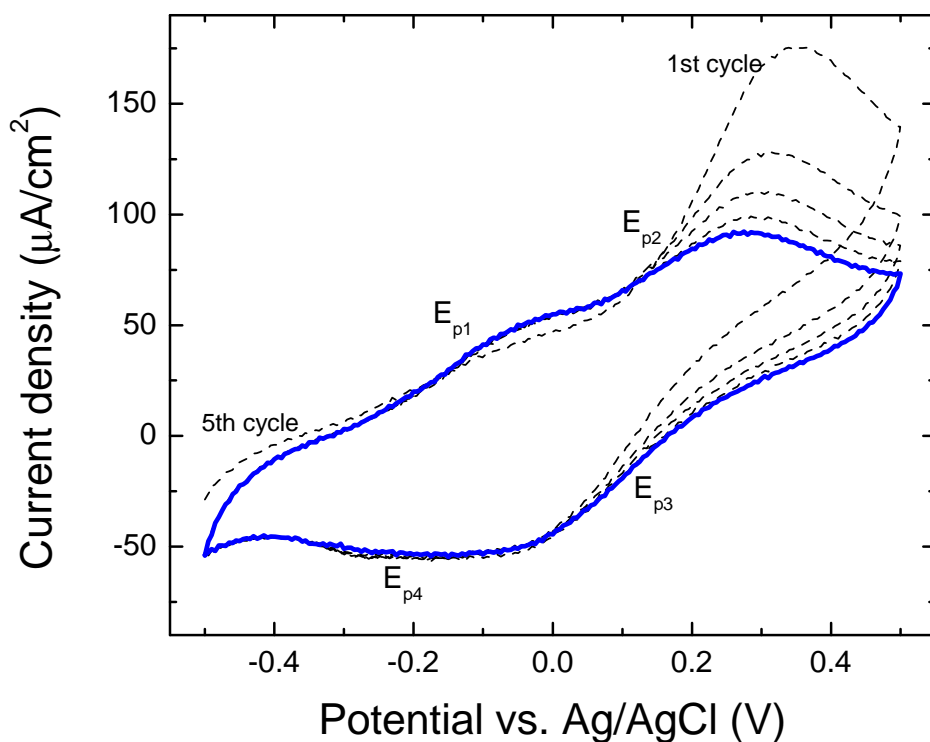
Figure 4-5 CV of NADH oxidation by poly-(MG)-modified GC electrode; scan rate 50 mV/s

Table 4-3 Inflection points of 5th cycle CV of NADH oxidation by poly-(MG) electrode

E_{p1} (V)	E_{p2} (V)	E_{p3} (V)	E_{p4} (V)
-0.13	0.19	0.14	-0.22

The 5th cycle of CV shown in Figure 4-5 possess very small features (peaks) that are not very distinctive, which is why the inflection points that are found mathematically were chosen to evaluate the reproducibility of the experiment when comparing the results to those obtained by the other labs. Most of the parameters met the reproducibility criteria except for E_{p2}, probably due to the fact that its value, unlike the other inflection points, decreases with the cycle number.

The lack of reproducibility in this last experiment across labs does not imply that the modular stack cell cannot work as standard platform, since this was already demonstrated with the previous experiments. The oxidation of NADH is a much more complex reaction that might not necessarily be well controlled by the researcher. In order to further characterize this reaction, an ex-situ spectrophotometric measurement of the actual amount of NADH that was oxidized was performed. The equivalent charge (Q_{eqv}) of oxidized NADH was calculated and compared to the analyzed charge surplus between the anodic and cathodic charges ($Q_a - Q_c = \Delta Q$) over the CV cycles. Table 4-4 summarized these values.

Table 4-4 Summarized results of NADH oxidized measured spectrophotometrically compared with charge measured through CV

Electrochemical			UV-vis spectrophotometry		
Total Q_a	*Total Q_c*	ΔQ	NADH oxidized	Q_{eqv}	$Q_{eqv}/\Delta Q$
($\mu C/cm^2$)	($\mu C/cm^2$)	($\mu C/cm^2$)	(μmol)	($\mu C/cm^2$)	
5.129	2.564	2.583	0.250	682.603	264.3

The electrochemical oxidation of poly-(MGH) is balanced with the chemical oxidation of NADH. Thus the equivalent charge associated with the NADH concentration drop that was measured ex-situ, can be directly compared to the surplus charge from the

electrochemical analysis. From Table 4-4 it is seen that this equivalent charge is 264 times higher than the oxidative charge surplus. This ratio indicates that the amount of charge measured electrochemically does not account for the amount of charge that would be theoretically expected, as based upon the amount of NADH determined to have been oxidized that was measured by spectrophotometric technique. Several factors that are beyond the researcher control could have originated this result (e.g. lower reaction rate of the electrochemical oxidation, irreversibility of reduction of poly-(MG$^+$)).

4.3. Conclusions

The experiments performed on this work were useful for assessing standardized experimental platform and protocols to allow cooperative research across different labs. Exchange of results, comparative analysis and collaborative pursuit of benchmark improvements in electrocatalytic electrode design and performances will be greatly facilitated by these standard protocols and platform. The modular stack cell was used to characterize GC electrodes regarding their performance in the presence of ferri-/ferrocyanide redox couple. The GC electrode was then modified by electrodeposition of poly-(MG) via cyclic voltammetry, and this electrode was finally tested for NADH oxidation capabilities. The reproducibility analysis is reported as a collaborative work[124] and it showed that the NADH oxidation by poly-(MG)-modified GC is still not completely understood and it requires further research.

Chapter 5. Structure and Electrochemical Properties of Electrocatalysts for NADH Oxidation

Two different azine monomers were chose to conduct this study: methylene green and methylene blue. Figure 5-1 shows the chemical structures for the two monomers. Preliminary work has already been done with methylene green in a stackable modular cell in a cross-laboratory research[124] depositing an electroactive film of its polymer on glassy carbon electrodes and showing its electrocatalytic activity with respect to NADH oxidation. Methylene blue is of interest, because it is purchased as a 97.0 % pure sample whereas methylene green is 50.5% pure with large (33.8%) impurities of methylene blue. Therefore, evaluation of methylene blue will help us understand if the NADH oxidation at poly-(methylene green) is due to the high concentration of methylene blue present or due to the methylene green.
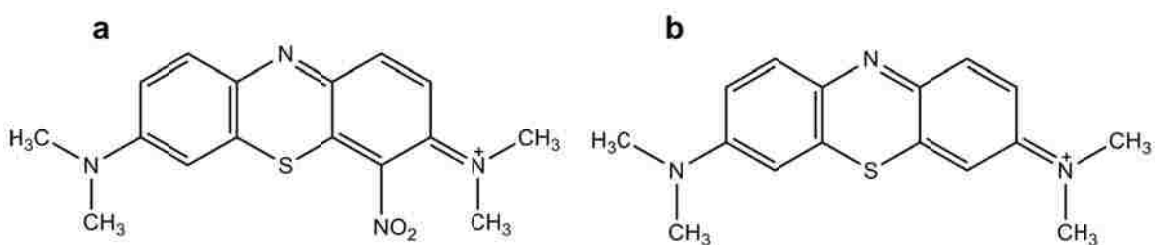
Figure 5-1 Chemical structure of: a) methylene green, and b) methylene blue

In order to characterize these poly-azine films, HR-SEM, X-ray photoelectron spectroscopy (XPS) and nuclear magnetic resonance (NMR) were chosen. HR-SEM allows us to examine the morphology of the thin polymeric film forming on the glassy carbon electrode during polymerization. XPS measures elemental composition and

55

chemical state of the elements present in our materials, allowing for deriving possible binding strategies of polymers. Proton NMR allows for us to analyze the formation or removal of C-H, N-H, O-H, or S-H bonds. This provides information about the chemical reactions occurring during polymerization.

5.1. Experimental

Methylene green (Fluka Cat. 66870), methylene blue (Mallinckrodt Chemicals Cat. 5891-57), malate dehydrogenase (MDH) from porcine heart (USB products from Affymetrix Cat. 18665), L-(-)-malic acid (Sigma Cat. M1000), NADH (Sigma Cat. N6005), and NAD$^+$ (Fluka Cat. 43407) were used without further purification. All other chemicals were of reagent grade. NADH and NAD$^+$ stock solutions were prepared with phosphate buffer, pH 7.0. Enzyme stock solution was prepared with TRIS buffer, pH 7.0. L-malic acid was prepared with distilled water and its pH was adjusted to 7.4 with concentrated NaOH. Electrochemical measurements were carried out in a one-compartment electrochemical cell containing platinum gauze as the counter electrode and Ag/AgCl/3.0 M KCl reference electrode (CH Instruments Inc.). All potential values are given against this reference. Glassy carbon (GC) plates (SPI Supplies, 25 mm x 25 mm x 1 mm) and glassy carbon rods (CH Instruments Inc., 3 mm diameter) were used as working electrodes. Prior to use, the working electrode was polished with alumina (BAS Polishing kit, Al$_2$O$_3$, 1 μm) to a mirror finish.

5.1.1. Poly-azine preparation

Methylene blue and methylene green were polymerized on glassy carbon surfaces electrochemically by cyclic voltammetry. The electropolymerization of the two azines

was carried out by cyclic voltammetry at a scan rate of 50 mV/s. The monomer concentration in the growing-solution was 0.5 mM in the presence of 0.1 M KNO_3. All of the monomer solutions were prepared in phosphate buffer pH 7.0. In every case, the potential sweep range was different according to the established procedures. All three of them were deposited under an oxygen-depleted environment. Electropolymerization was carried out for 1, 2, 10, 20 25 and 50 cycles on the planar GC for XPS and NMR analysis. The electrochemical instrument used for all the electrochemical analysis (electrodeposition and chronoamperometric curves) was Gamry Reference 600 Pontentiostat/Galvanostat/ZRA.

5.1.2. NADH oxidation

Poly-(methylene green) was chosen to be tested with respect to NADH oxidation. Amperometric curves were obtained at 0.05 V vs. Ag/AgCl by consecutive additions of the substrate from a 25 mM NADH stock in pH 7.0 phosphate buffer. A calibration curve was consecutively obtained from the steady-state current data.

5.1.3. L-malic acid oxidation in the presence of MDH

A poly-(MG)-modified GC electrode was put in pH 7.0 phosphate buffer electrolyte in the presence of the enzyme and MDH (50 µg/mL), and its cofactor NAD^+, in excess (5 mg/mL). L-Malate (substrate of MDH) amounts were added every 300 seconds from a 1 M stock in order to obtain an amperometric curve to show the catalytic activity of the enzyme. A calibration curve was consecutively obtained from the steady-state current data.

5.1.4. X-ray photoelectron spectroscopy (XPS)

Angle-resolved XPS (ARXPS) spectra were acquired by a Kratos AXIS Ultra photoelectron spectrometer using a monochromatic Al Kα source operating at 300W. The base pressure was 2×10^{-10} torr, and operating pressure was 2×10^{-9} torr. Charge compensation was accomplished using low energy electrons. Standard operating conditions for good charge compensation are –4.1 V bias voltage, -1.0 V filament voltage and a filament current of 2.1 A. The MG and MB samples polymerized at 1, 10, 25 and 50 cycles were analyzed at three different Take-off-angles of 90, 50 and 15°. Clean glassy electrode was also analyzed at the same angles as a reference. The reported ARXPS data represent averages from 2-3 areas per sample. The survey of each area is done first, followed by the recording of high-resolution spectra of C 1s, O 1s, N 1s and S 2p for all the samples. Linear background was used for elemental quantification of C1s, N1s, O1s and S 2p spectra. Quantification utilized sensitivity factors provided by the manufacturer. All the spectra were charge referenced to the aliphatic carbon at 284.8 eV. Curve fitting was carried out using individual peaks of constrained width, position and 70% Gaussian/30% Lorentzian line shape.

5.1.5. Nuclear magnetic resonance (NMR)

A solution of each dye solution described above was prepared and degassed. A 10 cm x 10 cm square of Toray paper was used for the working electrode. The same cyclic voltammetry parameters for electropolymerization as described above were employed on the working electrode for 2 or 20 scans. The electrode was rinsed with water. Then, the working electrodes were treated with acetone to dissolve the polymer off of the Toray paper and into solution. The solution was dried. The remaining solid was dissolved in

1000 µL of deuterated acetone and added to an NMR tube. Methylene green monomer, water, acetone, methanol and a blank were also added to deuterated acetone and run in the NMR for comparison. 128 scans of proton NMR were run on a 400 MHz Ultrashield™ Bruker NMR for each sample.

5.2. Results and discussion

5.2.1. Electropolymerization of azines

A change of color on the GC electrodes can be directly observed after the electrochemical polymerization is done. Poly-(MG) appears to be golden green, whereas poly-(methylene blue) (poly-(MB)) appears to be blue shifted. This color change is indicative of the formation of a layer of new material on the surface of the electrodes. Figure 5-2 shows cyclic voltammograms (1st and 50th cycle) that were obtained for deposition of the two azines. A significant increase in the current density from the first to the last cycle indicates the enhancement of the electrochemical accessible surface area (EASA) of the electrode which also implies deposition of a polymer film on the surface of the carbon electrode. Furthermore, a shift of the initial potential peak (0.010 V for MG and -0.140 V for MB) to more anodic regions (0.472 V for MG and 0.285 V for MB) is observed in all cases when comparing the first and the last cycles. This observation could indicate an increase in the amount of electroactive species confirming that the polymer film has been formed on the surface of the GC. Certain differences can be observed across monomers. On the first cycle, MG shows two oxidation peaks (a small one at -0.164 V and a bigger one at 0.010 V) whereas the other monomer only shows one peak. However, these two peaks shown by MG combine into only one peak by the 50th cycle of polymerization (at

0.472 V).The extra peak observed in the first cycle of methylene green polymerization corresponds to the contamination of methylene blue in the starting material. This was confirmed when this peak increased in intensity when methylene blue's percentage is increased in the starting material. The extra anodic peak in the cyclic voltammograms is due to impurity of the methylene green. The largest initial oxidative peak of MG is observed at a more anodic potential than that of MB, which is indicative of the nitro functional group's affect on the redox potential. It can be observed in every case that the electropolymerization process that dominates is oxidative, as reported elsewhere.[25, 70, 71, 230]
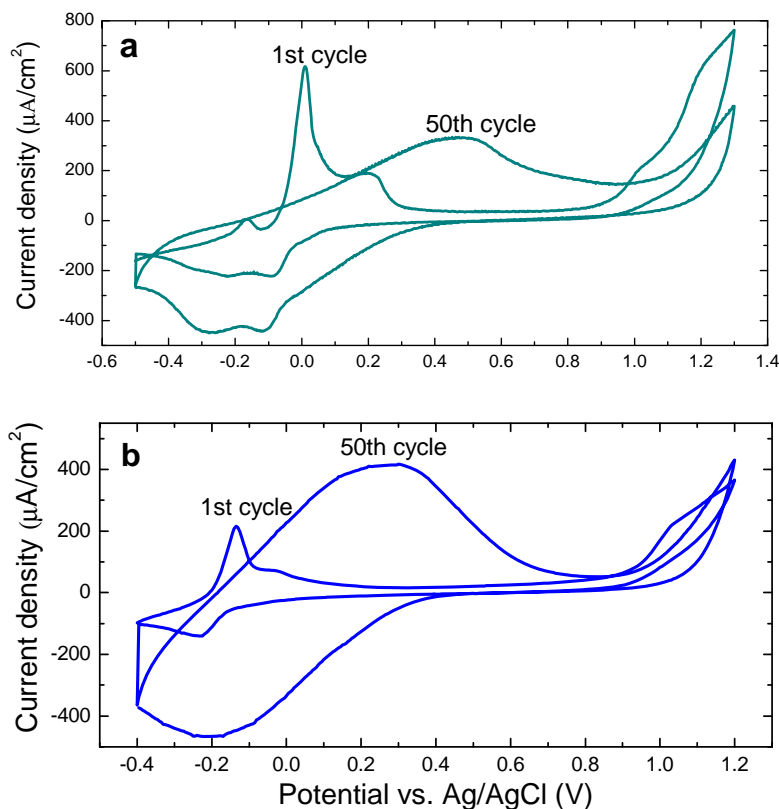
Figure 5-2 1st and 50th cycle electropolymerization of: a) methylene green, and b) methylene blue.

Scan rate: 50 mV/s; monomer concentration: 0.5 mM in 0.1 M KNO$_3$

Cyclic voltammetry is used as the polymerization procedure, since a reductive step is also necessary for formation of these poly-azines. From a general perspective, the two monomers show a very similar behavior regarding their electrochemical polymerization. For this reason and due to the fact that our biofuel cell research has previously utilized poly-(MG) and the similarities described regarding characterization, electrocatalytic activity measurements are reported for only poly-(MG) modified electrode.

5.2.2. Characterization

X-ray photoelectron spectroscopy (XPS)

Table 5-1 shows elemental quantification results for poly-(MG) and poly-(MB) samples polymerized for 1, 10, 25 and 50 cycles at three take-off-angles of 90, 50 and 15 degrees. Results from blank glassy carbon electrode and powder MG and MB monomers are also shown for reference. Blank electrode samples have 1.4-.1.7 atom% of N and negligible amounts (0.14-0.27 atom%) of S. The MG sample prepared by 1 cycle of voltammetric deposition has ~12 % N and 2.5-3% S, while smaller amounts of N (5.1%) and S (1.6%) are detected for MB sample prepared by 1 cycle. A slight enrichment of C and depletion of O towards the sample/air interface is detected for both samples. The composition of polymerized MG sample is very similar to that of the monomer, with slightly larger O and fewer C amounts. The composition of poly-(MB) is more different from that of the monomer, with lower N and S and higher O concentrations. The poly-(MG) sample prepared by 10 voltammetric cycles has even more N and S, with both of those being slightly more enriched towards the electrode/polymer interface. The poly-(MB) sample prepared by 10 voltammetric cycles has twice as much N and S as the 1-cycle sample.

The composition is stable for both polymers formed by greater than 10 deposition cycles.

Stable composition is achieved faster for MG sample than for MB.

Table 5-1 Elemental Quantification of carbon, nitrogen, oxygen and sulfur, on poly-(MG)- and poly-(MB)-modified electrodes during different deposition cycles

90 deg	C %	1sN %	1sO %	1sS 2p %	50 deg	C %	1sN %	1sO %	1sS 2p %	15 deg	C %	1sN %	1sO %	1sS 2p %
Blank	85.7	1.4	12.6	0.27	**Blank 50**	86.1	1.7	12.0	0.18	**Blank 15**	80.1	1.7	18.0	0.14
MG 1	71.7	11.9	13.4	3.0	**MG 1 50**	72.3	11.6	13.1	2.9	**MG 1 15**	76.4	9.7	11.6	2.4
MG 10	68.3	13.7	14.7	3.4	**MG 10 50**	68.4	12.8	15.4	3.4	**MG 10 15**	70.1	10.9	16.1	2.9
MG 25	66.6	12.5	17.8	3.1	**MG 25 50**	67.6	11.5	17.9	3.0	**MG 25 15**	69.9	10.8	16.7	2.6
MG 50	67.8	12.2	16.8	3.2	**MG 50 50**	68.1	11.2	17.8	2.9	**MG 50 15**	69.9	8.4	19.3	2.4
MG powder	75.3	13.4	8.2	3.1										
MB 1	81.0	5.1	12.3	1.6	**MB 1 50**	80.7	5.8	11.6	1.9	**MB 1 15**	75,6	7,1	14.6	2.7
MB 10	69.1	11.4	15.9	3.5	**MB 10 50**	69.2	11.5	15.5	3.8	**MB 10 15**	70.9	9.5	16.5	3.1
MB 25	69.3	10.9	15.9	3.9	**MB 25 50**	70.1	10.7	16.0	3.3	**MB 25 15**	72,8	8.7	15.3	3.3
MB 50	69.4	11.3	15.5	3.7	**MB 50 50**	70.2	11	15.3	3.6	**MB 50 15**	73,4	8,7	14.3	3.6
MB powder	79.5	11.5	5.5	3.5										

Deconvolution results for C, N and S for all samples are shown Table 5-2. Figure 5-3 shows curve fitted N 1s high resolution spectra for MG and MB monomer and poly-(MG) and poly-(MB) deposited by 10 deposition cycles. Both monomers have pyridine N (399.8 eV) and protonated amine (401.6 eV) types of N detected, while MG also has the nitro group (406 eV). In addition to these peaks, both polymerized samples have a new peak at 400.2 eV detected. This peak is being formed primarily at the expense of a decrease of pyridinic N. At 10 deposition cycles, increase in all types of nitrogen, except

nitro nitrogen is detected. The increase in pyridinic and 400.2 eV peak from 1 to 10 voltammetric cycles is much stronger for MB due to overall more dramatic increase in N concentration. For a larger number of cycles, only a slight change in overall N chemistry is observed for both poly-(MG) and poly-(MB) in comparison with the 10-deposition cycles sample.

Table 5-2 High resolutions spectra, 0 take off angle

	C						N				S	
	C=C	C-S, C*CO	C-N=C, C-N-R$_3$/ C-NO$_2$/ C=N-(CH$_3$)$_2$	C-O	C=O	N-C=O	C-N=C	CNarH	C=N-(CH$_3$)$_2{}^+$	NO2	C-S	SO$_3$
	284.7	*285.5*	*286.1*	*286.9*	*287.7*	*288.4*	*399.4*	*400.2*	*401.6*	*406*	*164.3*	*167.7*
Blank	43.7	18.6	7.8	4.5	3	6.2	0.27	0.26	0.5	0.43	0.23	0.32
MG powder	20.2	36.5	6.1	2.1	3.3	4.6	9.68	0	1.59	4.01	2.1	1.2
MG1	24.6	15.9	15.8	2.6	3.6	5.4	0.9	5.5	0.49	4.17	2.2	0.81
MG10	17.1	16	17	4.7	3.1	5.7	1.16	7.11	1.23	3.98	2.68	1.11
MG25	17.7	16.5	13.9	6	1.3	8.3	1.09	3.93	0.74	5.75	2.33	0.57
MG50	22.9	17.5	11.7	3.3	1	8	0.49	4.17	0.41	5.81	2.33	1.04
MB powder	20.2	40.4	8.0	1.4	2.6	5.3	11.2	0	1.3	-	2.5	1.4
MB1	44.6	12.0	10.2	2.9	5.2	6.1	2.45	2.01	0.65	-	1.07	0.55
MB10	24.7	24.4	8.5	1.2	3.0	7.3	6.29	4.52	0.56	-	2.80	0.74
MB25	23.3	22.5	11.0	3.4	3.4	5.7	6.88	3.30	0.75	-	2.80	1.06
MB50	20.7	23.1	11.1	3.0	3.0	6.3	5.74	4.88	0.72	-	2.74	0.99
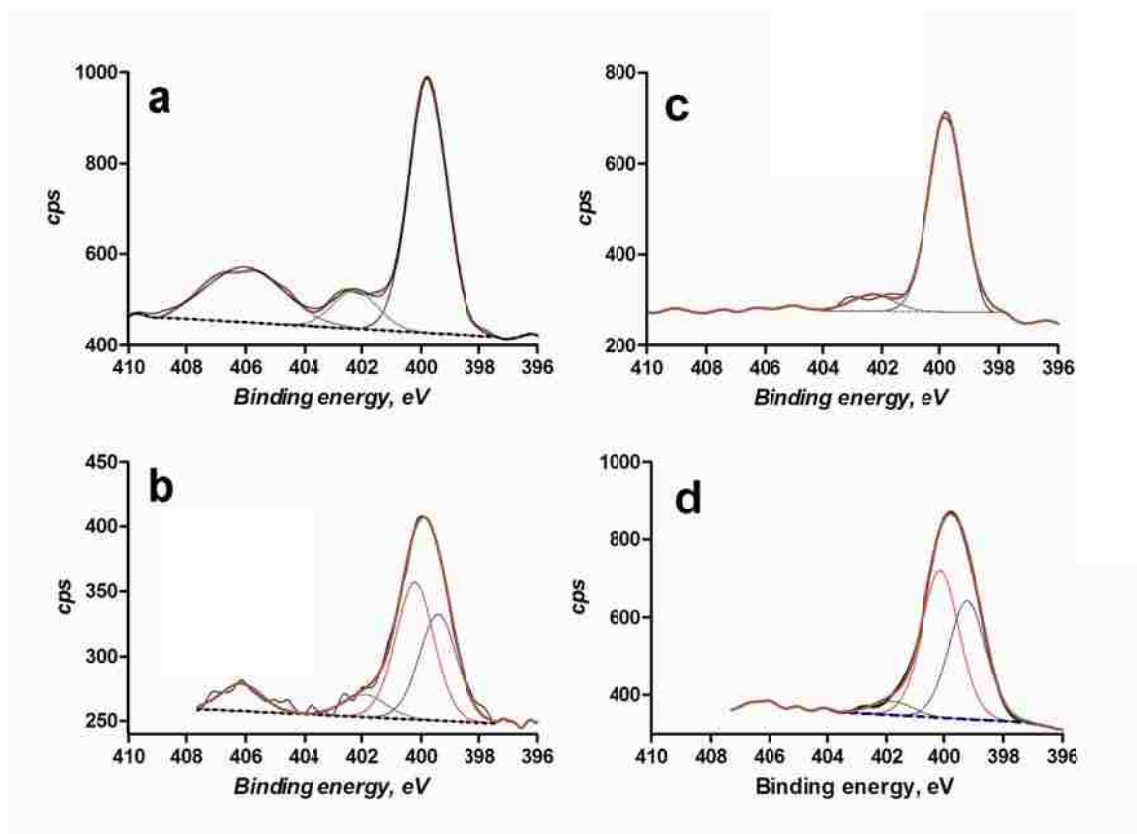
Figure 5-3 High Resolution Spectra of Nitrogen: a) methylene green monomer, b) poly-(methylene green), c) methylene blue monomer and d) poly-(methylene blue)

The new peak at 400.2eV detected for the poly-(MG) and poly-(MB) samples may have several sources of origin, including: secondary amines, amide and urethane. Deconvolution of C 1s high resolution spectra shows increase in the peak at 286.1 eV, especially for poly-(MG) sample, while all other peaks either decrease or stay unchanged. This peak is where all types of C-N bonds that are pyridinic or amines. Conversion of pyridinic N in the monomer to protonated N in the polymer is thus confirmed. Protonation of pyridinic N is accompanied by oxidation of the protonated amine in the monomer. The small decrease in the intensity of the peak at 401.6 eV (protonated amines) for both MG and MB confirms this. One of the possible places where polymer is

being formed is through the formation of a ring-N(CH$_3$)-ring bond [70]. A decrease in aromatic carbons which would participate in such a bond and an increase in the peak at 286.1 eV (C-N) confirm this type of polymerization. MB undergoes more dramatic changes during polymerization that MG does, as manifested by very different carbon structure for 1 and 10 cycles. Alternative ring-to-ring coupling, which is suggested in the literature [70, 73] is not possible to confirm by XPS, as new bonds that are being formed have exactly the same binding energy (BE) as the origin species. No change in nitro group is observed indicating that this moiety does not participate in polymerization of MG. Two types of S, i.e. C-S and S-O, are detected for both monomer and all polymerized samples. XPS, thus, confirms (1) reduction of pyridinic nitrogen to secondary amine, (2) oxidation and removal of proton on the protonated amine and (3) formation of a ring-N(CH3)-ring type of bonding between monomer units.

Nuclear magnetic resonance (NMR)

In order to study the polymer structure, poly-(MG) and poly-(MB) were analyzed with proton NMR. The most significant change between the spectra of the monomers versus polymers was a doublet at 7.58 ppm changed to two quartets at 7.53 and 7.63 ppm. This is indicative that there is an addition of protons added for the polymer near the two protons responsible for the doublet at 7.58 ppm. These and other NMR data values are reported in Table 5-3. From NMR simulations using ChemExper, the peaks in this area of the NMR spectrum are a result of the protons located two carbons away from the nitrogen in the thiazine ring. Thus, the NMR data does not show a loss of the proton two carbons away from the nitrogen in the ring, but rather an addition of protons elsewhere on the structure. Also, for both poly-(MG) and poly-(MB), a new peak appeared in the NMR

spectra for the polymers at 4.08 ppm. ChemExper predicts that this proton peak is from the addition of a proton onto a carbon near the sulfur atom.

Table 5-3 ^{1}H NMR data of representative peaks unique to each monomer or polymer. (Data provided by Prof. Shelley Minteer's group in Saint Louis University)

Compound	[1]H (ppm)
MG monomer	7.52, 7.61, 7.57
Poly-(MG)	4.08, 6.77, 7.53, 7.63
MB monomer	2.81,3.38,7.37,7.53,7.63
Poly-(MB)	4.08, 7.53, 7.62

In comparison to each other, the NMR spectrum for poly-(MG) had a single peak at 6.77 ppm that was not in the monomer's spectrum and poly-(MB) had a new singlet peak at 7.37 ppm. From NMR simulations, it indicates that the singlet at 6.77 ppm may be from the addition of a proton at the carbon farthest from the NO_2 group. As for poly-(MB), the simulation indicates that the peak at 7.37 ppm is from a proton added on to a carbon in the ring.

Representative proton peaks from the monomer of MB at 2.81, 3.38 and 7.99 ppm are not present in the spectra for the polymer of MB. NMR simulations indicate that the peaks at 2.81 and 3.38 ppm are caused from the protons of the methyl groups. Therefore, at least one link of the polymer may be at one of the carbons or nitrogens that are not part of the thiazine backbone structure. The broad peak at 7.99 ppm obtained from analyses of MB is not present for either poly-(MB) formed from two voltammetric scans or 20 voltammetric scans. Simulations correspond to the proton two carbons away from the sulfur.

Thus, NMR spectra suggest that protons are being lost during the electrochemical synthesis of both poly-(MG) and poly-(MB). It is also deduced that protons are added to the thiazine backbone when poly-(MG) or poly-(MB) is formed. There is evidence that poly-(MB), in particular, may be forming a link at a carbon or nitrogen that is not part of the thiazine backbone as well as at the carbon that is two atoms away from the sulfur. This is consistent with the conclusions from the XPS data as well.

Scanning electron microscopy (SEM)

SEM micrographs were taken from poly-(MG) deposited for 50 cycles on a GC plate. Figure 5-4 shows a representative micrograph of a poly-(MG) modified GC plate. This image shows evidence of the conformal character of the poly-(MG) film growth on the surface of the GC electrode. This observation coincides with the literature for two-dimensional supporting materials like platinum foil.[141]
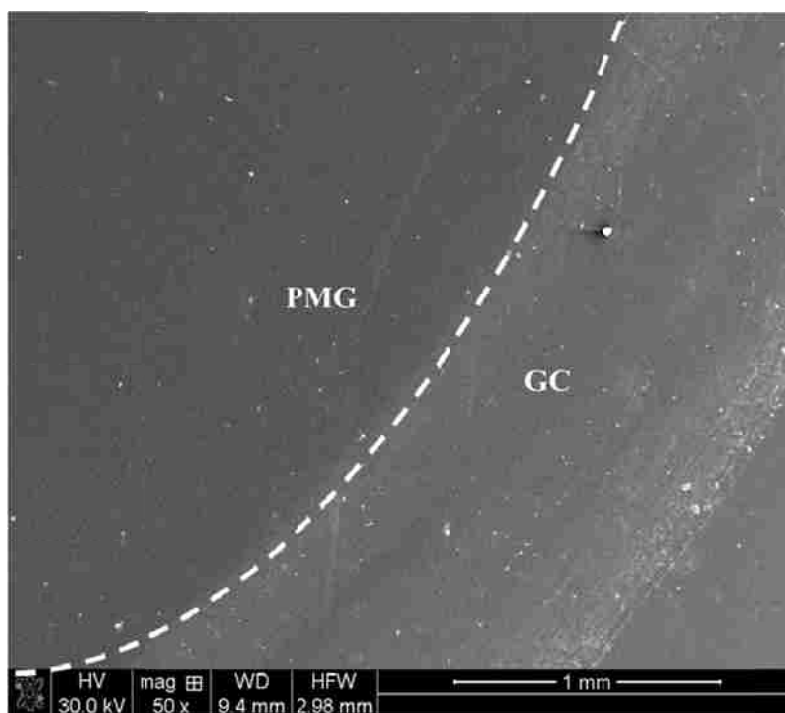
Figure 5-4 SEM micrograph of poly-(MG)-modified GC electrode

5.2.3. NADH oxidation electrocatalysis

One of the goals of this investigation is to demonstrate the role of poly-(MG) as an electrocatalyst for NADH oxidation. Poly-(MG$_{(ox)}$) reacts with NADH, subsequently regenerating poly-(MG$_{(red)}$) and active NAD$^+$. An electrochemical response of such process would be given by the following reaction:

$$\text{poly-(MG}_{(ox)}) + \text{NADH} \longrightarrow \text{poly-(MG}_{(red)}) + \text{NAD}^+ + \text{H}^+ + 2e^- \quad \text{(Eq. 5-1)}$$

In order to investigate the catalytic ability of the poly(MG) films with respect to NADH oxidation, a hydrodynamic voltammogram was obtained. This was done applying different potentials to a poly-(MG)-modified electrode at different NADH concentrations, and recording the steady-state current for each potential. The formal potential of MG in aqueous solution is found to be -0.07 V vs. SCE[58, 231] (-0.025 V vs. Ag/AgCl), whereas the formal potential for NADH oxidation is -0.56 V vs. SCE[47] (-0.515 V vs. Ag/AgCl). The potential range chosen was between -0.3 V and 0.35 V, since the poly-(MG) catalyst will ultimately determine the electrode operating potential. Figure 5-5 shows the curves for three different NADH concentrations in solution. These curves were obtained by plotting the steady-state currents versus the applied potentials. Concentration dependence is observed for applied potentials greater than 0 V vs. Ag/AgCl. This observation indicates that NADH oxidation may occur at potentials as low as 0 V vs. Ag/AgCl in the presence of poly-(MG) as the electrocatalyst. Even though an optimal biofuel cell anode will perform at a lower open circuit voltage, this result can be considered as a good step forward to decreasing the overpotential of NADH oxidation.
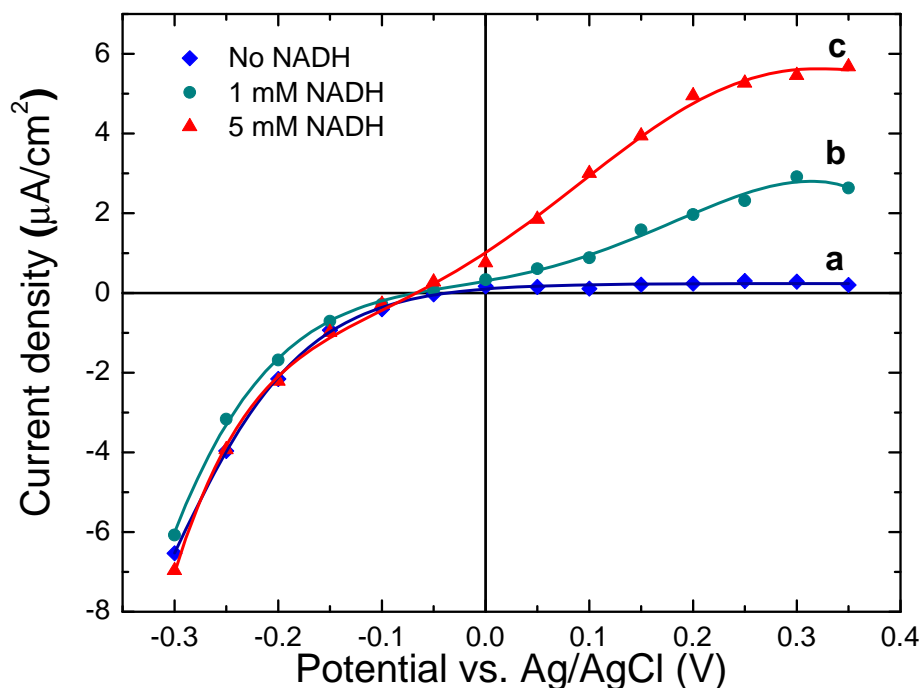
Figure 5-5 Hydrodynamic voltammogram of poly-(MG)-modified electrode: a) in absence of NADH, b) in 1 mM NADH and, c) in 5 mM NADH

Once the possible operating potential of the poly-(MG)-modified electrode was determined, the amperometric response was measured for NADH oxidation. Figure 5-6 is a representative curve that was obtained by performing consecutive additions of NADH in the presence of a poly-(MG)-modified GC electrode at an applied potential of 0.05 V vs. Ag/AgCl, showing the dependence of the current density with respect to the concentration of NADH. A maximum current of 3.13 $\mu A/cm^2$ is observed in this curve at a concentration of NADH of 12 mM, but the concentration dependence curve shows that higher current densities are possible by increasing the substrate concentration. For concentrations higher than 8 mM of NADH, deviation from linearity (dashed line, Fick's law) is observed, and a behavior that resembles Michaelis-Menten kinetics (pseudo-mono

molecular kinetics) is acquired with apparent maximum current of 7.1 ± 0.4 $\mu A/cm^2$.

Further discussion on this type of observation is presented in Chapter 6. These results are

valuable since they show how poly-(MG) can be a good candidate for NADH oxidation.
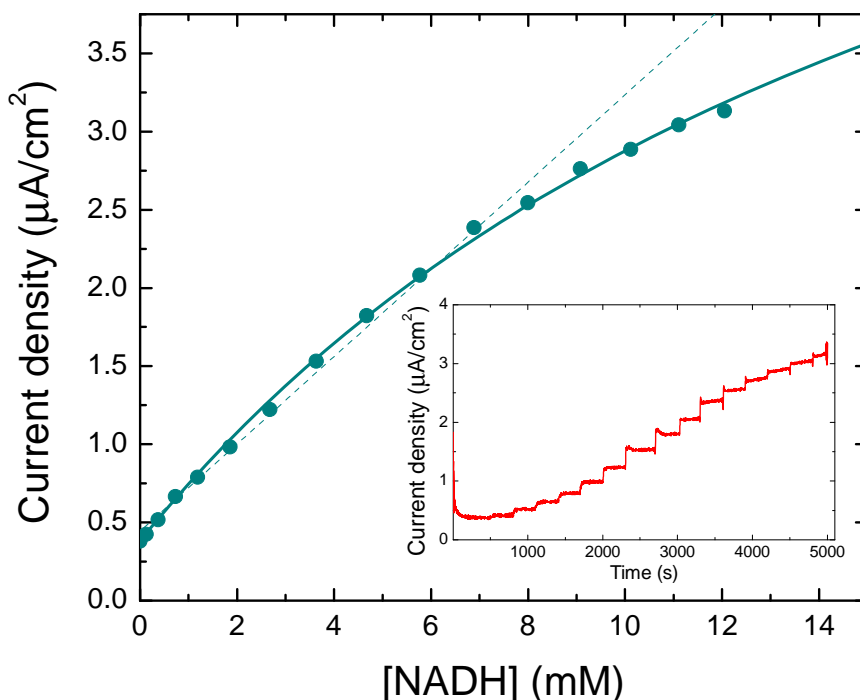
Figure 5-6 Amperometric current dependence with NADH additions in a poly-(MG) modified GC electrode at 0.05 V vs. Ag/AgCl. Inset: Chronoamperometric response

5.2.4. Enzyme catalyzed malate oxidation

In order to further demonstrate the catalytic effect of electropolymerized poly-(MG) films

towards NADH oxidation, NAD-dependent enzyme bioelectrocatalysis at a poly-(MG)

electrode was evaluated. Malate dehydrogenase (MDH) was chosen as a NAD-dependent

enzyme that is readily available and can be used without further purification. MDH plays

the role of catalyzing the oxidation of malate, while reducing NAD^+ to NADH. Figure

5-7 shows a schematic of the reaction cycle for malate oxidation in the presence of MDH at a poly-(MG)-modified carbon electrode.
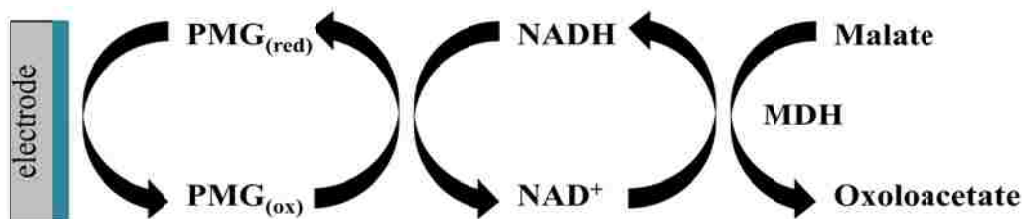
Figure 5-7 Reaction schematic for malate oxidation in the presence of MDH and poly-(MG)-modified electrode

Since the NADH/NAD$^+$ cofactor is not actually bound to the enzyme, it has to be added to the solution, so NAD$^+$ can diffuse to the enzyme and react and NADH can then diffuse to the electrode and be oxidized by poly-(MG). For this experiment, MDH was free in solution with its active cofactor NAD$^+$ and a poly-(MG)-modified GC electrode was employed for the amperometry. An amperometric curve was obtained by measuring the amperometric current response of the poly-(MG)/NAD$^+$/MDH system to consecutive additions of the substrate at an applied potential of 0.1 V vs. Ag/AgCl. A current density vs. concentration calibration curve was plotted and it showed typical Michaelis-Menten dependence that is expected from enzymatic catalysis (shown in Figure 5-8). The maximum current density was 1.55 ± 0.03 μA/cm^2 at substrate concentration as high as 700 mM. The apparent Michaelis-Menten behavior shows that the current density reaches a plateau where the current density acquires a relatively constant value. The apparent Michaelis-Menten constant was found to be $K_M^{app} = 60 \pm 4$ through an Eadie-Hofstee fit (inset in Figure 5-8). This fit also showed that a kinetic controlled regime is observed at low sensitivity (I/C) values whereas for

higher sensitivity values diffusion limitations start to occur.
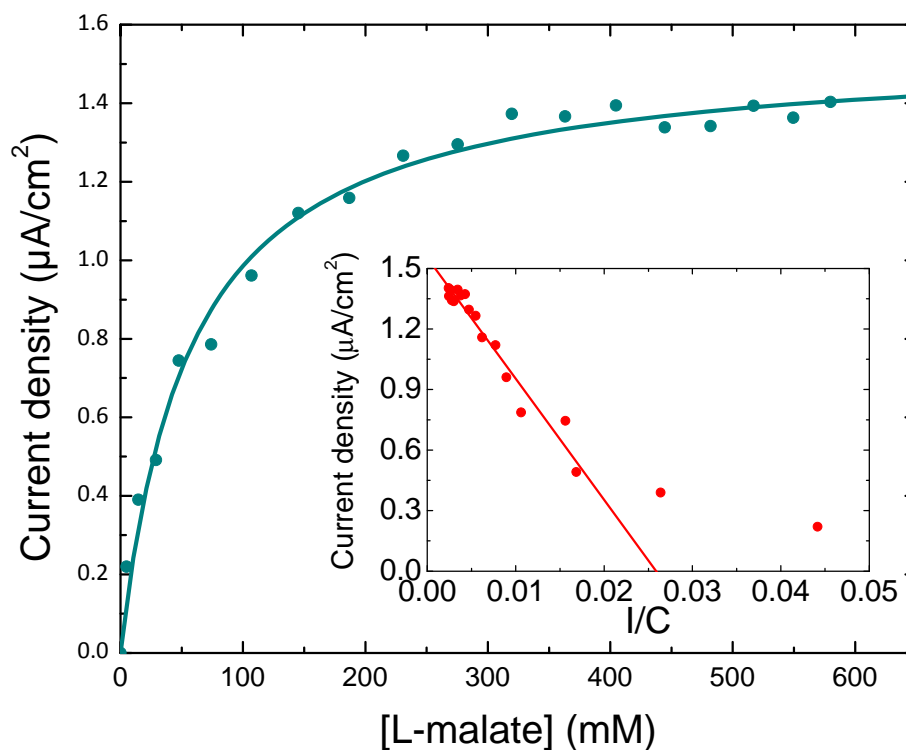
Figure 5-8 Michaelis-Menten behavior for amperometric response of poly-(MG)/NAD+/MDH system to consecutive additions of malate at 0.1 V vs. Ag/AgCl applied potential. Inset: Eadie-Hofstee fit

5.3. Conclusions

The presented characterization studies have shown that different mechanisms are involved in the electrochemical polymerization of azines. An oxidative step was observed during electropolymerization and also confirmed by a proton's removal shown in NMR and confirmed by XPS. A reductive step was also observed during electropolymerization and confirmed by proton's addition shown in XPS. HR-SEM gave us important information about the morphology of the polymer film grown on GC electrodes, creating a layer that is conformal to the underlying substrate. Furthermore, the electrocatalytic activity of poly-(MG) towards NADH oxidation was observed at potentials as low as 0.05

V vs. Ag/AgCl. Electrocatalytic activity studies in the presence of MDH elucidate how

poly-(MG) electrodes can be good electrocatalysts for future bioanode integration.

Chapter 6. Flow-Through 3-D Biofuel Cell Anode for NAD$^+$-Dependent Enzymes

In the previous chapter the work of structural and electrochemical characterization poly-(MG) polymers grown on glassy carbon electrodes was presented, demonstrating their ability to oxidize NADH at potentials as low as 0.05 V vs. Ag/AgCl.[232] Once a mediator for NADH oxidation has been chosen, one can move forward to targeting other design considerations for biofuel cell anodes based on NAD$^+$-dependent enzymes.

In order to build a biofuel cell that can achieve maximum power densities the electrode design needs to move from "flow-by" to "flow-through".[187] A key design point is the electrode material. It is necessary to choose an electrode material for the anode that can support mass transport of the fuels while providing a high surface area. Reticulated vitreous carbon (RVC) is a novel open-pore foam material with exceptionally high void volume and high surface area[233] that makes it a desired choice for flow-through electrodes. This material is based on vitreous carbon which is why its chemical properties can be expected to be the same and make it an attractive material for modification via electropolymerization of MG for NADH oxidation catalysis.

Furthermore, an immobilization technique for NAD$^+$-dependent enzymes is to be provided in order to obtain higher enzyme stabilities and increased lifetimes. Chitosan has been chosen due to its biocompatibility, versatility and ability to form three-dimensional porous scaffolds that support mass transport while enhancing the enzyme stability. This chapter describes how the best immobilization conditions were chosen for the enzyme studied, as well as a scaling up of the 2-D electrodes to 3-D structures.

6.1. Experimental

Methylene green (Fluka Cat. 66870), L-(-)-malic acid (Sigma Cat. M1000), NADH (Sigma Cat. N6005), NAD$^+$ (Fluka Cat. 43407), alcohol dehydrogenase (ADH) from *Saccharomyce cerevisiae* (Sigma Cat. A3263, 347 un/mg), ethanol (200 proof, VWR Cat. 89125172), chitosan (CHIT) (medium molecular weight, Aldrich Cat. 448877), multi-walled carbon nanotubes (MWCNTs) (20-30 nm outer diameter, 10-30 μm length, 95 wt% purity from www.cheaptubesinc.com) and concentrated acetic acid (EMD Chemicals Cat. EMAX0073P5) were used without further purification. All other chemicals were of reagent grade. Malate dehydrogenase (MDH) from porcine heart (USB products from Affymetrix Cat. 18665, 2580 un/mg) was purified by dialysis (Slide-A-Lyzer MINI dialysis units and concentrating solution from Thermo scientific) with TRIS buffer pH 7.03 in three steps (30 minutes, 1 hour and 30 minutes) against 500 mL of buffer. The final MDH stock solution contained 1 mg MDH/10 μL TRIS buffer. Chitosan was pretreated before use to achieve a final deacetylation degree of 95% by autoclaving for 20 minutes at 121°C in 40 wt% NaOH solution, filtrated, washed with DI water and pH 8.0 phosphate buffer and dried in a vacuum oven at 50°C for 24 hours.[234] A 1 wt% CHIT stock solution was prepared in 0.25 M acetic acid and its pH was then adjusted to 5.8 with concentrated NaOH and stored at room temperature with stirring. A MWCNTs/CHIT solution was prepared from this stock solution with a final concentration of 2.5 wt% of MWCNTs. NADH and NAD$^+$ stock solutions were prepared with phosphate buffer, pH 7.01. L-malic acid was prepared with distilled water and its pH was adjusted to 7.4 with concentrated NaOH. Electrochemical measurements were carried out in standard three-electrode electrochemical cell containing platinum wire as

the counter electrode, Ag/AgCl/3 M KCl reference electrode (CH Instruments Inc.) for the two-dimensional working electrodes. A stackable flow through electrochemical cell with platinum mesh (100 mesh, Alfa Aesar Cat. 10282) as the counter electrode and the same reference electrode as the previous cell was used for three-dimensional working electrodes. The schematic if this apparatus is shown on Figure 6-1 and Figure 6-2. All potential values are given against Ag/AgCl. Glassy carbon (GC) rods (CH Instruments Inc., 3 mm diameter) are referred to as "2-D working electrode" and reticulated vitreous carbon (RVC) (Electroanalytica, 60 ppi) is referred to as "3-D working electrodes". Prior to use the GC electrode was polished with alumina (Alumina slurry from Electron Microscopy Sciences, 1, 0.5 and 0.03 µm) to a mirror finish. RVC electrodes were pretreated with oxygen plasma cleaning for 15 seconds for hydrophilization of their surfaces. Quanta 3-D FEG Scanning Electron Microscope was used for imaging.
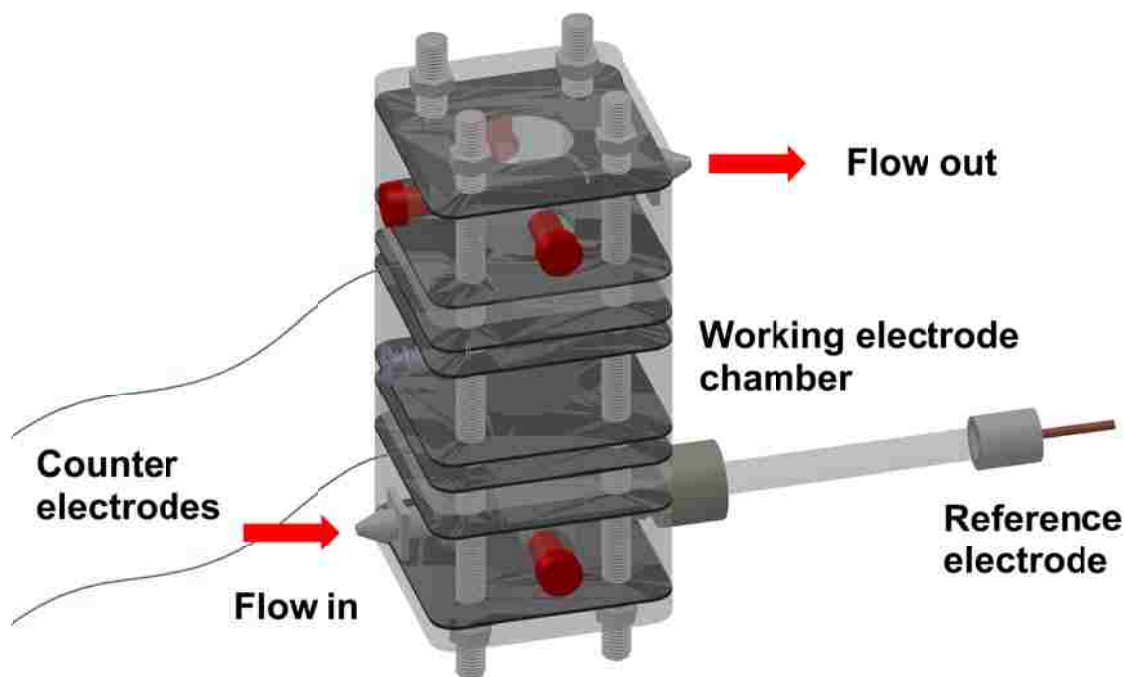
Figure 6-1 Schematic of stackable cell with 3-D RVC working electrode
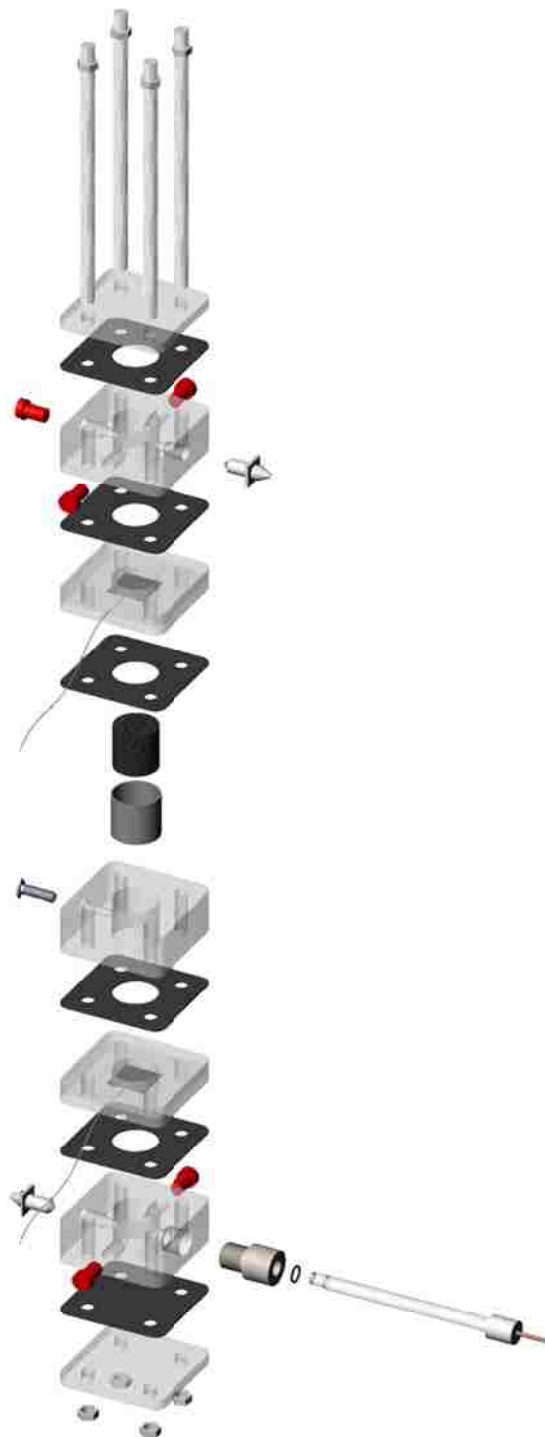
Figure 6-2 Exploded 3-D drawing of the modular stack cell for flow through operation with RVC working electrode

6.1.1. *Poly-(methylene green) electrode preparation*

Poly-(MG) catalyst was deposited on GC and RVC electrodes electrochemically by cyclic voltammetry according to a standard procedure previously reported.[124, 232] The electropolymerization of MG was carried out by cyclic voltammetry under a scan rate of 50 mV/s in a potential range from -0.5 V to 1.3 V vs. Ag/AgCl. The monomer concentration in the growing-solution was 0.5 mM in the presence of 0.1 M KNO$_3$ in 50 mM phosphate buffer pH 7.01. Poly-(MG) was deposited under an oxygen-depleted environment. Electropolymerization was carried out for 10, 25, 50 and 200 cycles on the RVC for SEM imaging in order to determine a deposition mechanism. Deposition of 10 cycles was used for all of the catalytic experiments. The electrochemical instrument used for all the electrochemical analysis (electrodeposition and chronoamperometric curves) was Gamry Reference 600 Pontentiostat/Galvanostat/ZRA.

6.1.2. *Enzyme immobilization*

Chitosan polymeric scaffolds were used for immobilizing malate dehydrogenase by entrapment. Both chitosan and CNTs-chitosan scaffolds were prepared according to procedures presented by Cooney et al. [143, 144, 212, 215] For GC electrodes, 25 μL droplets of Chit/(CNTs)/NAD$^+$/MDH (10 μL chitosan: 0.35 mg NAD$^+$: 1 μL MDH) were cast and frozen at -4°C overnight. This was followed by freeze-drying for 1 hour in order to remove water from the scaffolds. For RVC electrodes, 500 μL of Chit/CNTs/NAD$^+$/MDH (same ratio as GC electrodes) were added to the electrode and frozen at -4°C overnight. Freeze-drying was performed for 4 hours in order to eliminate water from the scaffold. The amount of ADH immobilized in GC and RVC electrodes

was calculated based on the enzyme's activity in order to obtain comparable results to those of MDH.

6.1.3. NADH oxidation

Poly-(MG) modified electrodes were tested with respect to NADH oxidation. Amperometric curves were obtained at 0.05 V vs. Ag/AgCl by consecutive additions of the substrate (25 mM NADH stock). A calibration curve was consecutively obtained from the steady-state current data.

6.1.4. L-malate oxidation in the presence of MDH

Poly-(MG)-modified electrodes with immobilized MDH were tested towards L-malate oxidation (pH 7.01 for GC electrodes, pH 6.3 for RVC electrode) in the presence of excess (5 mg/mL) NAD$^+$ cofactor. L-Malic acid (substrate of MDH) amounts were added every 300 seconds (1 M stock) in order to obtain an amperometric curve to show the catalytic activity of the enzyme. The applied potential was 0.05 mV vs. Ag/AgCl for every electrode. A calibration curve was consecutively obtained from the steady-state current data. In the case of RVC electrodes in the flow through cell, the buffer solution was pumped through the peristaltic pump at a speed of 3 mL/min. Similar experiments were performed with ADH for ethanol oxidation.

6.1.5. MDH bioanode polarization curves

Galvanostatic and potentiostatic polarization curves were obtained for the 3-D RVC electrode with immobilized MDH while flowing 500 mM L-malate at a speed of 3 mL/min. A pH 6.3 PBS buffer was used for all experiments since it has been shown to be the optimal pH for both MDH based bioanode and laccase based biocathodes, which are later integrated in a biofuel cell (Chapter 7).

6.2.   Results and discussion

6.2.1.   L-malate oxidation on 2-D poly-(MG)-modified electrodes

Electrochemical characterization of three 2-D GC electrodes was performed. Table 6-1 shows how each electrode was prepared. GCA was modified with poly-(MG) and MDH was immobilized into a chitosan scaffold. GCB and GCC both had immobilized MDH in a MWCNTs/CHIT scaffold, but only GCC had been pre-modified with a poly-(MG) film. GCB did not contain the electrocatalyst for NADH oxidation in order to determine if MWCNTs play a role in NADH oxidation. The NAD$^+$ cofactor was added in excess in order to ensure that the losses of cofactor to the bulk are minimized, and to optimize the electrochemical conversion of NAD$^+$ at the interface of the electrode.

The three electrodes were tested by chronoamperometry at an applied potential of 0.05 V vs. Ag/AgCl in order to determine the enzyme's activity towards L-malate oxidation. All of the steady-state current measurements were normalized with respect to the enzyme loading (Figure 6-3). By comparing electrode GCA to GCB and GCC, we can observe that the enzyme immobilized onto the unmodified GC electrode shows very little activity towards L-malate oxidation in comparison with the GC electrodes that were modified with poly-(MG). This observation is a clear indication of the catalytic effect for NADH oxidation of poly-(MG) electrocatalysts and demonstrates their utility when integrated with NAD$^+$-dependent enzymes. The immobilized enzyme on the poly-(MG)-modified electrodes always showed higher current responses than the enzyme free in solution (data not shown). This was to be expected since the immobilization method provides the enzyme stability and closeness to the electrode surface and therefore to the catalyst for NADH re-oxidation.
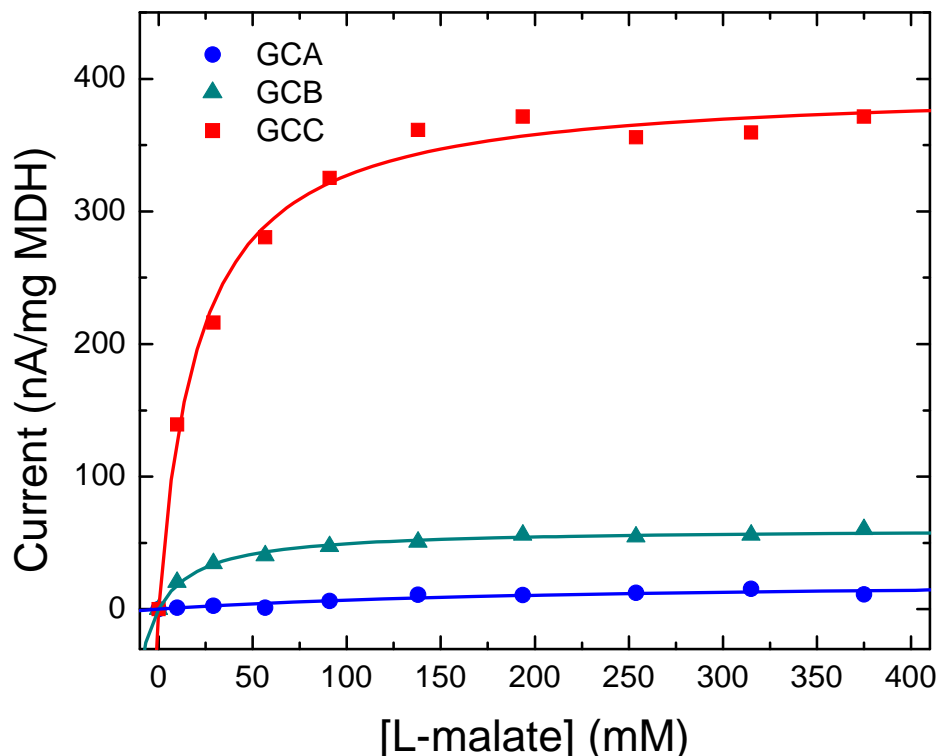
Figure 6-3 Michaelis-Menten kinetics for MDH on electrodes GCA-C. Applied potential: 0.05 V vs. Ag/AgCl

The small activity observed at GCA can be attributed to the presence of MWCNTs in the immobilization matrix and it could suggest that there is some catalytic effect of the MWCNTs towards NADH oxidation as it has been previously reported in the literature.[61] Such effect might be caused by some metal traces that are usually present in MWCNTs (iron and nickel) and can be observed by energy dispersive X-ray spectroscopy (EDS) when imaging MWCNTs. Furthermore, if we compare electrodes GCB and GCC, we can also observe that immobilization in MWCNTs/CHIT scaffold resulted in a much higher current response. The addition of MWCNTs into the chitosan scaffold results in an increased micro-porosity (pores in the range of 100-200 μm) of the immobilization

matrix, and thus increased overall electrochemical accessible surface area. In comparison with the chitosan scaffold which contains larger macro-pores and higher void volume, the MWCNTs/CHIT scaffold allows for higher residence times of NAD$^+$ cofactor resulting in higher conversion of the enzyme's substrate.

Apparent Michaelis-Menten constants (K_M^{app}) were estimated for the three electrodes and also summarized on Table 6-1.. It is important to notice that they are apparent because they account for all of the reactions occurring in the system (oxidation of NADH, reduction of NAD$^+$ and oxidation of enzyme's substrate). The three electrodes showed the typical Michaelis-Menten kinetics behavior which is to be expected for enzymatic electrodes. Electrodes GCB and GCC showed very similar K_M^{app} values (23 ± 3 and 21 ± 2 mM, respectively) and GCC showed a K_M^{app} that was much higher (200 ± 100). This can be explained by the fact that there is because of the absence of poly-(MG) on electrode GCB, there is no oxidation of NADH. By missing this essential step in the sequence of reactions, the enzymatic oxidation of the substrate is not favored, which is consequently reflected in the value of K_M^{app}. Figure 6-3 and i_{max} (Table 6-1) show clearly a 6.5-fold current increase by incorporating the same amount of enzyme into a conductive MWCNTs embedded scaffold design (electrode GCC) compared to a non-conductive scaffold design (electrode GCB). These results helped us understand which immobilization technique proves to be more effective for the enzyme studied to further transfer the system to a three-dimensional bioanode design. The following sections discuss such a design.

6.2.2. Electropolymerization of poly-(MG) on 3-D electrodes

Poly-(MG) was successfully deposited on RVC three-dimensional electrodes by the standard protocol previously described. Due to the hydrophobic nature of the electrode material, it was necessary to pre-treat it with oxygen plasma cleaning. This material was chosen because of its technological advantages including open pore structure that provide a high surface area to volume ration, high conductivities and low resistance to flow that allow for the mass transport of the fuels.

Poly-(MG) was deposited while varying the number of deposition cycles in order to determine the mechanism of growth of the polymer. Figure 6-4 shows a representative voltammogram of the poly-(MG) deposition on a piece of RVC for 10 cycles at a scan rate of 50 mV/s performed in a flow through system.
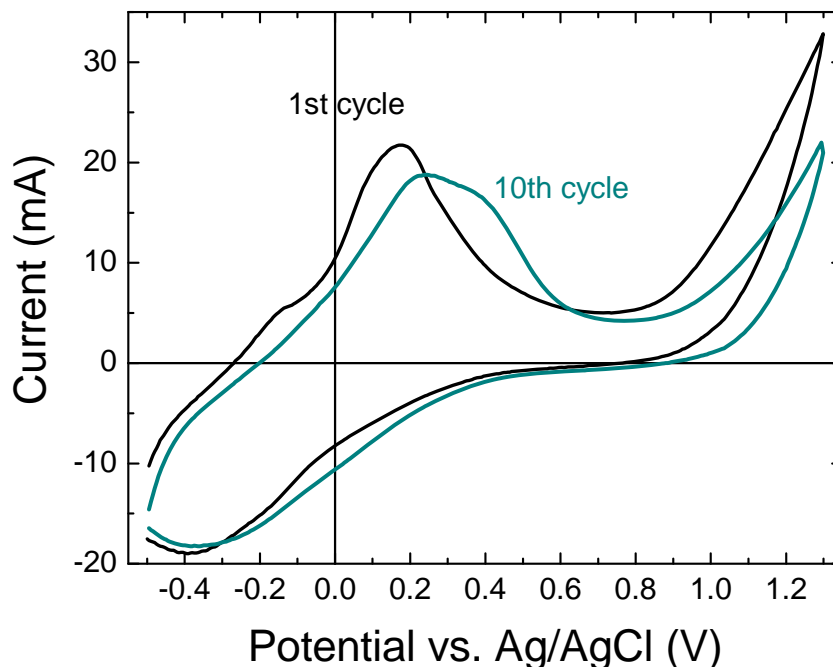
Figure 6-4 Poly-(MG) deposition on RVC 60 ppi, 10 cycles, 50 mV/s

All samples were later characterized by SEM. Figure 6-5(a-d) shows the micrographs that were taken from the four different poly-(MG)-modified RVC samples. The first thing we observed when analyzing these samples is the fact that poly-(MG) was deposited on the RVC materials in the form of particles instead of a film as we had previously observed for the case of planar GC. This particulate formation can be attributed to both the surface tension intrinsic to the highly porous RVC material and its inertness. This observation is in agreement with previous reports found in the literature describing discontinuous deposition of metallic particles.[233]
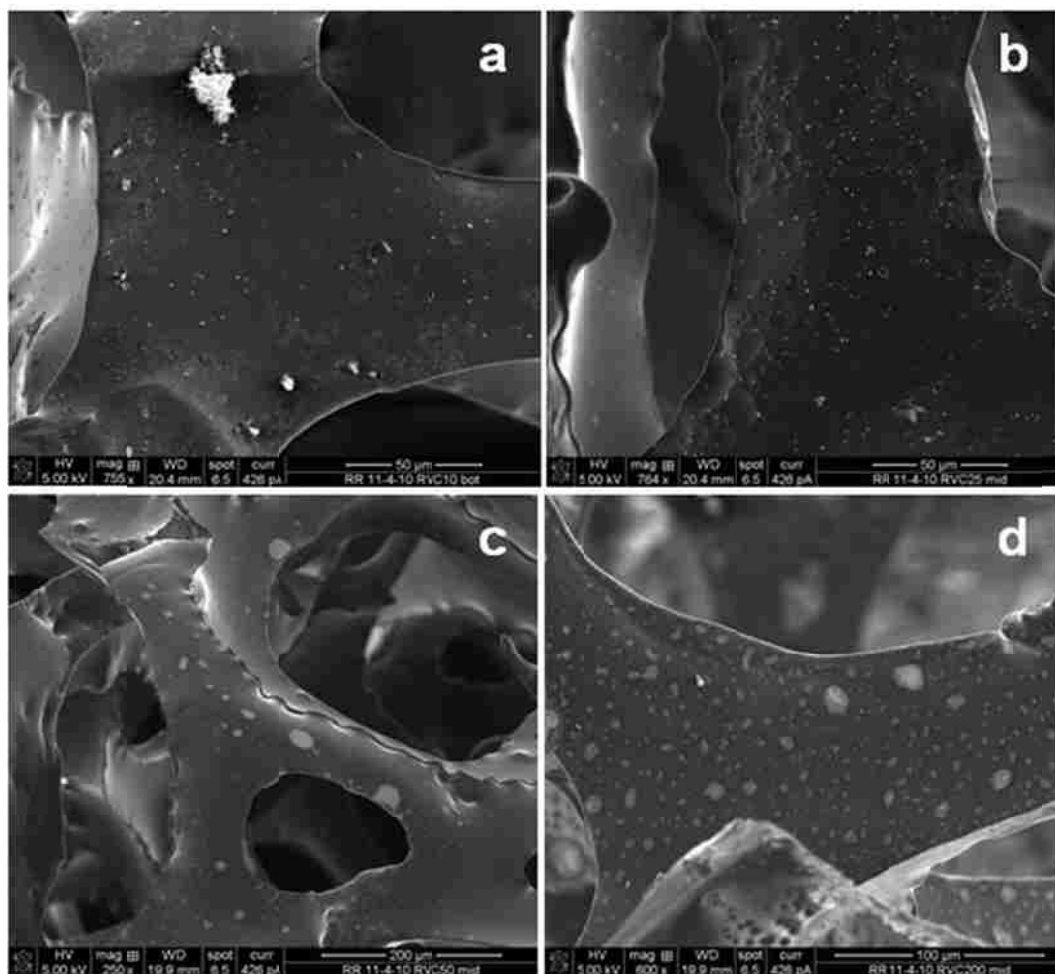
Figure 6-5 SEM micrographs of poly-(MG)-modified RVC by various deposition cycles: a) 10 cycles, b) 25 cycles, c) 50 cycles, d) 200 cycles

With the micrographs we were also able to observe that for higher deposition cycles (higher deposition times), the amount and size of particles was increased. It is also evident that the particle size distribution becomes less uniform with higher deposition times. This is typical of a progressive nucleation mechanism,[235] in which the particles are deposited progressively in time resulting in a broad size distribution of the particles. This observation of the nucleation mechanism is consistent with our past results of electrodeposition of metal particles on RVC materials.[236]

6.2.3. *NADH oxidation by poly-(MG)-modified 3-D electrodes*

After studying the morphology of the poly-(MG)-modified RVC electrodes, we were interested in studying their electrochemical performance as electrocatalysts for NADH oxidation. It was expected that the electrodes would oxidize NADH due to their similarity to GC electrodes. Chronoamperometric measurements were performed on each electrode in order to evaluate their performance as electrocatalysts. The current response to NADH additions of each electrode was recorded at steady-state conditions.

Figure 6-6 shows the steady-state current response dependence with the concentration of NADH for each electrode. In every case we obtained a non-linear dependence that resembles a Michaelis-Menten type of kinetics. This observation is in agreement with the model proposed by Gorton et al. [55] for mediator-modified electrodes for NADH oxidation and that have also been reported elsewhere.[36, 57, 237] From this data we can also observe the decrease in catalytic activity of poly-(MG) with increase of the thickness of the polymer given by the number of deposition cycles. Similar observations have been widely reported in the literature for other NADH mediators.[9, 36, 41, 44, 45] This fact has been attributed to the low partition coefficient of NADH and the diffusion coefficient of

NADH within the polymer.[36] Despite this behavior of the polymer catalyst, this experimental observation helps us build an electrode with a layer of polymer particles thin enough to reach their best electrocatalytic activity towards NADH oxidation. The electrode modified by 10 CVs showed the highest i_{max} (1700 ± 200 µA), at least double the amount of current of the electrode prepared by 200 deposition cycles, and was therefore chosen for the bioanode design.
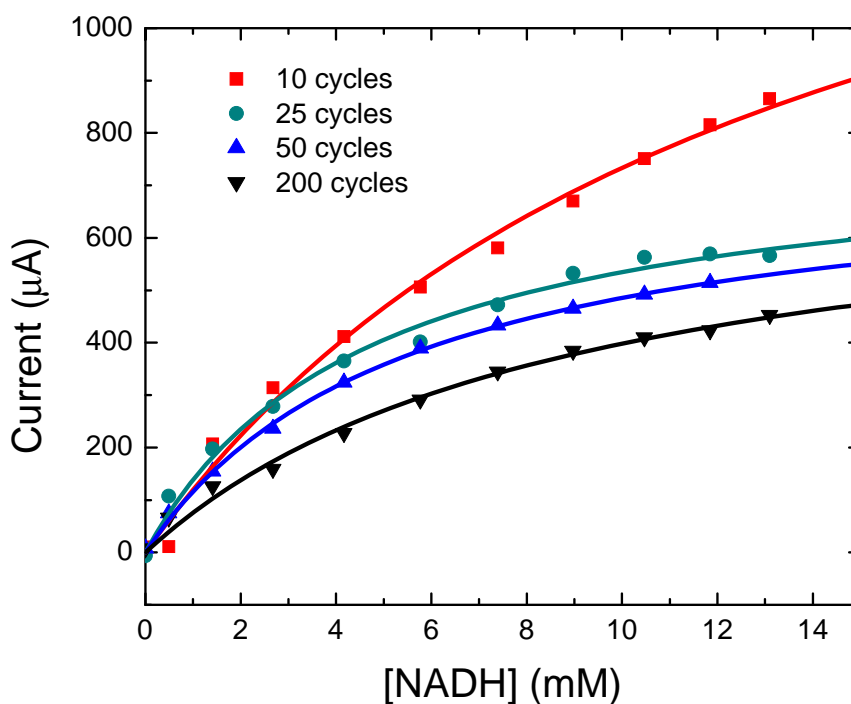
Figure 6-6 Amperometric response to consecutive additions of NADH to poly-(MG)-modified RVC

6.2.4. *L-malate oxidation on 3-D poly-(MG)-modified electrode*

Once the appropriate design conditions were determined for the MDH-based anode, it was build and tested in a flow-through system. The first parameter was the deposition cycle which was determined to be 10 cycles for higher current responses as previously

discussed. The second parameter was the immobilization technique for MDH. The technique used was freeze-dried MWCNTs/CHIT scaffold which had yielded a higher current response due to increased enzyme loading and conductivity.

Figure 6-7 shows the comparison of the 3-D poly-(MG)-modified RVC electrode and the 2-D poly-(MG)-modified GC electrode, both with the same immobilization technique for MDH (

Figure 6-7a) and ADH (

Figure 6-7b). This figure shows an apparent Michaelis-Menten behavior that can be observed for both systems.
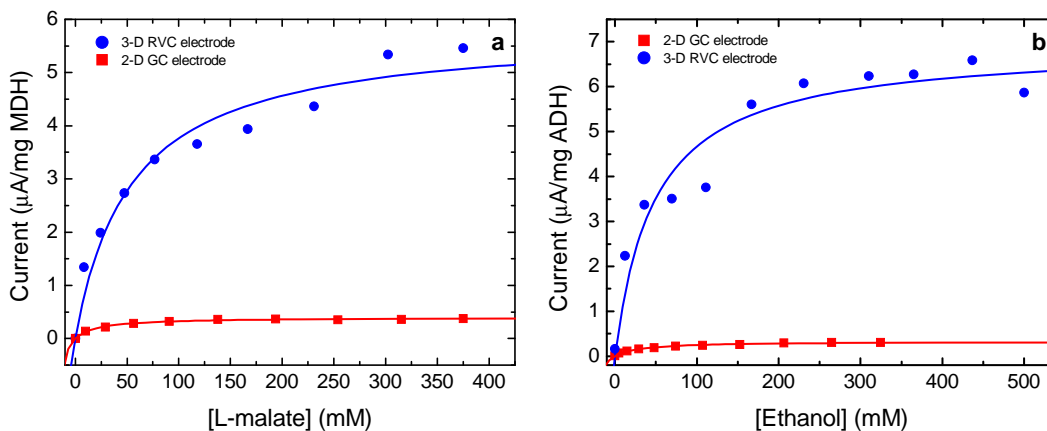
Figure 6-7 Michaelis-Menten kinetics on 2-D and 3-D poly-(MG)-modified electrodes for: a) MDH and b) ADH

It can be observed that higher current densities per amount of enzyme immobilized can be achieved in a 3-D system for both enzymes. This increase in current density (15-fold for MDH, 21-fold for ADH) coincides with the earlier observed current amplification (Figure 6-3) due to introduced three-dimensionality on GC electrodes.

Furthermore this identical kinetic behavior on both carbonaceous materials (GC and RVC) confirms similar depositing and catalysis mechanism of poly-(MG). Flow-through operation of the system also allows for higher residence times resulting in higher oxidation of the substrate. Table 6-1 also summarizes the kinetic parameters obtained for the 3-D MDH and ADH electrodes.

It is important to consider that the large volume and surface area of RVC can actually accommodate higher amounts of enzymes than the amount used in these experiments and this would significantly increase the performance of the 3-D bioanode for biofuel cells.

Table 6-1 Summary of Michaelis-Menten parameters obtained electrochemically for GC and RVC electrodes

Electrode	Preparation	K_M^{app} (mM)	i_{max} (μA/mg enzyme)
GCA	Unmodified GC with MDH immobilized in a MWCNTs/CHIT scaffold	200 ± 100	0.022 ± 0.007
GCB	Poly-(MG)-modified GC with MDH immobilized in a CHIT scaffold	23 ± 3	0.061 ± 0.001
GCC	Poly-(MG)-modified GC with MDH immobilized in a MWCNTs/CHIT scaffold	21 ± 2	0.395 ± 0.008
RVCA	Poly-(MG)-modified RVC with MDH immobilized in a MWCNTs/CHIT scaffold	50 ± 10	5.8 ± 0.4
GCD	Poly-(MG)-modified GC with ADH immobilized in a MWCNTs/CHIT scaffold	32 ± 4	0.33 ± 0.01
RVCB	Poly-(MG)-modified RVC with ADH	50 ± 10	6.9 ± 0.4

immobilized in a MWCNTs/CHIT scaffold

6.2.5. *Polarization curves of MDH 3-D bioanode*

After studying the kinetics of MDH immobilized in MWCNTs/CHIT scaffold in 3-D poly-(MG)-modified RVC electrode and demonstrating that it is catalytically active oxidizing L-malate, we constructed polarization curves. Figure 6-8 shows the polarization curves obtained under controlled-current and controlled-potential conditions.
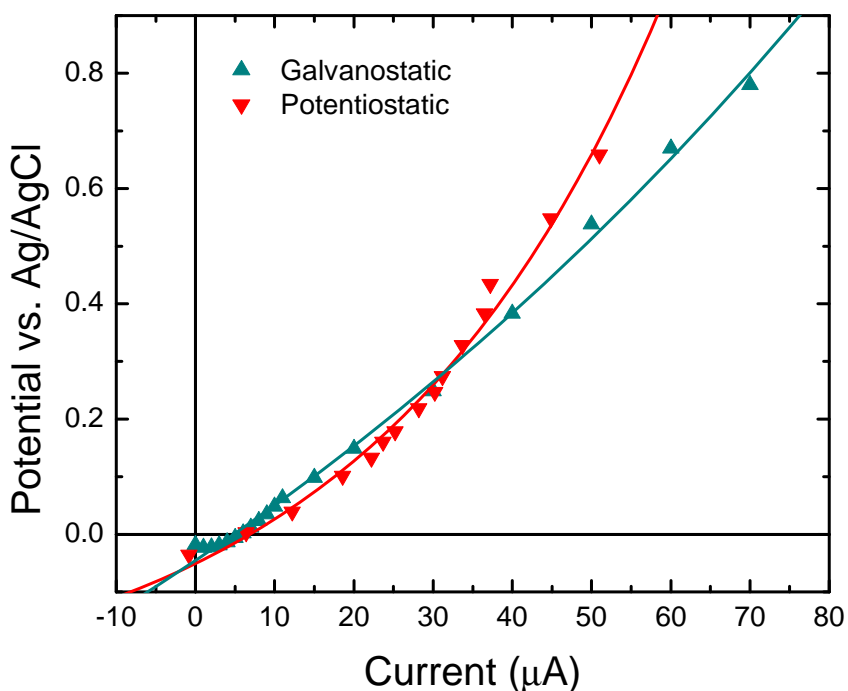
Figure 6-8 Polarization curves measured in galvanostatic and potentiostatic mode of MDH 3-D bioanode in flow through cell

The open circuit potential (OCP) for this bioanode was of -35 mV vs. Ag/AgCl, with limiting currents near 70 μA. This result is promising for the construction of a fully enzymatic biofuel cell.

6.3. Conclusions

This work has approached different design considerations for building a 3-D bioanode for NAD⁺-dependent enzymes. The electropolymerization of MG was achieved for the first time onto the surface of porous RVC. The resulting poly-(MG) was deposited in the form of particles due to low wetting (hydrophobicity) of the electrode surface. The mechanism of growth of these catalyst particles was determined to be progressive via visual observation by SEM. This study also elucidated that low number of deposition cycles (i.e. 10 cycles) for poly-(MG) deposition results in higher catalytic activity for NADH oxidation, at low potentials (50 mV vs. Ag/AgCl). MWCNT/s/CHIT suspension was found to be the best immobilization technique compared to CHIT for MDH, due to the conductivity and higher surface area introduced by the use of MWCNTs. The 3-D RVC electrode modified with poly-(MG) and integrated with the immobilized MDH was tested in a flow-through 3-D modular stack cell and yielded the highest current densities per amount of immobilized MDH. The construction of the polarization curve for the 3-D bioanode based on MDH allowed us to demonstrate its potential capabilities for integration into a fully enzymatic biofuel cell, starting at operating open circuit potential of -35 mV vs. Ag/AgCl and with limiting currents near 70 μA.

Chapter 7. Fully Enzymatic Flow-Through Biofuel Cell

This chapter covers the construction and evaluation of two fully enzymatic biofuel cells based on the previously studied NAD^+-dependent enzymes (MDH and ADH). In order to create a membrane-free biofuel cell, both the anode and cathode must operate with the same electrolyte and thus at the same pH. So far, we have only studied the behavior of the anodic enzymes at neutral pH values, but in order to integrate the anode with the cathode a compromise has to be made regarding the optimal operating conditions for both electrodes.

Typically, multi-copper oxidases enzymes like laccase are very active at acidic pH values lower than 5 (pH 4.5 for laccase from *Trametes versicolor*) and NAD^+-dependent enzymes are active at slightly basic or close to neutral pH values (pH 7.4 for MDH and pH 8.8 for ADH). Our research group has developed immobilization techniques for laccase from *Trametes versicolor* that allow for the enzyme to be active at pH values as high as 6.3. Therefore it has been necessary to explore the performance of poly-(MG) catalysts as well as NAD^+-dependent MDH and ADH at such pH values.

This chapter starts with pH studies that were performed with poly-(MG) and NAD^+-dependent enzymes in order to determine the optimal operating conditions for the enzymatic biofuel cell in terms of supporting electrolyte. In addition, it describes the assembly of two flow-through fully enzymatic biofuel cell models and presents their evaluation and performances.

7.1. Experimental

Methylene green (Fluka Cat. 66870), L-(-)-malic acid (Sigma Cat. M1000), NADH (Sigma Cat. N6005), NAD$^+$ (Fluka Cat. 43407), alcohol dehydrogenase (ADH) from *Saccharomyce cerevisiae* (Sigma Cat. A3263, 347 un/mg), laccase from *Trametes versicolor* (Sigma Cat. 53739, 25.5 un/mg), chitosan (CHIT) (medium molecular weight, Aldrich Cat. 448877), ethanol (200 proof, VWR Cat. 89125172), multi-walled carbon nanotubes (MWCNTs) (20-30 nm outer diameter, 10-30 μm length, 95 wt% purity from www.cheaptubesinc.com), dimethyl sulfoxide (DMSO, Sigma), 1-Pyrenebutyric acid N-hydroxysuccinimide ester (PBSE 95%, Sigma-Aldrich Cat. 457078), carbon black (XC72R, Cabot), and concentrated acetic acid (EMD Chemicals Cat. EMAX0073P5) were used without further purification. All other chemicals were of reagent grade. Malate dehydrogenase (MDH) from porcine heart (USB products from Affymetrix Cat. 18665, 2580 un/mg) was purified by dialysis (Slide-A-Lyzer MINI dialysis units and concentrating solution from Thermo scientific) with TRIS buffer pH 7.03 in three steps (30 minutes, 1 hour and 30 minutes) against 500 mL of buffer. The final MDH stock solution contained 1 mg MDH/10 μL TRIS buffer. Chitosan was pretreated before use to achieve a final deacetylation degree of 95% by autoclaving for 20 minutes at 121°C in 40 wt% NaOH solution, filtrated, washed with DI water and phosphate buffer pH 8.0 and dried in a vacuum oven at 50 °C for 24 hours.[234] A MWCNTs/CHIT solution was prepared with 1 wt% CHIT 0.25 M acetic acid stock solution to a final concentration of 2.5 wt% of MWCNTs. Citrate, acetate, phosphate and TRIS buffers were prepared by following standard protocols at different pH values. NADH stock solutions were prepared with each buffer. L-malic acid was prepared with distilled water and its pH was adjusted

to 7.4 with concentrated NaOH. Electrochemical measurements were carried out in a stackable flow through electrochemical cell with platinum mesh (100 mesh, Alfa Aesar Cat. 10282) as the counter electrode and Ag/AgCl/sat KCl reference electrode (CH Instruments Inc.) when working in the three-electrode setup. For the fuel cell experiments (two-electrode setup) the cathode was connected to the potentiostat as the working electrode and the anode was connected as the counter and reference electrodes. All potential values are reported against Ag/AgCl. RVC 60 ppi was used for the anode supporting material and it was pretreated with oxygen plasma cleaning for 15 seconds for hydrophilization of their surfaces.

7.1.1. pH dependence of NADH oxidation reaction studies

GC electrodes were modified by electropolymerization of MG as described in previous chapters. Cyclic voltammetry in 1 mM NADH in eleven different buffer solutions were performed for three cycles between -0.5 and 0.5 V vs. Ag/AgCl. The pH values studied ranged between 3.00 and 8.98. After recording the CV, the half-wave potentials were determined.

7.1.2. MDH pH dependence studies

MDH was immobilized on poly-(MG)-modified electrodes in a MWCNTs/CHIT scaffold as described on Chapter 6. Two PBS buffers (pH 5.8 and pH 6.98) were used as supporting electrolyte for chronoamperometric measurements with consecutive additions of L-malate. The steady-state currents were plotted against the concentration of substrate.

7.1.3. Anode design

Two enzymatic anodes were built for these experiments. The supporting material for both anodes was RVC 60 ppi modified with poly-(MG) as previously described by 10

deposition cycle ns. The immobilization technique for both enzymes (MDH and ADH) was freeze drying of MWCNTs/CHIT. For MDH anode the amount of enzyme 1 mg/100 µL chitosan and for ADH it was 3 mg/100 µL.

7.1.4. Cathode design

The gas-diffusion cathode consists of two layers, a gas diffusion and a catalytic layer. About 80 mg of carbon black XC72R with a teflon content of 35 wt% were placed into a round dye of about 2 cm diameter and pressed by hand onto a nickel mesh (Alfa Aesar Cat. 39704) that serves as current collector. About 10 mg of teflonized multi-walled carbon nanotubes (3.5 wt% PTFE) were evenly distributed on top the gas diffusion layer. Both layers were fused together by pressing for 1 minute at 1 klbs in a hydraulic press to a final thickness of 0.5 mm 4 mg PBSE (1-Pyrenebutyric acid N-hydroxysuccinimide ester) in 0.5 mL DMSO were allowed to soak into the catalytic layer for about 2 hours the electrode was rinsed with DMSO and water and 4mg/ml laccase in PBS (pH 6.3) were cross-linked at +4 °C over night. Figure 7-1 shows SEM micrographs of the gas diffusion cathode indicating its layers.
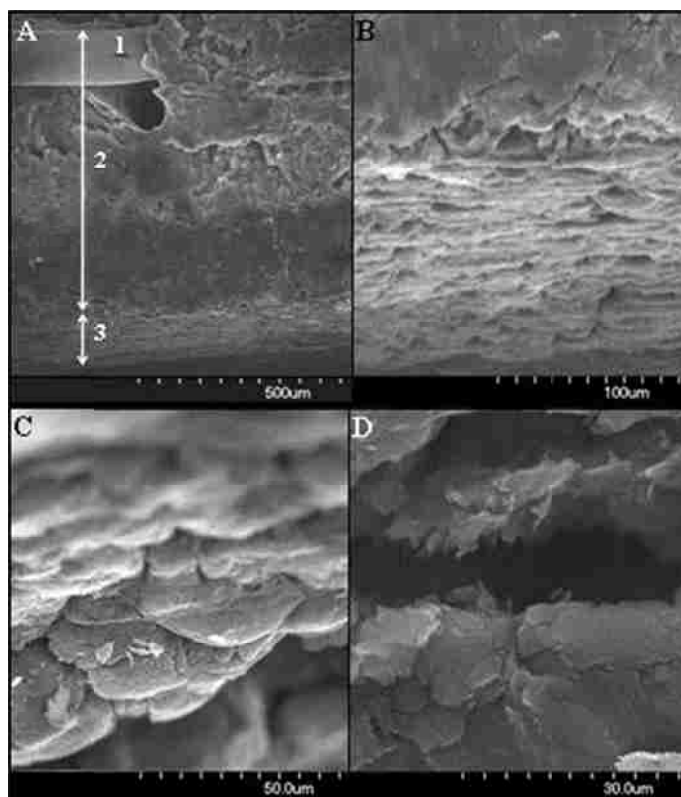
Figure 7-1 SEM images of different magnification of gas diffusion electrode. (A) shows a cross section of (2) gas diffusion and (3) MWCNT catalytic layer with (1) nickel mesh, gas diffusion layer was made of carbon black with 35wt% PTFE. Images B – D show higher magnification SEMs of MWCNT catalytic layer with 3.5wt% PTFE as binder. Images provided by Carolin Lau

7.1.5. *Enzymatic biofuel cell construction*

Figure 7-2 shows a photograph of the fuel cell assembly consisting of the laccase-cathode (lower plate), two counter electrodes (platinum mesh), the MDH-anode and a reference electrode. The cell was setup in this configuration so both anode and cathode could be studied separately and their individual polarization curves could be built before running the complete fuel cell. For the ADH-laccase fuel cell the fuel solution consisted of 475 mM ethanol and ~1.5 mM NAD^+, and for the MDH-laccase fuel cell the fuel solution contained 500 mM L-malate and ~1.5 mM NAD^+. Polarization curves were obtained in both potentiostatic (controlled potential) and galvanostatic (controlled current) regimes.
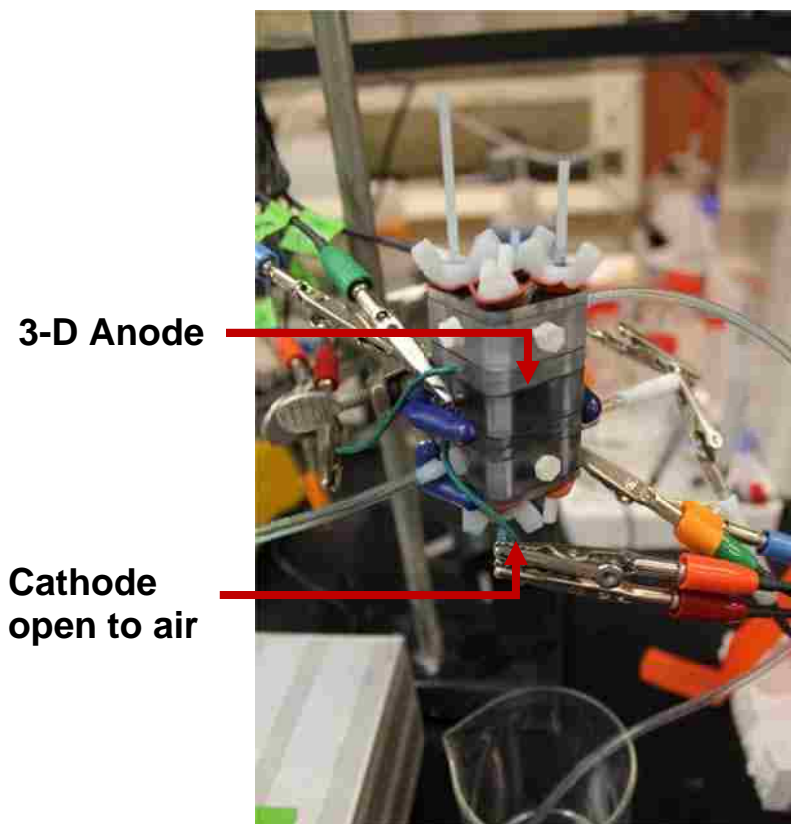
Figure 7-2 Photograph of flow-through enzymatic fuel cell with reference and counter electrodes for individual analysis of anode and cathode

7.2.   Results and discussion

7.2.1. pH dependence of NADH oxidation reaction

Several experiments of NADH oxidation in different buffer electrolytes were performed by cyclic voltammetry, and for every voltammogram obtained the half-wave potential of NADH oxidation was determined. This was made by finding the position of the inflection point (first derivative of current) corresponding to the highest peak. Figure 7-3a shows a representative of cyclic voltammograms of poly-(MG)-modified GC electrodes in the presence of 1 mM NADH indicating the position of their half-wave potentials for the oxidation reaction. It can be observed that for the voltammogram performed in higher pH

(pH = 8.20) electrolyte, the catalytic current is at least two times higher than that of the one performed in lower pH (pH = 3.00). Moreover, the half-wave potential is lower for the higher pH value. Figure 7-3b shows the linear dependence of the half-wave potential with increasing pH. In this graph it is seen that the half-wave potential value decreases with increasing pH value. Since the use of NADH oxidation catalysts attempts to lower the overpotentials for this reaction, higher pH values are more desirable than lower pH values. Furthermore, phosphate buffer presented the most stable and reproducible behavior in comparison with the other buffers, particularly TRIS buffer which would also be desirable for high pH values.
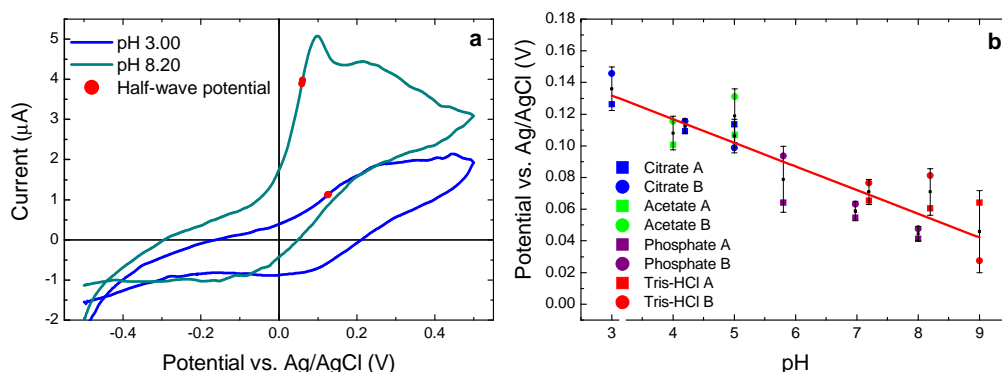
Figure 7-3 a) Cyclic voltammograms of poly-(MG)-modified GC electrodes in 1 mM NADH at different pH values, b) half-wave potential dependence with pH for NADH oxidation. A and B denote repetitions of each experiment

7.2.2. MDH behavior at different pH electrolytes

Phosphate buffer has been the electrolyte of choice through all the work presented, and the experiments presented in the previous section that it has definitely been an appropriate choice. In order to combine the bioanode and biocathode, it was necessary to

determine whether the studied anodic enzymes will work at the cathode conditions. Thus, the kinetics of immobilized MDH was studied in two different buffers: pH 6.98 PBS since all of the previous data was obtained in that buffer, and pH 5.8 PBS since the laccase for the cathode has usually been studied in that buffer at UNM. Figure 7-4 shows the Michaelis-Menten data obtained from chronoamperometric experiments demonstrating that MDH follows the expected enzyme kinetic behavior even at a pH lower than its optimal pH. The Michaelis-Menten constant obtained at lower pH conditions was higher ($K_M^{app} = 49 \pm 3$ mM) compared to the one obtained at neutral pH ($K_M^{app} = 20 \pm 2$ mM) which shows better reaction kinetics at neutral pH. However, the fact that the enzyme is still active at slightly acidic pH is very encouraging for integration in a membrane-free biofuel cell with a laccase cathode.
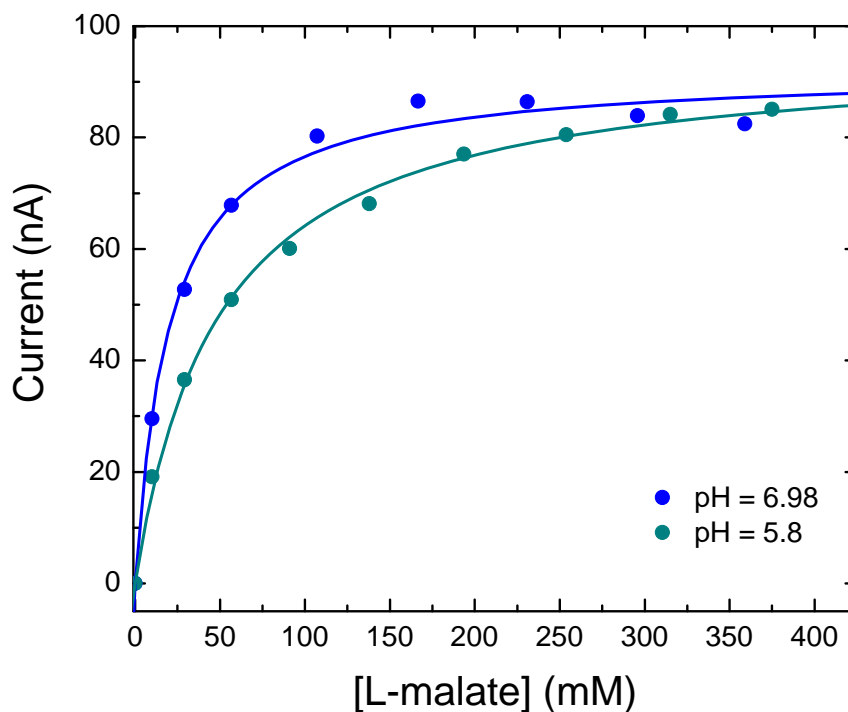
Figure 7-4 Michaelis-Menten behavior of MDH at different pH electrolytes

7.2.3. MDH-laccase biofuel cell

Polarization curves were constructed for the anode, cathode (controlled-potential regime) and biofuel cell under both controlled-potential and controlled-current regimes. Evidently, for the case of fuel cells evaluation under of the system under controlled-current regime is more appropriate since we are interested in observing the voltage output that the fuel cell can sustain, but it was necessary to also perform the controlled-potential experiment in order to have an idea of the operational current range of the device.

Figure 7-5 shows an open circuit voltage 0.584 V for the MDH-laccase biofuel cell which is in agreement with current values reported in the literature for enzymatic biofuel cells (0.6 V).[238]
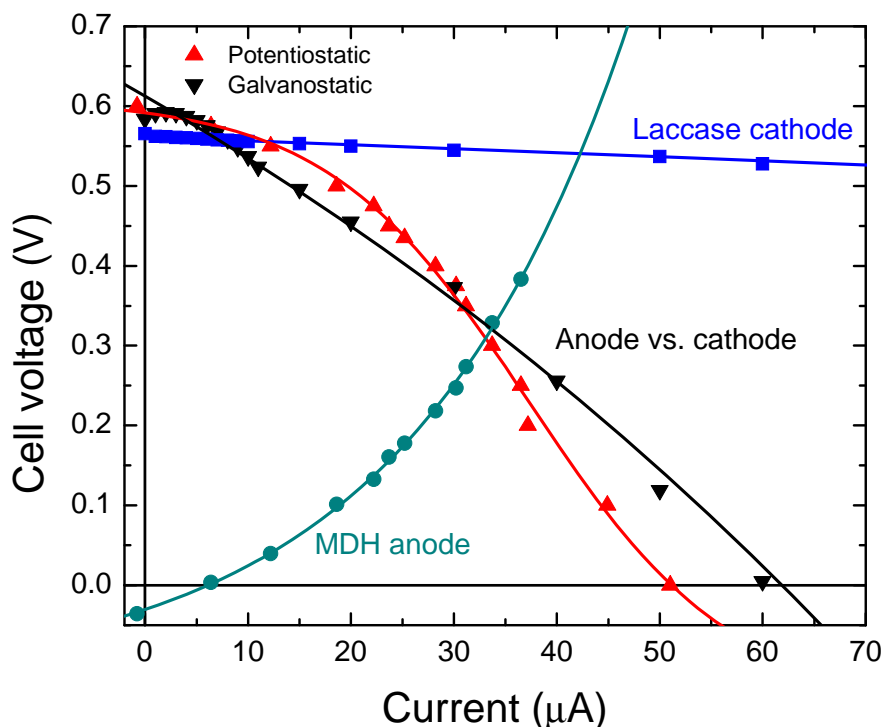
Figure 7-5 Polarization curves of: (●) MDH-anode, (■) laccase-cathode, and (▲, ▼) biofuel cell. L-malate concentration: 500 mM. OCV = 0.584 V

From Figure 7-5 it is clearly observed that the MDH-anode is very limited by ohmic losses and transport limitations. The laccase-cathode on the other side, only presented small kinetic losses in the current operation range of the anode. The biofuel cell polarization curve shows a kinetic-limited behavior for current lower than μA where the sustained voltage is almost independent of the current. For current higher than 10 μA ohmic losses are observed and the anode limits the performance of the biofuel cell only reaching a maximum current of about 65 μA.

Figure 7-6 shows power curves that were constructed for the MDH-laccase biofuel cell per volume of the anode and per area of the cathode. The volume of the anode was determined to be ~1.5 cm^3 and the area of the cathode ~1.3 cm^2. A maximum power density of ~9 μW/cm^2 can be observed in this figure. This value is also in good agreement with reports for enzymatic biofuel cells based on a single dehydrogenase enzyme.[239, 240]

The maximum power per unit volume (of anode) is found to be ~8 μW/cm^3. Current biofuel cell technologies report their maximum current and power outputs per unit area, but for scaling-up of biofuel cells reporting outputs per unit volume is more significant.
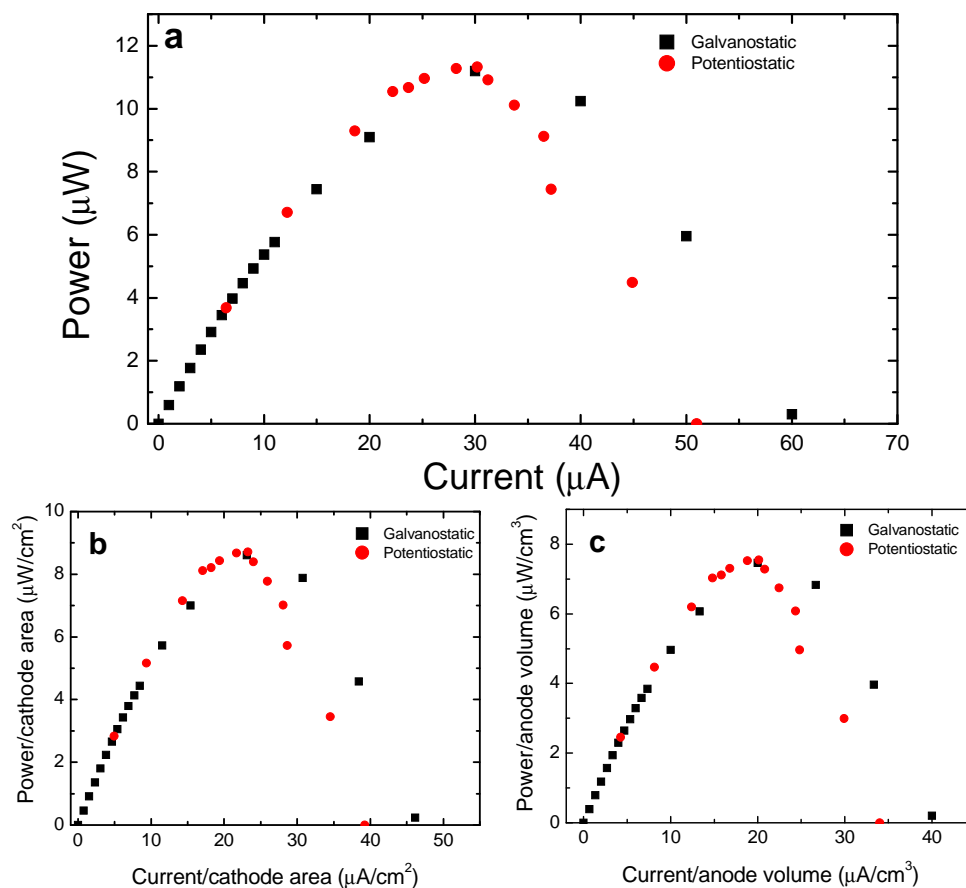
Figure 7-6 Power curves of MDH-laccase biofuel cell in 500 mM L-malate: a) raw power curve, b) power curve per area of the cathode, c) power curve per volume of the anode

7.2.4. ADH-laccase biofuel cell

A second biofuel cell was design with the same laccase-cathode and an ADH-anode. Figure 7-7 shows the open circuit potential curves obtained for each electrode, as well as the cell voltage curve. The OCP of the anode approached –0.05 V vs. Ag/AgCl while the OCP of the cathode approaches 0.58 V vs. Ag/AgCl. This adds to a maximum cell voltage of 0.63 V for the biofuel cell. However, Figure 7-7 shows a cell voltage of 0.61 V close to steady-state. The small loss in voltage could have been due to prolonged

operation of the biofuel cell by the time the curve was recorded and thus loss in enzymatic activities.
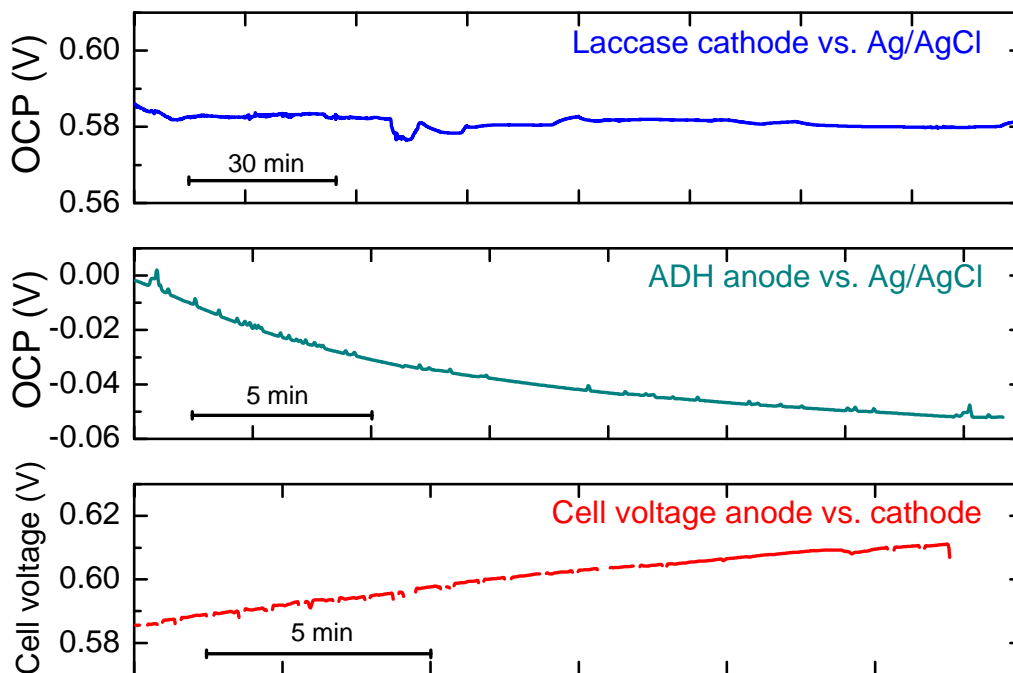
Figure 7-7 Open circuit potentials of laccase-cathode and ADH-anode, and cell voltage of biofuel cell.

Figure 7-8 shows the polarization curves of the anode and cathode (obtained in potentiostatic regime) and the biofuel cell (galvanostatic regime).

In the current operating range the cathode shows the typical behavior of an air breathing electrode with kinetic limitations at low currents, ohmic losses between 30 and 150 μA and a very sudden drop in potential at higher currents due to transport limitations given by the diffusion of air. This biofuel cell sustained an OCV of 0.618 V, slightly higher than that of the MDH-laccase biofuel cell.
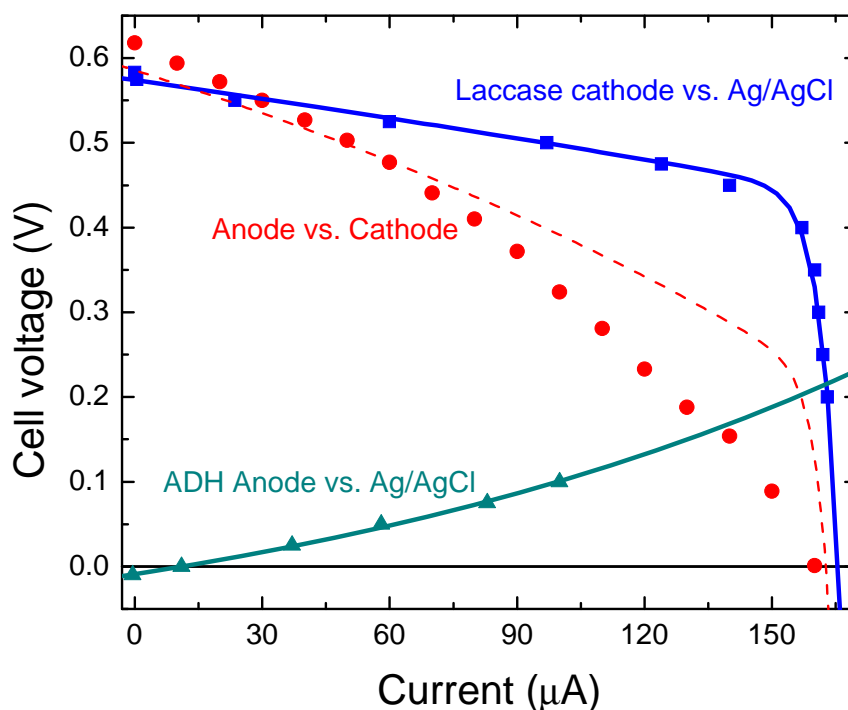
Figure 7-8 Polarization curves of: (▲) ADH-anode, (■) laccase-cathode, and (●) biofuel cell. Red dashed line represents the theoretical full cell polarization curve. Ethanol concentration: 475 mM. OCV = 0.618 V

For both of the biofuel cell studies, it is observed that the anode is the limited electrode, and mainly by ohmic losses. This is consequence of various design aspects. First of all, the supporting electrolyte only contained a total salt concentration of 0.4 M that compared to what is usually used in other devices (e.g. batteries) is very low. Enzymes however, could be inactivated at high salt concentrations, which is why the choice of electrolyte concentration needs to be carefully studied. Moreover, the 3-D design and dimensions of the anode introduce a substantial separation between the electrodes. This macroscopic separation (~1 cm) between the anode and the cathode and

the flow of low conductive ions significantly contribute to the ohmic losses in the biofuel cell.

Figure 7-9 shows power curves that were constructed for the ADH-laccase biofuel cell in the same way as those for the MDH-laccase one. The maximum power density was determined to be ~25 µW/cm^2 which is almost three times higher than that obtained for the MDH-laccase biofuel cell. In terms of volumetric density the maximum power was ~21 µW/cm^3.
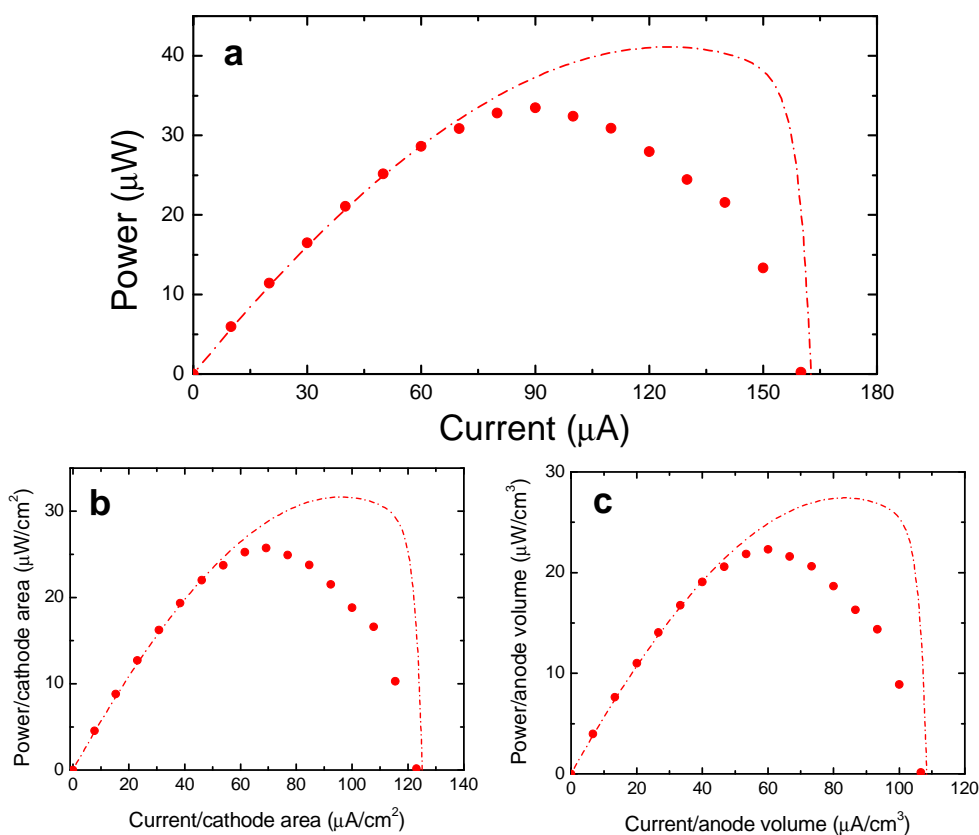
Figure 7-9 Power curves of ADH-laccase biofuel cell in 475 mM ethanol: a) raw power curve, b) power curve per area of the cathode, c) power curve per volume of the anode

Despite certain shortcomings, the work described in this chapter presents a functional yet not fully efficient biofuel cell with a single-enzyme anode that will build that serves as a platform for new biofuel cell designs and optimizations. Although the current design allows for high residence time of the fuels thanks to the large dimensions of the anode, it has the disadvantage of macroscopic separation between the anode and cathode and therefore long path for the ionic flow. In this design both the ionic and mass flow are in parallel ("co-flow") as described in Figure 7-10a.

Paper based electrodes could offer an alternative design in which the separation between the cathode and anode would be minimal due to the small width of both electrodes. However, if the flow of the fuel is maintained as the current design the residence time of the fuel would also be minimal, reducing then the conversion of the fuel. In this case, a "cross-flow" (Figure 7-10b) design in which the fuel travels in parallel to the electrode surfaces maximizing the residence time; while the ionic flow remains orthogonal to the electrodes, would improve the biofuel cell performance by reducing ohmic losses.
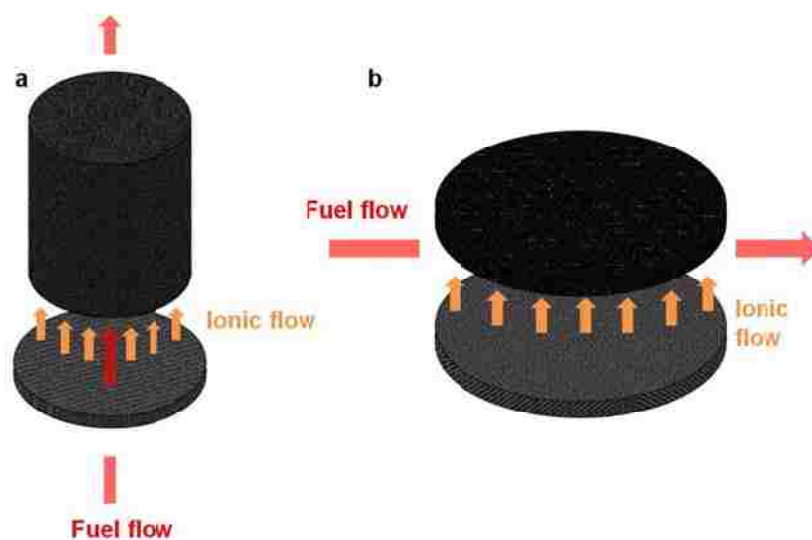
Figure 7-10 Anode-cathode configuration in a)"co-flow"and b) "cross-flow"design

7.3.   Conclusions

Two membrane-less fully enzymatic biofuel cells based on a single NAD^+-dependent enzyme were built and evaluated in a flow-through operation. The MDH-laccase demonstrated limitations in the anode performance that were reflected in a limiting current ~65 µA, and maximum power densities of ~9 $µW/cm^2$ or ~8 $µW/cm^3$ (at 0.373 V). The ADH-laccase showed higher performance achieving limiting current ~160 µA and maximum power densities of ~26 $µW/cm^2$ or ~22 $µW/cm^3$ (at 0.372 V). This higher performance of the ADH-laccase is due to the higher enzymatic activity of ADH that has previously been observed. This single-enzyme design serves as a model for future multiple-enzyme anodes that will have the capacity of multi-step oxidation of biofuels generating even larger current and power densities.

Large ohmic losses characterized the both anodes resulting in polarization curves that resemble resistive behavior. This ohmic effect was a consequence of the low conductivity of the supporting electrolytes as well as the macroscopic separation between the anode and the electrode. Improvements in design have been suggested including the utilization of paper electrodes that will allow for the electrodes to be placed in most immediate contact, and "cross-flow" between the ionic and mass flows.

Chapter 8. Modeling of Malate and Ethanol Oxidation Coupled with Electrochemical NADH Oxidation on Poly-(Methylene Green) Surface

This chapter presents the use of a MATLAB model to simulate and predict the behavior of the 3-D bioanode output by varying design parameters. The model that is used was provided by the research group of Prof. Scott Calabrese Barton's group at Michigan State University. The description and utilization of the model in multi-step enzymatic anode is presented in a recent manuscript by Kar et al.[241]

In summary, the model was designed by Kar et al.[241] for catalytic oxidation of substrates by NAD^+-dependent enzymes coupled with NADH oxidation catalyzed by poly-(MG) in a flow-through bioanode. The model was originally built for a 3-D Toray paper electrode but since it is geometry independent it can be also utilized in different systems. Figure 8-1 shows the schematic of the flow-through electrode for enzymatic oxidation of L-malate that is used in Chapters 7 and 8 and that has been simulated through this model.

This numerical simulation can provide the information about the impact of different design parameters in the performance of the biofuel cell. The following section describes the mathematical treatment and model development provided by Kar et al.[241]

Outlet: L-malate and NAD⁺
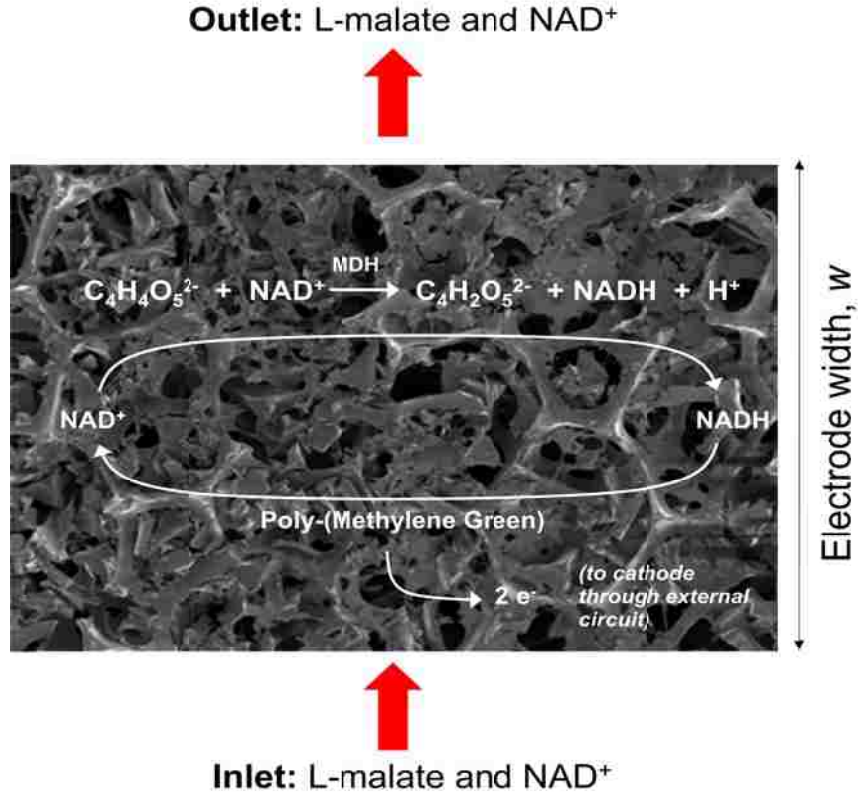
Figure 8-1 Schematic of the flow-through electrode for malate oxidation

8.1. Description of the model

The bioanode is assumed to have uniform cross-section and a thickness w of 1.2 cm for the RVC 3-D electrode in the stackable biofuel cell. The RVC void volume is assumed to be filled with the immobilization phase which is permeable to all aqueous species and consists of MWCNTs/CHIT containing MDH with fixed concentration. L-malate, NAD⁺ co-factor and electrolyte are mobile and flow and diffuse into the electrode from one end (inlet) and exit out of the electrode from the other end (outlet) with a linear velocity v that can be calculated with the known flow rate provided by the pump and the cross-sectional area of the RVC compartment. The electrons generated by the enzyme (MDH) catalyzed oxidation (Eq. 8-1) are transported via aqueous NADH to the catalytic electrode (poly-

(methylene green)) surface, where NADH is electro-catalytically re-oxidized (Eq. 8-2), transferring the electrons to the solid phase. The enzymatic oxidation reaction of L-malate involves the transfer of two electrons to one molecule of NAD^+ and all reactions area assumed to be irreversible. Oxidation of L-malate is given by Eq. 8-1 and the electrochemical reaction for NAD^+ regeneration is given by Eq. 8-2:

$$C_4H_4O_5^{2-} + NAD^+ \xrightarrow{MDH} NADH + C_4H_2O_5^{2-} + H^+ \qquad \text{(Eq. 8-1)}$$

$$NADH \xrightarrow{PMG} NAD^+ + H^+ + 2e^- \qquad \text{(Eq. 8-2)}$$
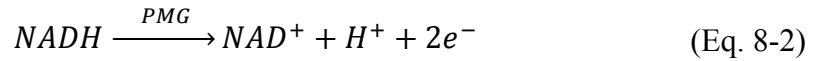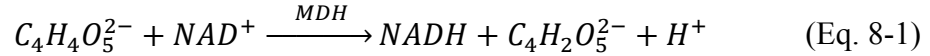
By neglecting transport limitations on the scale of the electrode pores, the system can be treated as one-dimensional with steady state and the material balances for L-malate, NAD^+ and NADH can be described by Fick's law for a system with diffusion, convection and chemical reaction,[242] and they are given (below) by Eq. 8-3, 8-4 and 8-5 respectively.

$$D_{Mal}\frac{d^2C_{Mal}}{dx} - v\frac{dC_{Mal}}{dx} = R_{MDH} \qquad \text{(Eq. 8-3)}$$

$$D_{NAD^+}\frac{d^2C_{NAD^+}}{dx} - v\frac{dC_{NAD^+}}{dx} = R_{MDH} - R_{NADH} \qquad \text{(Eq. 8-4)}$$

$$D_{NADH}\frac{d^2C_{NADH}}{dx} - v\frac{dC_{NAD^+}}{dx} = -R_{MDH} + R_{NADH} \qquad \text{(Eq. 8-5)}$$

Where D_{Mal}, D_{NAD^+} and D_{NADH} (cm^2/s) correspond to the diffusivities of L-malate, NAD^+ and NADH respectively; C_{Mal}, C_{NAD^+} and C_{NADH} (moles/cm^3) correspond to the concentrations of L-malate, NAD^+ and NADH respectively; v (cm/s) is the flow velocity of the fuel and co-factor; and R_{MDH} and R_{NADH} are the rates of reactions of MDH and NADH.

For simplicity, Kar et al. chose a ping-pong bi-bi[243] mechanism to describe the kinetics of the oxidation of substrates by NAD^+-dependent enzymes, and it is expressed in the following equation for the L-malate oxidation reaction:

$$R_{MDH} = \frac{k_{cat,MDH} C_{MDH} C_{NAD^+} C_{Mal}}{K_{NAD^+} C_{Mal} + K_{Mal} C_{NAD^+} + C_{NAD^+} C_{Mal}} \qquad \text{(Eq. 8-6)}$$

Where K_{NAD^+} and K_{Mal} are the Michaelis-Menten constants for the cofactor (NAD^+) and substrate respectively; the latter being obtained from the electrochemical data. $k_{cat,MDH}$ is the total reaction rate of the enzyme (assuming L-malate oxidation is faster than cofactor reduction) that can be obtained from the electrochemical data of Michaelis-Menten kinetics for L-malate oxidation by the equation:[244]

$$k_{cat} = \frac{i_{max}}{nFA} \qquad \text{(Eq. 8-7)}$$

With *n* the number of electrons transferred (two), *F* Faraday's constant and A the surface area of the electrode. The electrode reaction rate (R_{NADH}) can be described by Eq. 8-8 and it includes a NADH concentration dependence term (first term in braces) and a potential dependent term (second term in braces):

$$R_{NADH} = ak \left\{ \frac{C_{NADH}}{K_s + C_{NADH}} \right\} \left\{ \frac{e^{\frac{V-U}{\beta}}}{1 + e^{\frac{V-U}{\beta}}} \right\} \qquad \text{(Eq. 8-8)}$$

The first term in Eq. 8-8, *a*, is the specific area per unit volume of the electrode (cm^2/cm^3). The second term, *k*, is the rate constant for NADH oxidation, which is related

to the maximum steady-state current density NADH oxidation, i_{NADH}, on the surface of

poly-(MG) and can be determined from electrochemical data with the following equation:

$$k = \frac{i_{NADH}}{nF} \qquad \text{(Eq. 8-9)}$$

In Eq. 8-8 the first term is expressed in terms of the concentration of NADH, C_{NADH}

and K_S (the dissociation constant of the substrate catalyst complex) which resembles a

Langmuir isotherm type of kinetics as previously described for NADH oxidation. The

second term in braces is a Nernstian expression for potential dependence. The parameters

β (V/decade) and U (V vs. Ag/AgCl) are Tafel slope and redox potential, respectively; V

is the anode potential. K_s, β and U can be obtained from electrochemical data for NADH

oxidation.

Moreover, Kar et al.[241] developed non-dimensional material balance equations (from

Eq. 8-3 to 8-5) by normalizing all species concentrations by the bulk concentration of L-

malate, C_{Mal}, normalizing position within the electrode by the electrode thickness, w, and

normalizing all diffusivities to the L-malate diffusivity D_{Mal}; and by further multiplying

both sides of the material balance equations by $w^2/D_{Mal}C_{Mal}$ yielding Eq. 8-10 to 8-12:

$$\frac{d^2C'_{Mal}}{dx'^2} - Pe\frac{dC'_{Mal}}{dx'} = r_{MDH} \qquad \text{(Eq. 8-10)}$$

$$\delta_{NAD^+}\frac{d^2C'_{NAD^+}}{dx'^2} - Pe\frac{dC'_{NAD^+}}{dx'} = r_{MDH} - r_{NADH} \qquad \text{(Eq. 8-11)}$$

$$\delta_{NADH}\frac{d^2C'_{NADH}}{dx'^2} - Pe\frac{dC'_{NADH}}{dx'} = r_{NADH} - r_{MDH} \qquad \text{(Eq. 8-12)}$$

Where C'_{Mal}, C'_{NAD+} and C'_{NADH} are dimensionless concentrations, δ_{NAD+} and δ_{NADH} are dimensionless diffusivities, obtained by normalizing the dimensional diffusivities by the diffusivity of L-malate. $Pe = v\,w\,/\,D_{Mal}$ is the Peclet number, a ratio of the rate of convection to the rate of diffusion. Moreover, Kar et al.[241]

$$r_{MDH} = \frac{Da_{MDH}C'_{NAD+}C'_{Mal}}{[\sigma_{NAD+}C'_{Mal} + \sigma_{Mal}C'_{NAD+}C'_{Mal}]} \qquad \text{(Eq. 8-13)}$$

In Eq. 8-13 the Damkohler number is introduced and it is defined as:

$$Da_{MDH} = \frac{k_{cat}E_{MDH}w^2}{D_{Mal}C_{Mal}} \qquad \text{(Eq. 8-14)}$$

Eq. 8-13 also includes non-dimensional Michaelis-Menten constants $\sigma_{NAD+} = K_{NAD+}/C_{Mal}$ and $\sigma_{Mal} = K_{Mal}/C_{Mal}$. In a similar way, the electrode reaction rate is expressed in non-dimensional form:

$$r_{NADH} = Da_{NADH}\frac{C'_{NADH}}{(\sigma_S + C'_{NADH})} \qquad \text{(Eq. 8-15)}$$

With the Damkohler number given by:

$$Da_{NADH} = \left\{\frac{w^2ka}{D_{Mal}C_{Mal}}\right\}\left\{\frac{e^{\frac{V-U}{\beta}}}{1 + e^{\frac{V-U}{\beta}}}\right\} \qquad \text{(Eq. 8-16)}$$

And $\sigma_S = K_s/C_{Mal}$

Kar et a.[241] made assumptions of fixed concentrations of L-malate and NAD^+ at the electrode-electrolyte interface at the inlet while the concentrations of all other species were considered zero. Assumptions of zero gradients for all species at the outlet were used. The boundary conditions for the non-dimensional mass balances result in:

$$C'_{NAD^+} = C_{NAD^+}/C_{Mal}; \ C'_{NADH} = 0 \ \text{at} \ x' = 0 \qquad \text{(Eq. 8-17)}$$

$$\frac{dC'_{Mal}}{dx'} = \frac{dC'_{NAD^+}}{dx'} = \frac{dC'_{NAD}}{dx'} = 0 \ \text{at} \ x' = 1 \qquad \text{(Eq. 8-18)}$$

Finally, the current per unit area, i (A/cm^2) can be obtained by integrating the dimensionless rate of NADH oxidation (r_{NADH}) over the dimensionless electrode length, x' as described in Eq. 8-19:

$$i = \left(\frac{nFD_{Mal}}{w}\right) \int_0^1 r_{NADH} dx' \qquad \text{(Eq. 8-19)}$$

8.2. Determination of parameters

Several of the necessary parameters needed to simulate Eq. 8-19 have already been mentioned in the previous section but Table 8-1 includes all remaining parameters that were employed in the simulation.

Table 8-1 Parameters and nominal values used in the simulation

Parameter	Value (units)	Source
Electrode area per unit volume, a	40 cm^2/cm^3	RVC 60 ppi[233]
Anode potential, V	0.6 V	[241]
Electrode width, w	1.2 cm	Experimental conditions
Reversible potential for NADH oxidation, U	0.0708 V vs. Ag/AgCl	Fit Figure 8-2
Exchange current density for NADH oxidation, i_0	5.65 x 10^{-6} μA/cm^2	Fit Figure 8-2
Surface adsorption constant for NADH, K_S	1.8 x 10^{-5} moles/cm^3	Fit Figure 5-6
Tafel slope, β	0.056 V/decade	Fit Figure 8-2
Velocity of fuel and cofactor solution, v	4.2 cm/s	Experimental parameters
Enzyme concentration, C_{MDH}	2.857 x 10^{-7} moles/cm^3	Experimental conditions
Turnover number for MDH, k_{cat}	2.505 s^{-1}	Fit Figure 6-7
Michaelis-Menten constant for mediator, K_{NAD^+}	1.4 x 10^{-7} moles/cm^3	[241]
Michaelis-Menten constant for substrate, K_{Mal}	5 x 10^{-7} moles/cm^3	Fit from Figure 6-7
Bulk concentration, C_{Mal}	0.5 x 10^{-3} mol/cm^3	Experimental conditions
Bulk concentration of NAD$^+$, C_{NAD^+}	1.5 x 10^{-6} mol/cm^3	Experimental conditions
Diffusivity of L-malate, D_{Mal}	4 x 10^{-6} cm^2/s	Assumed as diffusivity of methanol[241]
Diffusivity of NAD$^+$ D_{NAD^+} and NADH, D_{NADH}	3.3 x 10^{-8} cm^2/s	[241]

Figure 8-2 presents the fit of curve c from Figure 5-5 (5 mM NADH) that was used to obtain the parameters of the Nernstian term in equation 8-8.
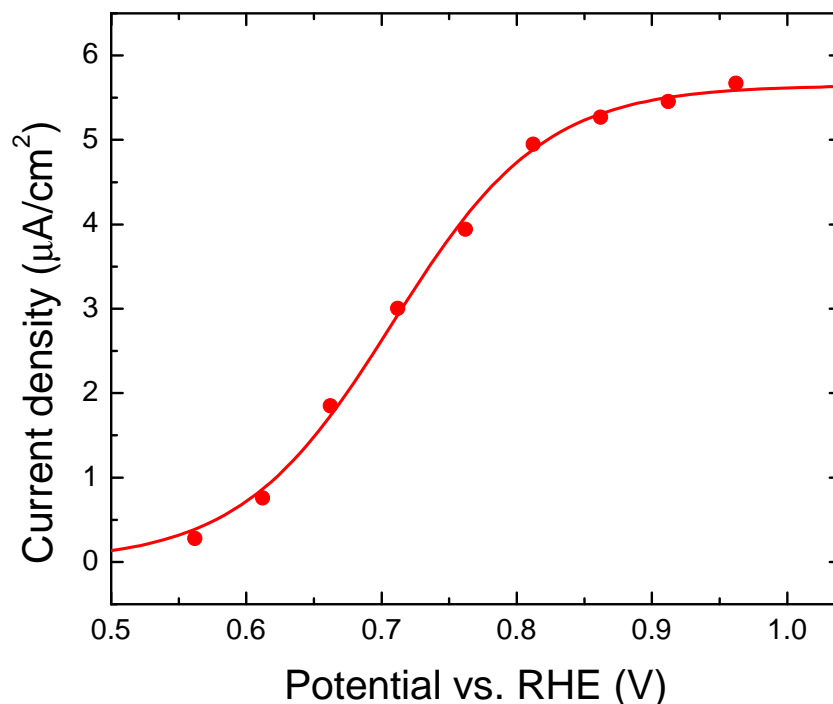
Figure 8-2 Polarization curve of poly-(MG)-modified GC in 5 mM NADH for determination of U, i_0 and β

8.3. Simulation of L-malate oxidation by MDH coupled with NADH oxidation

Provided the MATLAB code to model Eq. 8-19 and all experimental parameter from Table 8-1, an initial simulation of the system was ran. The output of the simulation is shown in Figure 8-3 and it describes the current density with respect to the position (width) at the electrode. This first simulation shows that during the first millimeter of the anode, the resulting oxidative current density does not reach steady state behavior. This clearly indicates that for the enzymatic system that was simulated, there is a limitation when building very thin electrodes with orthogonal flow, probably due to low activity of the system. Thus, high residence times are necessary for high conversion of species at the electrode surface.

This observation is in agreement with the hypothesis discussed in the previous chapter where we proposed that for a paper based anode, parallel flow of the fuel with high residence time would be beneficial.
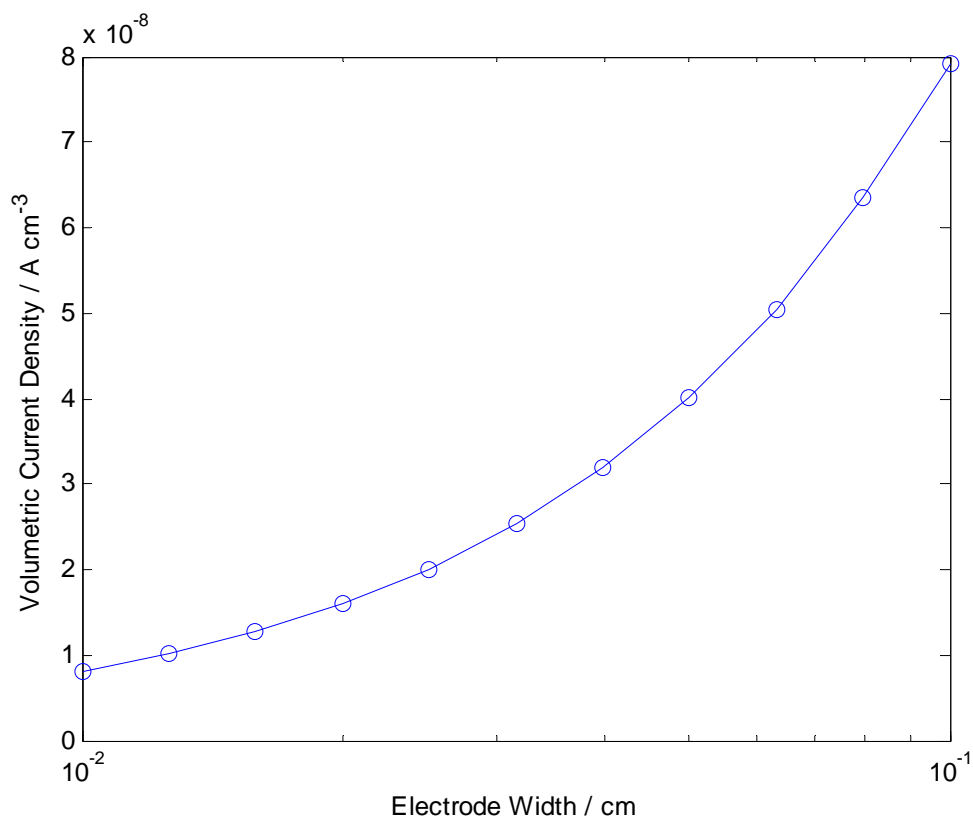
Figure 8-3 MATLAB simulation of current density per volumetric unit with respect to the position at the electrode. Equation 8-19 was simulated.

Currently, the simulation model is not developed to describe biofuel cells with such high flow velocities. Further modification and simulations will be necessary in order to evaluate the effect of fuel, co-factor and enzyme concentrations, cell potential, electrode surface area, and surface area per unit volume of the electrode material and thus optimize the bioanode design for improved performance. This model could also be extended to multi-enzyme enzymatic electrodes mimicking metabolic processes.

Chapter 9. Conclusions and Outlook

The principal objective of this work was to engineer a biofuel cell anode for NAD^+-dependent enzymes while developing a platform technology that can be used for mono- or multiple enzyme systems. This goal was achieved by carrying out specific task that helped building the technology step-by-step. The achievements of each task are summarized here:

Standardized Characterization of Electrocatalytic Electrodes

These experiments were useful for assessing standardized experimental platform and protocols to allow cooperative research across different labs. They also provided information about the electropolymerization of MG onto glassy carbon surfaces and about its catalytic activity towards NADH oxidation.

Structure and Electrochemical Properties of Electrocatalysts for NADH Oxidation

Through this study further electrochemical characterization of the poly-(MG)-modified GC was achieved and its catalytic activity towards NADH oxidation was again demonstrated. Structural characterization of poly-(MG) films on GC electrodes was possible by the use of analytical techniques like XPS and NMR. Both XPS and NMR confirmed that electropolymerization of MG consists of an oxidative step, and XPS also confirmed the reductive step that is also observed in cyclic voltammetry. Furthermore, XPS suggests that a ring-N-(CH$_3$)-ring bond is possible. HR-SEM provided important information about the morphology of poly-(MG) onto GC electrodes which appears to have a conformal character. And ultimately, the electrocatalyst proved to be functional in combination with a NAD^+-dependent enzyme (MDH) for electrocatalytic oxidation.

Flow-Through 3-D Biofuel Cell Anode for NAD+-Dependent Enzymes

The immobilization of MDH in different chitosan scaffolds showed that the addition of MWCNTs into the immobilization matrix enhanced the electrocatalytic activity of the enzyme by increased conductivity and electrical wiring provided by the nanotubes as well as higher electrochemically accessible surface area. Moreover, the electropolymerization of MG was achieved on the 3-D structure of RVC and its catalytic activity towards NADH oxidation was established. The best deposition conditions were determined for the 3-D to achieve the highest catalytic activity. The growth of poly-(MG) onto this material was different than the growth on the 2-D GC electrode and it its morphology was studied via SEM and found to be in the form of particles instead of a conformal film coating. 3-D electrodes were tested in combination with NAD+-dependent MDH and ADH which showed Michaelis-Menten kinetics. Lastly, the utility of 3-D electrode design was proven in the construction of a single-enzyme anode based on NAD+-dependent MDH with OCP of -35 mV vs. Ag/AgCl.

This design resulted in a common technology platform for bioanodes that can be used for any NAD+-dependent enzyme due to two contributing factors: the presence of poly-(MG) as the NADH electrocatalyst, and the use of chitosan or modified-chitosan scaffold that can accommodate different or multiple enzymes for multi-step oxidation of fuels.

Fully Enzymatic Flow-Through Biofuel Cell

In the last set of experiments, a laccase-cathode was integrated with two different NAD+-dehydrogenase anodes to construct a biofuel cell. The first biofuel cell was a MDH-laccase system with L-malate as the fuel. This cell sustained an OCV of 0.584 V with maximum power densities of ~9 $\mu W/cm^2$. The second biofuel cell was a ADH-laccase

system fueled by ethanol. It sustained a slightly higher OCV of 0.618 V with ~25 $\mu W/cm^2$. In both systems the main losses were due to resistance limitations. The fairly low concentration of electrolytes combined with the macroscopic separation of the electrodes originated ohmic losses. However, these biofuel cells based on a single-enzyme anode demonstrated to be in agreement with the literature.

Future Outlook

Several challenges are still to be overcome in enzymatic biofuel cell technologies. The bioanode that has been designed can be improved and optimized in various ways. First of all, chitosan can be hydrophobically modified to enhance enzyme's activity, stability and lifetime. Furthermore, multiple enzymes can be immobilized in chitosan scaffolds in order to achieve complete oxidation of biofuels that would originate higher current and power densities.

However, the major challenge is posed by ohmic losses, which means that the electrode configuration in continuous-flow design needs to be re-considered. We have proposed that a "cross-flow" configuration (Figure 7-10) with a paper-based anode would help by placing the electrodes in most immediate contact while allowing for long residence time of the biofuel (high conversion rates). Such a design should diminish ohmic losses in the cell voltage and improve the limiting current and thus power output of the biofuel cell.

Appendix A. Entrapment of Enzymes and Carbon Nanotubes in Biologically Synthesized Silica: Glucose-Oxidase Catalyzed Direct Electron Transfer

Dmitri Ivnitski,[a] Kateryna Artyushkova,[a] Rosalba A. Rincón,[a] Plamen Atanassov,[a,*]

Heather R. Luckarift,[b,*] and Glenn R. Johnson[b]

[a] *The University of New Mexico, Department of Chemical and Nuclear Engineering, Albuquerque, NM 87131, USA*
[b] *Air Force Research Laboratory Microbiology and Applied Biochemistry, 139 Barnes Drive, Suite 2, Tyndall AFB, Florida 32403, USA*

Abstract

This work demonstrates a new approach for building bioinorganic interfaces by integrating biologically derived silica with single-walled carbon nanotubes to create a conductive matrix for immobilization of enzymes. Such a strategy not only allows simple integration into biodevices but presents an opportunity to intimately interface an enzyme and manifest direct electron transfer features. Biologically synthesized silica/carbon nanotube/enzyme composites are evaluated electrochemically and characterized by means of X-ray photoelectron spectroscopy. Voltammetry of the composites displayed stable oxidation and reduction peaks at an optimal potential close to that of the FAD/FADH$_2$ cofactor of immobilized glucose oxidase. The immobilized enzyme is stable for a period of one month and retains catalytic activity for the oxidation of glucose. It is demonstrated that the resulting composite can be successfully integrated into functional bioelectrodes for biosensor and biofuel cell applications.

Keywords: electron transfer; glucose oxidase; nanocomposites; photoelectron spectroscopy; silica immobilization.

A.1. Introduction

Direct bio-electrocatalysis of redox enzymes has attracted increasing attention for the development of the next generation of electronic nanoscale biomaterials and devices for industrial, clinical, environmental, space exploration, and defense applications.[183, 245-249] The fusion of electrocatalysis with biology, for example, facilitates the development and commercialization of disposable biochips with near perfect selectivity for a given target analyte.[247, 249] Efficient communication between enzyme and electrode can also aid the development of biofuel cells with high power output.[5, 245, 250, 251] Direct electron transfer (DET) between an enzyme and an electrode provides the most potential for miniaturization and high power output because the requirement for complex electron mediators is negated. In addition, an enzyme-electrode based on DET theoretically functions at a potential range that is close to the redox potential of the enzyme itself. Immobilization of enzymes for DET, however, has proven to be problematic as accessibility of the enzyme redox center and hence efficient transfer of electrons to the electrode is limited.

Glucose oxidase (GOx) is a widely studied enzyme, particularly with respect to DET, and as such provides a suitable model system applicable to the development of biosensors and biofuel cells.[252] GOx is a stable enzyme with high catalytic activity and an inexpensive substrate source; utilizing glucose as a widely available fuel. In aqueous solution at physiological pH, the redox potential of $FAD/FADH_2$ at the enzyme active site is negative and therefore well suited to operation at the anode of a biofuel cell.[5, 253, 254] The optimal redox potential of $FAD/FADH_2$, however, is only achieved under DET as employing redox mediators for anodic processes such as glucose oxidation requires the

use of a redox potential that is more positive than that of the enzyme active site. This leads to additional overpotential to facilitate charge transfer from the enzyme to the mediator and results in a decrease in the cell voltage. Several limitations therefore must be addressed for the successful application of GOx in direct bio-electrocatalysis. The FAD/FADH$_2$ redox center of GOx is located deep within the apoenzyme (approximately 13 Å) and hence the electron-transfer rate between the active site of glucose oxidase and the electrode surface is inherently slow.[252, 255, 256] Over recent years, efforts have been made to reduce the electron-tunneling distance between GOx and the electrode using different promoters.[5, 246, 247, 254-257] One strategy is to incorporate the enzyme into an electrically conductive matrix such as carbon nanotubes (CNTs), which potentially reduces the distance from the redox center of GOx to the CNTs, which then act as a microelectrode surface.[258] We have previously demonstrated the ability of multi-walled CNTs to be used as an efficient conductivity matrix for DET between the active site of GOx and a carbon electrode, indicating that CNTs successfully orientate the enzyme active site and redox-active cofactor with respect to the electrode surface. The resulting electron-transfer rate constant of approximately 2.4 s^{-1} indicated that the heterogeneous DET process was significantly greater than previously observed for unmodified electrodes. The three-dimensional network of electronically conductive CNT significantly increases the surface area for enzyme immobilization and provides an electronic circuit as a series of "nanowires" for the enzyme.[246, 253, 256] The work reported herein utilizes single-walled CNTs in place of multi-walled CNTs owing to their superior electron-transfer properties.

The crux of bio-electrocatalysis, however, is the development of enzyme-immobilization techniques that provide continuous electron transfer from the enzyme to the electrode, whilst maintaining high catalytic activity and enzyme stability. The majority of methods for enzyme immobilization utilize an inert support that serves no further specific catalytic function. When the immobilization support is an electrode or transducer surface, highly integrated functional enzymatic systems can be realized. Recent studies have demonstrated the remarkable versatility of a biomimetic silicification reaction as a means of enzyme immobilization.[259, 260] Biosilicification is a rapid ambient precipitation of silica mediated by a biological catalyst. A wide variety of peptides and proteins can catalyze the precipitation of silica and become encapsulated as the silica matrix forms.[261-264] The reaction provides an efficient method for enzyme immobilization and provides significant mechanical stability to the resulting silica matrix. Lysozyme, for example, catalyzes the formation of silica particles when mixed with a silicic acid precursor. The process is a one-step procedure and additional enzymes added during the reaction become entrained and retain a high level of catalytic activity.[265] Initial studies demonstrated that the technique was successful for immobilizing enzymes directly at a surface with retention of catalytic activity, but extension of the application to bio-electrocatalysis has not yet been demonstrated.[266] This work describes an approach to create a bio–nano interface suitable for direct electrochemistry of enzymes. Direct bio-electrocatalysis of glucose oxidation is demonstrated by entrapping GOx in a silica/CNT composite obtained through lysozyme-catalyzed synthesis of silica.

A.2. Experimental Section

Materials: GOx from Aspergillus niger (EC1.1.3.4), tetramethyl orthosilicate (TMOS), 99%, lysozyme from chicken egg white (EC3.2.1.17) and carboxylated single-walled carbon nanotubes were obtained from Sigma–Aldrich (St. Louis, MO). Toray carbon paper TGPH-060, was obtained from E-TEK, K, Somerset, NJ (now a division of BASF). Screen-printed electrodes were obtained from Alderon Biosciences Inc. (Durham, NC). All other reagents and chemicals were of analytical grade and obtained from standard commercial sources. Enzyme stock solutions were prepared in 0.1 M phosphate buffer (pH 7.0). All other solutions were prepared with deionized water and filtered before use.

Preparation of the enzyme/CNT/silica composites: GOx and CNT were immobilized on a screen-printed carbon electrode surface and on TP by entrapment within a silica matrix using a modification of immobilization methods described previously.[259, 260] For screen-printed carbon electrodes, lysozyme was nonspecifically adsorbed on the working carbon electrode surface by soaking the surface in a solution of lysozyme (0.5 mL, 25 mg mL^{-1}) and the excess removed by washing with phosphate buffer (0.1 M, pH 8). A homogeneous GOx/CNT suspension was prepared by sonicating CNT (2 mg) in phosphate buffer (1 mL, 0.1 M, pH 7) for 1 h. An aliquot (0.1 mL) of the CNT suspension was then mixed with GOx (3 mg) and sonicated for a further 20 min. The silica precipitation reaction mixture consisted of phosphate buffer (0.7 mL, pH 8), TMOS (0.1 mL, 1 M in 1 mM HCl) and GOx/CNT (0.1 mL in phosphate buffer, pH 7). The silica precipitation mix (20 mL) was dropped onto the lysozyme-modified surface and incubated for 30 min at room temperature to allow the silica to form. For the preparation of TP electrodes, the lysozyme-modified TP (prewashed by sonication) was placed into a

mini-column (prepared from micro-fuge filtration columns (Qiagen, lnc. Valencia, CA) modified to accommodate a circle of TP) and the precipitation mix was flowed through the minicolumn four times under gravity. Finally, both screen-printed carbon electrodes and TP modified with CNT, GOx, and silica were washed with water and dried before analysis.

Characterization of enzyme/CNT/silica composites: The surface morphology of the GOx/CNT/Silica modified carbon electrodes was visualized using a Hitachi (S-5200) SEM equipped with an energy dispersive spectrometer. The microscope was operated at 10 kV for imaging. No conductive coatings or other treatment were performed on the samples prior to SEM observations. XPS spectra were acquired using a Kratos AXIS Ultra photoelectron spectrometer using a monochromatic Al Ka source operating at 300 W (base pressure: $2x10^{-10}$ Torr, operating pressure: $2x10^{-9}$ Torr, 1 Torr=133.322 Pa). Charge compensation was accomplished using low-energy electrons. Standard operating conditions for good charge compensation were −4.1 V bias voltage, −1.0 V filament voltage and a filament current of 2.1 A. The sample surface survey was completed initially, followed by determination of high-resolution spectra of C1s, O1s, Si2p, and N1s for all samples. Take-off angles of 908 and 158 were selected for angle resolved studies, corresponding to $\approx$ 8–10 and $\approx$ 2 nm of the surface respectively. Data is presented as the average of 1–2 samples at 3–4 areas per sample. A linear background of C1s, N1s, O1s and Si2p spectra was used. Quantification- utilized sensitivity factors were provided by the manufacturer. All the spectra were charge referenced to the aliphatic carbon at 285 eV. Curve fitting was carried out using individual peaks of constrained width and shape. A 70% Gaussian, 30% Lorentzian line shape was used for the curve fits.

Determination of GOx surface concentration: The surface concentration of GOx was calculated from the equation $\Gamma=Q/nFA$, where Γ is the surface concentration of GOx, Q is the charge obtained from integration of the anodic peak, n is the number of electrons per oxidation of GOx ($FADH_2$) molecule, F is the Faraday constant, and A is the electrode surface area in contact with the electrolyte (electrochemically accessible surface area, EASA).[267] EASA was calculated using the capacitance of the electrode obtained from cyclic voltammetry in a potential region where no Faradic processes occur. In order to elucidate the EASA the specific capacitance for carbonaceous material (CNT) was assumed to be 20 mF cm^{-2}. The EASA of the Si- and CNT-modified carbon electrode was calculated to be 3.7 cm^2.

Electrochemical measurements: Electrochemical measurements were performed with a potentiostat/galvanostat (Princeton Applied Research, Model 263A) in a three-electrode cell with a 5 mL working volume and consisting of the silica/GOx/CNT working electrode, a carbon counter electrode and an Ag/AgCl reference electrode (Bioanalytical Systems Inc., Evansville, IN). The electrolyte solution was composed of equal volumes of phosphate buffer (0.1 M, pH 6.2) and KCl (0.1 M). Electrochemical experiments were carried out at 20 ± 0.5 °C. Cyclic voltammograms were used to calculate the electron-transfer rate constant using the method of Laviron.[268]

Determination of glucose oxidase activity: The enzymatic activity of GOx was determined according to the supplier's quality control test procedure (Sigma–Aldrich) with dextrose as substrate. For stability experiments, stock samples were incubated at 25 °C with shaking for 1 month. Aliquots were removed periodically for analysis of GOx activity. The pH profile of GOx was determined using the same glucose oxidase assay

adjusted to a range of pH values with 1 M NaOH. The immobilization efficiency (%) is calculated as a ratio of enzyme activity after immobilization, relative to free enzyme under identical experimental conditions.

A.3. Results and Discussion

Biocatalytic precipitation of silica composites containing GOx, were prepared on Toray carbon paper (TP), with and without the addition of CNT. Lysozyme provided the scaffold for silica formation and binds to the carbon-electrode surface by physical adsorption, negating any requirement for chemical modification or pretreatment of the TP. The morphology of the resulting silica precipitate was investigated by scanning electron microscopy (SEM). The filaments of TP were clearly visible by SEM (Figure A-1a) and following the silicification reaction, a surface-coated layer of silica can be clearly differentiated from the uncoated fibers.

The surface morphology of the TP appears more coarse, although still uniform, indicating that the silicification reaction occurred homogeneously on the surface (Figure A-1b). The majority of the silica forms as a network of fused particles in agreement with previous studies (Figure A-1c).[259] The presence of CNT embedded within the silica matrix is also evident (Figure A-1d).

X-ray photoelectron spectroscopy (XPS) was used to analyze the chemistry of the silica composite. XPS is a powerful technique allowing estimation of the elemental and chemical composition of the upper 10 nm of a surface and has been demonstrated as an effective tool to quantify protein immobilized or adsorbed during enzyme immobilization.[269-274]
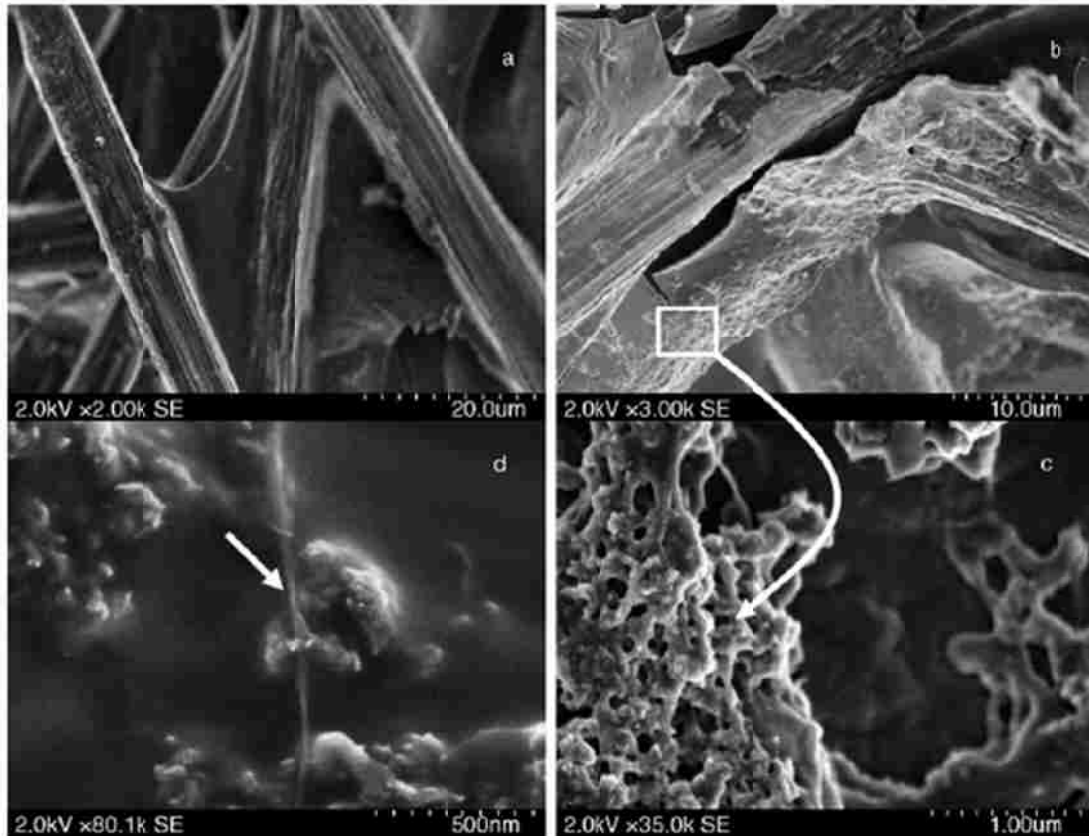
Figure A-1 SEM micrographs of carbon paper electrodes coated with a) lysozyme and b) silica at low magnifications and c–d) at high magnifications

The surface elemental composition and bonding with respect to C1s, O1s, N1s and Si2p core level spectra were determined at a surface depth of approximately 10 and 2 nm (Table A-1). TP alone, with or without CNT, exhibits the same elemental compositions with $\approx$ 2% oxygen, irrespective of sampling depth. Initially, the formation of silica resulting from reaction of lysozyme with hydrolyzed tetramethyl orthosilicate (TMOS) was analyzed as a control sample and was found to exhibit a significant increase in Si and N, as expected. The complete functional samples (i.e., silica on TP containing GOx and CNT) were composed of $\approx$ 5% N and $\approx$ 15% Si, confirming the presence of both the enzyme and a silica matrix. However, in the absence of CNT, a lower N signal (0.6%)

and relatively higher Si and O signals were observed, suggesting either a lower degree of enzyme immobilization or a more complete coverage of GOx by silica that blocks the encapsulated enzyme from XPS analysis. No changes in composition with depth were observed for any of the samples.

Table A-1 XPS elemental quantitative results. Values are represented as a percentage of the total. TP is Toray Carbon Paper

Sample	Depth	C1s	O1s	Si2p	N1s	O/C	N/C	N/O
	[nm]	[%]	[%]	[%]	[%]			
TP	10	97.1	2.9					
	2	97.6	2.4					
TP and CNT	10	97.6	2.4					
	2	98.5	1.5					
TP and silica	10	46.5	35.9	9.1	8.5	0.77	0.18	0.24
	2	45.7	35.5	10.3	8.5			
TP/silica/GOx	10	36.9	48.5	14	0.6	1.31	0.02	0.01
	2	37.2	49.1	13.8	0.7			
TP/silica/GOx/CNT	10	39.5	42.5	13.1	4.9	1.08	0.12	0.11
	2	35.4	45.6	14	5.1			
GOx		68.1	23.1		8.8	0.34	0.13	0.38
Lysozyme		65.2	19.1		15.7	0.29	0.24	0.82

XPS was also used to determine O/C and N/C ratios in an effort to obtain protein fingerprints for lysozyme and GOx. Analysis of soluble solutions of GOx and lysozyme, however, showed an O/C ratio of approximately 0.3 for both proteins, making distinction between the two difficult. In addition, the O/C ratios for composites containing silica were much higher owing to the excess of silica (SiO_2). The N/C ratio may therefore be a more appropriate measure of the interaction of enzyme chemistry at the surface. The N/C ratio predicted by the polypeptide sequences is much larger for lysozyme (0.24) than for GOx (0.13). For samples containing both GOx and lysozyme, an N/C ratio of 0.12 is very

close to that of GOx alone, which may indicate that the majority of enzyme detected by XPS is GOx. In comparison, in a GOx-free control, the ratio is much larger (0.18) as would be expected for lysozyme alone.

High resolution C1s and O1s spectra of each sample were obtained and deconvoluted using conventional curve fitting (Figure A-2) and quantitative results were calculated (Table A-2). The C1s spectrum of GOx has three main peaks corresponding to the following bonds: aliphatic C*H–CH (284.8 eV) that may have originated from surface contamination, oxydrilic C*–OH and amidic N–C*H–CO (286.6 eV), and N–CH–C*=O (288.3 eV), where the respective carbon species are marked by an asterisk. The analysis of the binding energies of the N1s (400.2 eV) and two peaks for O1s (532 and 533.2 eV) confirmed that these elements are attributable to the enzyme component. The C1s spectrum of lysozyme also has major peaks due to C–C and C–H carbon (284.8 eV), and higher binding energy peaks at 285.8 and 288.2 eV that are attributed to the C*–N and –C*O–NH– or –C*OO– carbon, respectively. Smaller peaks at 284.2 and 286.6 eV are thought to be due to contamination during preparation, but did not interfere with the chemical analysis.

High-resolution C1 s spectrum of the silica composite (containing lysozyme, GOx and CNT) contains features of both pure enzyme samples, that is, a dominant peak at 286.6 eV that corresponds to the spectra for GOx and a secondary signal at 285.8 eV that corresponds to the primary peak in the spectra of lysozyme. A background signal of Si–C was detected in all samples. High-resolution O1s spectra for pure enzymes and the silica composite all exhibit spectra corresponding to the presence of immobilized biomolecules (533 eV). In addition, the composite exhibits a high binding energy that can be attributed

to the presence of silica. Complete conversion of the TMOS precursor to silica is confirmed by the presence of a very small peak (O1s spectra) from a Si-OCH$_3$ bond at approximately 532 eV. The position of a single Si2p peak (not shown) at 104 eV also confirmed that all of the silicon present occurs as silica (silicon dioxide). XPS analysis allowed for a detailed understanding of the overall chemical composition of the silica composite and confirmed the formation of silica with the incorporation of both enzymes and CNT.
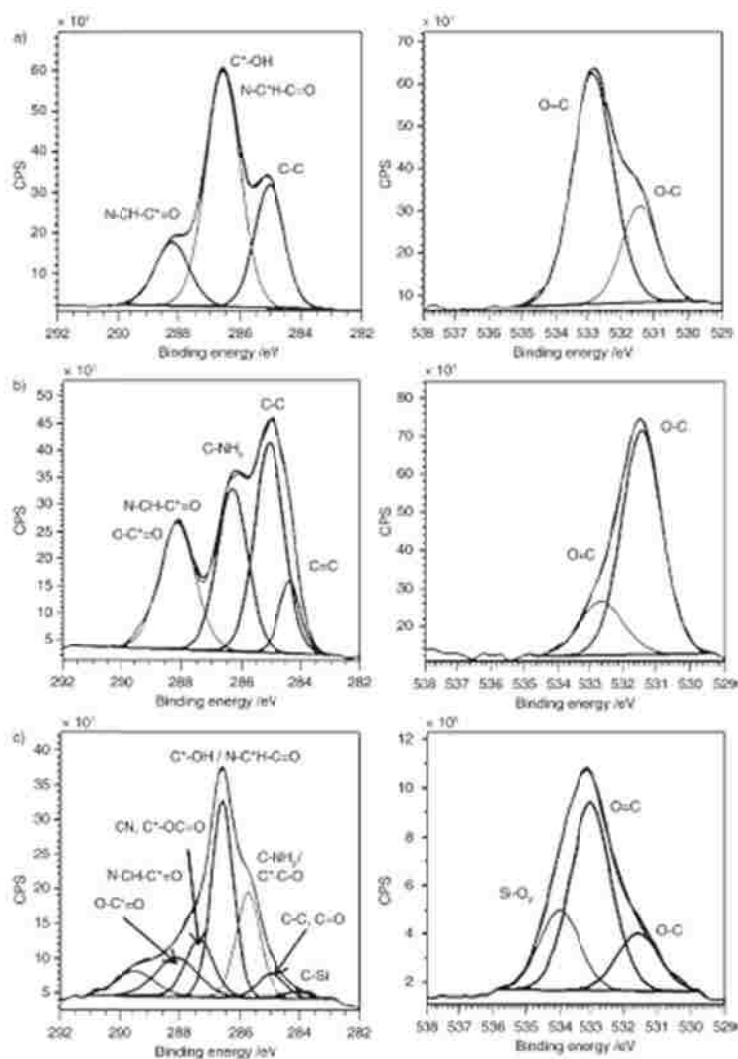
Figure A-2 XPS spectra of a) soluble GOx, b) soluble lysozyme, and c) silica composites with entrapped GOx and CNT

131

Table A-2 C1s and O1s deconvolution results of XPS analysis. Values shown are represented as a percentage of the total

	C-Si, C=C	C-C, C-H	C-NH$_2$, CO-NH, C*-C-N, C*-C-O	N-C*-H-C=O, C*-OH	CN, C*-O-C=O	N-CH-*C=O, O-C*=O	O-C	O=C	Si-O$_2$
Binding energy	284.2	284.8	285.8	286.6	287.2	288.2	531.9	533.2	534.1
GOx		27.1		57.4		15.5	23.8	76.2	
Lysozyme	12.3	13.9	38.8			35	78.7	21.3	
TP and silica	5.1	13.9	32.6	8.3	20.6	19.4		20.5	79.5
TP/silica/GOx/CNT	2.8	10.3	14.1	47.6	12.8	12.4	6	63.6	29.4

The initial microscopy and spectroscopy demonstrated the formation of a heterogeneous matrix composed of silica particles that encapsulate GOx and CNT, attached to TP as a model electrode surface. The electrochemical characteristics of the GOx/CNT composite were then investigated further by cyclic voltammetry. The key issue was to determine whether GOx can undergo DET when immobilized at a carbon electrode surface. Initially, the DET between the active sites of GOx and the electrode was investigated in the absence of glucose (i.e., no catalytic turnover). Two types of carbon electrodes (screen-printed and TP) showed similar behavior. The cyclic voltammograms of GOx/CNT modified carbon electrodes (Figure A-3, curve 2) show that a pair of well-defined redox peaks (reduction and oxidation) was observed. The formal redox potential is –406 mV at pH 6.2 versus Ag/AgCl, which is close to the redox potential of the FAD/FADH$_2$ cofactor in the enzyme. The redox peaks can be attributed to the redox reaction at the active site of GOx immobilized on the surface of the electrode.
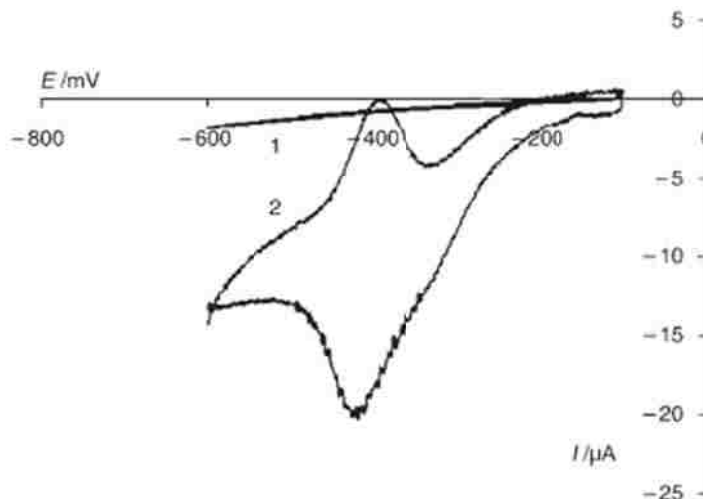
Figure A-3 Cyclic voltammogram of GOx modified electrodes. Line 1: GOx in silica; Line 2: GOx and CNT in silica. (Electrolyte described in text, scan rate is 20 mV s^{-1})

Control experiments in the absence of silica, which rely on nonspecific binding of GOx to TP, exhibit no electrochemical activity. In the presence of CNT but without silica in the matrix, DET has been successfully demonstrated.[258] Such experiments, however, rely on a material set where the CNT phase is synthesized directly on the TP matrix. Control experiments show no redox peaks in the absence of the CNT, despite the presence of GOx (Figure A-3, curve 1) suggesting that electrical contact between the redox center of GOx and the carbon electrode is provided by close proximity of the CNT, serving as a matrix of nanowires within the silica film. This hypothesis was validated by XPS analysis, which confirmed the co-immobilization of GOx with CNT inside the silica matrix. The intensity of the anodic and cathodic peak currents increases with increasing scan rate (Figure A-4a). In addition, there is a linear proportionality between the anodic and cathodic peak currents as the scan rate ranges from 40 to 250 mV s^{-1}, a typical characteristic of thin protein film electrochemical behavior (Figure A-4b). The electrochemical characteristics indicate that the reaction is not a diffusion-controlled

process and the redox peaks are from the surface-bound prosthetic group FAD of the GOx. The peak separations from 24 to 50 mV at a scan rate of 10–100 mV s^{-1} indicate that the heterogeneous pseudo-reversible electron-transfer process was fast. The calculated electron-transfer rate constant of 2.6 s^{-1}, is comparable to that previously reported for nanotube-modified electrodes and significantly greater than the magnitude reported for self-assembled monolayer electrodes.[253, 275, 276]
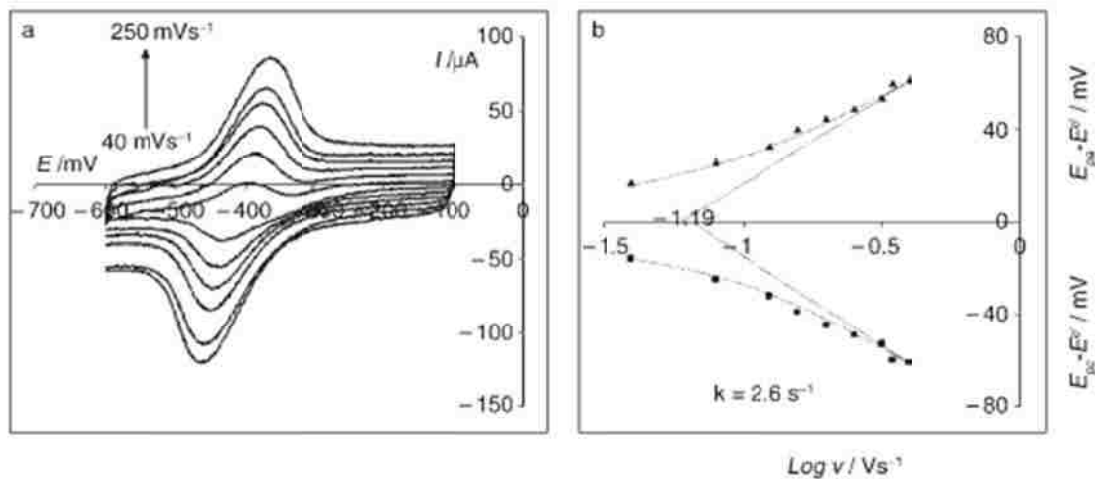
Figure A-4 a) Cyclic voltammograms of GOx and CNT in silica showing effect of increasing scan rate from 30 to 250 mV s^{-1} and b) the corresponding Laviron plot

The ability of glucose oxidase to simultaneously undergo DET with the electrode and retain its catalytic activity was confirmed by demonstrating the catalytic activity of the immobilized GOx/CNT in the presence and absence of glucose (Figure A-5). It was further confirmed by a standard non-electrochemical activity assay during stability studies of the immobilized enzyme, through the manifestation of its catalytic activity over a period of time (Figure A-6). Figure A-5 presents cyclic voltammetry observations of the redox transformations of FAD/FADH$_2$ associated with the active site of GOx immobilized in the CNT/silica matrix. In the presence of glucose, the anodic and cathodic

peaks are shifted significantly towards oxidative current values. This peak shift is as a direct result of enzyme activity and can be explained by an enzyme-activity-induced decrease in oxygen at the surface of the GOx-modified electrode.
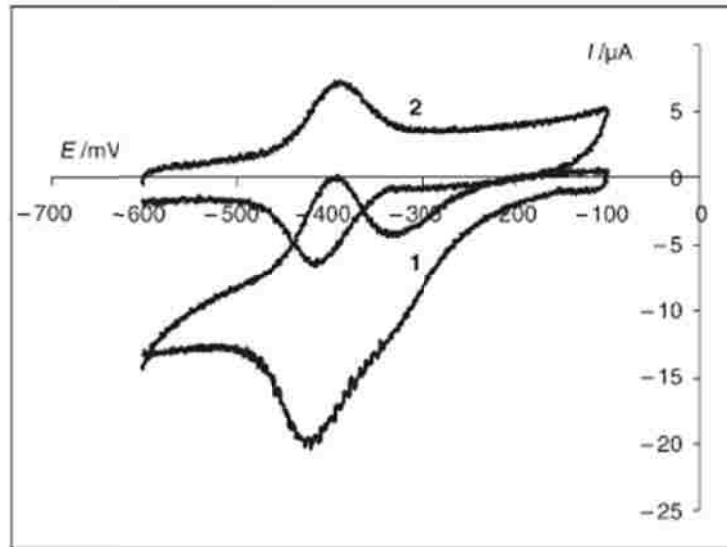
Figure A-5 Cyclic voltammograms of GOx and CNT in silica in the absence (Line 1) and presence (Line2) of 40 mM glucose at a scan rate of 20 mV s^{-1}
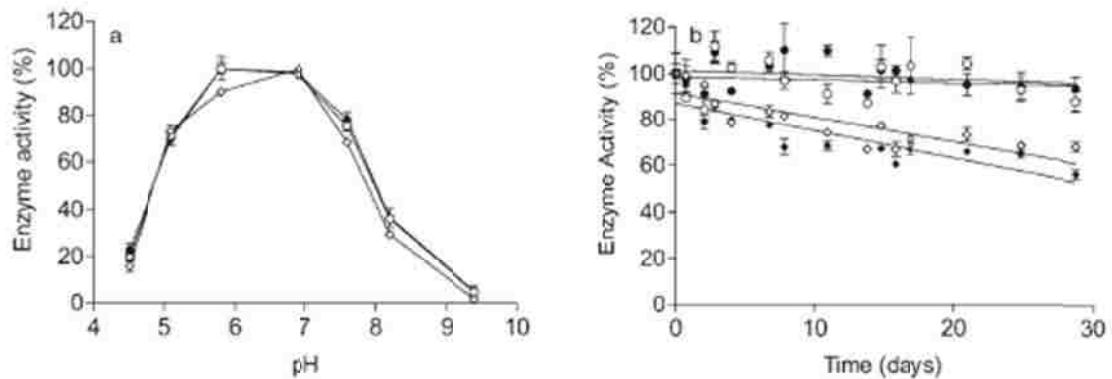
Figure A-6 Effect of silica immobilization upon the pH profile (a) and stability (b) of immobilized GOx. Key: soluble GOx (◊); soluble GOx and CNT (♦); GOx immobilized in silica (○); GOx and CNT immobilized in silica (●). Linear regression lines were calculated using GraphPad Prism (v3.03).

The surface concentration of GOx within the silica matrix (Γ) was calculated to be $\approx 2.5 \times 10^{-11}$ mol cm^{-2}, which, assuming the average effective diameter of a single GOx

molecule to be ≈ 6.0 nm, corresponds to a surface area of ≈ 4.2 cm^2. The total amount of

GOx immobilized (deposited) on the electrode surface was 4.1×10^{-9} mol, indicating that

less than 1% of the introduced GOx was electroactive in terms of DET, in good

agreement with previous studies.[277] The data suggests that the electrochemically active

GOx (2.5×10^{-11} mol) forms a monomolecular electroactive layer on the electrode surface.

The high efficiency of the biomimetic silicification reaction for the simultaneous

entrapment of CNT and GOx at an electrode surface is attributed to the mild

immobilization conditions that minimize enzyme denaturation and provides a

stabilization effect for the resulting composites. As such, we examined the stability of the

silica-entrapped GOx/CNT composite in respect to catalytic activity. Enzyme activity of

soluble GOx with glucose was comparable in the presence or absence of CNT (data not

shown). Silica encapsulation of GOx provided an immobilization efficiency of $\approx 18\%$

(17.9 ± 1.9). The immobilization efficiency of GOx in the presence of CNT was slightly

higher at $\approx 25\%$ (26.0 ± 0.55) and was attributed to nonspecific binding of GOx to the

CNT that provides a preliminary scaffold to stabilize the enzyme activity during

subsequent silica encapsulation.[278] The silica formation appears to cause some initial

inactivation of the enzyme because of the alkaline reaction conditions. Silica

immobilization of GOx was not as high as has been observed for other enzymes and this

is attributed to the loss of activity of GOx upon disparate changes in pH. Silica formation

from lysozyme requires pH>7, whereas GOx has a pI of 4.2. Although the silica

formation reaction is rapid (<2 min), some loss of enzyme activity upon rapid changes in

local pH may occur. The immobilized enzyme, however, retained its enzymatic activity

and retains a pH activity profile comparable to the native GOx suggesting that no

significant catalytic modification of the enzyme active site has occurred (Figure A-6a). In addition, silica-immobilized GOx is stable when stored at 25 °C for up to one month. Soluble GOx undergoes slow denaturation over time under the same conditions (Figure A-6b). The enhanced stability provided by silica encapsulation may therefore provide an opportunity to develop enzyme-based DET systems that can withstand continuous operation over a time frame that has not yet been realized.

A.4. Conclusions

In conclusion, we have demonstrated the potential to create bioinorganic functional nanomaterials that serve as a starting point for a variety of technology solutions. Potential applications include sensor systems, actuation devices and micropower sources. The immobilization of GOx in a silica matrix, doped with CNT, was demonstrated and supported efficient electrical conductivity. The high electroactive surface area of the composite confirms the understanding that intimate contact between the enzyme molecule and electrode surface is a prerequisite for DET bioelectrocatalysis.

The immobilization not only stabilized enzyme activity over a period of at least one month but also facilitates mediator-free DET coupled to the oxidation of glucose. The method of co-immobilization of enzyme and CNT based on a biomimetic silicification reaction demonstrates a number of advantageous properties including excellent film-forming ability, good adhesion, biocompatibility and bioelectrocatalytic properties. Enzyme immobilization with direct bioelectrocatalysis is widely applicable, for example, in mechanistic studies of enzyme reactions in biological systems. Primarily, however, the GOx electrode system demonstrated herein based on DET provides significant simplification and application to the design of an anode for biofuel cell applications. The

inherent change in electrochemistry of the system in the presence and absence of glucose as substrate, however, also provides a further opportunity to develop the system for sensitive glucose detection and application in the field of reagent-free glucose sensors.

Appendix B. Chemical polymerization and electrochemical characterization of thiazines for NADH electrocatalysis applications

Marguerite N. Arechederra[a], Courtney Jenkins[a], Rosalba A. Rincón[b], Kateryna Artyushkova[b], Plamen Atanassov[b], Shelley D. Minteer[a,*]

[a] Chemistry Department, Saint Louis University, St. Louis, MO 63103, United States
[b] Department of Chemical & Nuclear Engineering, Center for Emerging Energy Technologies, University of New Mexico, Albuquerque, NM 87131, United States
Published: Electrochimica Acta, 2010

Abstract

Electrochemically polymerized azines have been employed frequently as NADH electrocatalysts in biosensors and biofuel cells. However, some applications of these electrocatalysts do not lend themselves to electropolymerization. Therefore, this research investigates the chemical synthesis and application of poly(methylene blue) (PMB) and poly(methylene green) (PMG) in electrocatalysis. In an attempt to develop a simple synthesis for polymerized thiazines that could be immobilized on any surface, we investigated several polymerization protocols that are described in this paper. Structural analyses imply that the chemically synthesized polymers are chemically unique in comparison to the electropolymerized polymers. Amperometric investigations were used to compare the catalytic activity of chemically and electrochemically synthesized polymers as electrocatalysts for the oxidation of NADH and the chemically synthesized polymers were employed at the bioanode of a methanol/air biofuel cell to show their utility for this application.

Keywords: NADH electrocatalysts, thiazine, poly(methylene green), poly(methylene blue), biofuel cells.

B.1. Introduction

Poly(methylene green) (PMG) and poly(methylene blue) (PMB), both polymerized thiazine dyes, have been researched for their application as NADH electrocatalysts in biofuel cells.[6, 229] For biofuel cells, the bioanodes consist of a thin layer of the polymerized electrocatalyst coated with NAD-dependent dehydrogenase enzymes.[6] These enzymes catalyze the oxidation of the fuel and reduce NAD^+ to NADH. The NADH is then oxidized by the PMG or PMB at the electrodes surface to regenerate NAD^+. This bioanode system has been implemented in glucose,[88, 208] pyruvate,[7] malate,[144] and alcohol biofuel cells.[66, 229, 279] Besides their use in biofuel cells, PMG and PMB have been studied in a similar manner for enzymatic biosensor applications.[66, 69, 280]

Both methylene green (MG) and methylene blue (MB), shown in Figure B-1, are electrocatalysts for NADH. Their catalytic activity is due to their structural similarities to the flavonoid that is responsible for the catalytic oxidation in nature[281, 282] and because their half wave potentials are more positive than that of NADH.[88]
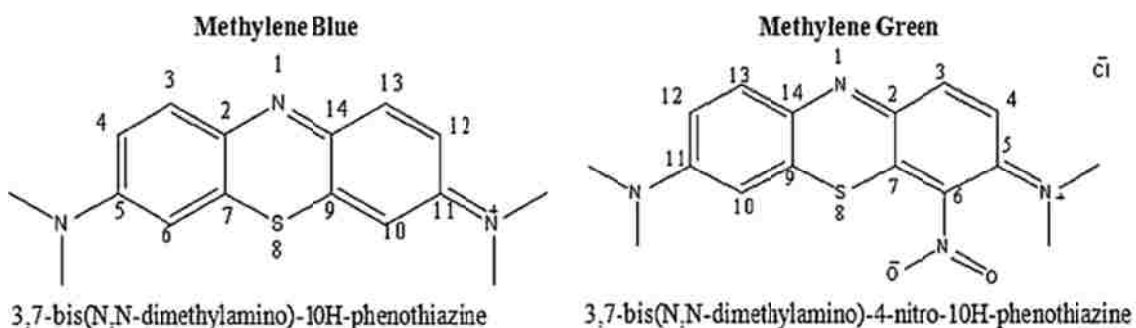
Figure B-1 Chemical structure of the monomers, labeled carbons and names according to IUPAC chemical nomenclature

In order to better understand the structure of the polymers and the functional relationship to their uses, the electrochemistry of the polymers has also been analyzed in detail in several papers with differing electropolymerization protocols.[70, 124, 141, 227, 232]

Although electropolymerized polymers have shown their use in applications and their catalytic activity, there are some applications where electropolymerizing is not feasible. For this reason, it is important to consider chemical synthesis approaches, which have been employed for other conducting polymers. For example, chemical syntheses for polymerizing aniline and dimethylaminoaniline have already been developed.[283, 284] In this paper, we employ two chemical synthesis approaches in making PMG and PMB. These chemical synthesis protocols are modifications of the protocols employed in the references above for aniline and dimethylaminoaniline. We were interested in using Ce^{3+} as an initiator in acidic conditions since Hand and Nelson showed that this protocol can cause direct coupling of dimethylaminoaniline cationic radicals.[283] In another experiment of interest, aniline undergoes oxidative polymerization as described by Yasuda and Shimidzu through a Fe^{3+} catalyst and more mild conditions.[284] We had postulated that MG and MB would undergo similar polymerization chemistry as aniline and dimethylaminoaniline in the protocols described, due to their similarities in functional groups and aromatic nature.

In the present paper, we are reporting the modification of a glassy carbon electrode with chemically polymerized PMG and PMB and comparing them to electropolymerized PMG and PMB. The redox chemistry was studied first in order to determine which polymers would be ideal candidates for electrocatalysis. The kinetics of the electrocatalysts are also reported. We have proposed structural features of the polymers

based on UV–vis, nuclear magnetic resonance (NMR), and X-ray photoelectron spectroscopic (XPS) chemical analyses. Finally, we compared the performance of the chemically and electrochemically synthesized polymers as electrocatalysts in a methanol/air biofuel cell to show their utility for this application.

B.2. Experimental

Materials and electrode preparation

All of the chemicals used were of analytical grade and used without further purification. All aqueous solutions were prepared using 18 MΩ water. Tetrabutylammonium bromide modified Nafion was prepared by a previously established procedure.[208] A CH Instruments 650a potentiostat interfaced to a PC was used for all experiments along with a glassy carbon electrode (GCE) as the working electrode, a saturated calomel electrode (SCE) as the reference electrode and platinum mesh as the counter electrode, unless otherwise stated. Prior to the film depositions or immobilization, the GCEs were polished with 0.05 μm alumina on Buehler polishing pads and washed thoroughly. The GCEs used for electropolymerization of polymers were pretreated by running cyclic voltammetry from −2.0 to 2.0 V at a scan rate of 0.05 V/s in concentrated nitric acid for four segments or until a constant background was reached.

Electrochemical synthesis

The working electrode was placed in a solution of pH 7.0 phosphate buffer with 0.5mM monomer and 0.1M KNO3, which had been purged with nitrogen for 1 h. The film was formed by 12 segments of cyclic voltammetry at a scan rate of 50 mV/s and a potential window between −0.6 and 1.3 V for PMB and −0.5 and 1.3V for PMG. After polymerization, the electrodes were rinsed with water and allowed to dry before use.

Chemical synthesis and immobilization

PMB and PMG were chemically synthesized using a protocol similar to that described by Yasuda and Shimidzu[284] in the oxidative polymerization of aniline. 0.28 g of monomer (MG or MB), 91.7 mL water and 8.3 mL of concentrated HCl were mixed and cooled in a dry-ice bath overnight. This was followed by the addition of 0.81 g of iron(III) chloride.[284] The polymers were purified with gravimetric filtration using successive rinses of 1 M hydrochloric acid, 1 M ammonia, 1-methyl-2-pyrrolidone, methanol, and diethyl ether.[284] This protocol resulted in a PMB product that appeared black and a PMG solid product that appeared dark green, almost black. These products will be referred to as Yasuda PMB and Yasuda PMG for the remainder of the paper.

Using a protocol similar to Hand and Nelson[283] for the oxidative polymerization of aniline analogues, a solution of 0.25 g of monomer (MG or MB), 62.5 mL methanol and 12.5 mL concentrated H_2SO_4 was cooled in a dry-ice bath overnight followed by the addition of 0.42 g cerium(IV) sulfate and 0.69 g ammonium cerium(IV) nitrate. The color of the PMB product was gold and that for PMG was cranberry. These products will be referred to as Hand PMB and Hand PMG for the remainder of the paper.

In order to produce a porous layer of the chemically synthesized polymers on glassy carbon electrodes, a solution of 0.71 mg of PMB (or 0.81 mg of PMG) was mixed with 5.0 mL of acetonitrile. A drop of the solution was pipetted on the glassy carbon electrodes and the electrodes were dried in a vacuum desiccator.

Voltammetric evaluation of PMG and PMB

To evaluate the electrochemical properties of the PMG and PMB films, the polymer modified glassy carbon electrodes were equilibrated in 10m M pH 7.4 phosphate buffer

with 1 M sodium nitrate. Cyclic voltammograms were obtained on the GCEs at a scan rate of 50 mV/s. The potential window used was −0.5 to 0.5 V versus SCE.

NADH electrocatalysis studies

The electrochemical experiments were carried out in a traditional three-electrode electrochemical cell. A Ag|AgCl (saturated KCl) reference electrode was used for these experiments and a platinum counter electrode. Amperometry was performed in pH 7.4 phosphate buffer with 1M sodium nitrate with an application of +200mV versus Ag|AgCl upon the addition of 0.1, 1, 10, 25 and 50 mM NADH. Plots of current versus concentration were utilized to determine the V_{max} and the corresponding k_{cat} for each polymer.

Methanol/air biofuel cell

Toray paper electrodes were used for the bioanodes. For the electrochemically synthesized polymers, a thin film of methylene blue or methylene green was electropolymerized onto the surface utilizing the electropolymerizing procedure described above. The electrodes were rinsed with 18 MΩ water three times and allowed to air dry overnight.

In order to immobilize the chemically synthesized polymers, we used a similar protocol to that for the NADH experiments. However, we added a stabilizing agent. The stabilizing agent, tetrabutylammonium fluoride (TBAF), was chosen since the electro-negativity of fluoride in the salt makes it a good candidate to interact with the positively charged polymers thus preventing them from being as soluble in buffer and enzyme casting solution. So, each polymer was immobilized on the bioanode by mixing 0.71 mg

of PMB (or 0.81 mg of PMG) and 0.01 M TBAF in 5.0 mL of acetonitrile. 50 μL of the mixtures were pipetted onto the electrodes and dried in a dessicator for at least 2 h.

Next, the azine coated electrodes were coated with a casting solution containing a mixture of Nafion suspension and enzyme solution. 1 mg of NAD+ and 1 mg of alcohol dehydrogenase were added to 1 mL of pH 7.4 phosphate buffer and vortexed. 200 μL of enzyme buffer solution was mixed with 100 μL of tetrabutylammonium bromide modified Nafion® polymer suspension. The mixture was vortexed for at least 2 min a 3000 rpm. 50 μL of enzyme/Nafion casting solutions were pipetted onto 1 cm^2 of Toray carbon paper electrode that was previously coated with either a chemically synthesized polyazine or electropolymerized with an azine and left to air dry in the refrigerator for at least 24 h. Once dry, the electrodes were soaked in electrolyte/coenzyme solution in the refrigerator for at least 24 h. Electrolyte and coenzyme solution was 10 mM pH 7.4 phosphate buffer containing 6 M of sodium nitrate and 1.5 mM of NAD$^+$. This sodium nitrate concentration was sufficiently high to minimize cell resistance. Electrochemical measurements were carried out in a custom fabricated test cell as described in Arechederra et al.[285] Toray carbon paper was used for the bioanode as described above and commercial gas diffusion electrodes containing Vulcan XC-72 with 20% platinum (PEMEAS E-TEK) were used for the cathode and hot pressed against the Nafion® NRE-212 PEM (Sigma).

Analytical characterization techniques

For NMR, the polymers were dissolved in 600 μL of methanol-d_4. 128 scans of proton NMR were run on a 400 MHz Ultrashield^{TM} Bruker NMR for each sample. For UV–vis spectroscopy, analyses were obtained with a UV-2501 PC Shimadzu instrument. The

electrochemically synthesized polymer was studied by polymerizing them onto indium tin oxide coated glass microscope slides and the monomers and chemically synthesized polymers were dissolved in methanol and acetonitrile, respectively. XPS analysis of the polymer layers was performed on a Kratos AXIS Ultra photoelectron spectrometer using a monochromatic Al Kα source operating at 300 W. All of the spectra were charge referenced to the aliphatic carbon at 284.8 eV. Individual peaks of constrained width, position and 70% Gaussian/30% Lorentzian line shape were used for curve fitting. XPS of powders was performed for the monomer and chemically synthesized polymers. Analysis of the electropolymerized polymers on GCEs were performed as well.

B.3. Results and discussion

We synthesized PMG and PMB utilizing two different chemical protocols. The first protocol derived from Hand and Nelson employed cerium as an oxidant.[283] The synthesis derived from Yasuda and Shimidzu employed iron instead.[284] Whereas the protocol derived from Hand and Nelson used a much more powerful oxidant, we postulated that this difference may be a determining factor in the resulting PMG and PMB polymers, as well as their electrochemical and electrocatalytic activity.[283] The protocols for the two syntheses resulted in solid polymer precipitating out of solution and a color change was noted for each of the polymers as discussed in Section 2.

The electrochemistry for each polymer was studied using cyclic voltammetry within the potential window of −0.5 to 0.5 V. This window was chosen, since it is the potential window typically employed for evaluating the electrochemistry of the electropolymerized polymers. Representative cyclic voltammograms are shown in Figure B-2. For reference, the electrochemically synthesized polymers are labeled with the abbreviation ES in the

figures. There were no defined redox peaks for the polymers produced from the Hand protocol signifying a gross structural change to the monomer. The half wave potentials for the polymers formed from the Yasuda protocol were at −0.009 and 0.174 V versus normal hydrogen electrode (NHE) for PMB, which compare to peaks at −0.025 and 0.013 V versus NHE for the electropolymerized PMB. The half wave potentials for Yasuda PMG were at 0.023 and 0.196 V versus NHE, which compare to peaks at −0.011 and 0.209 V versus NHE for the electropolymerized PMG. Since the Hand polymers did not have any peaks within the potential region of interest, we did not proceed with the study of them for our NADH studies.
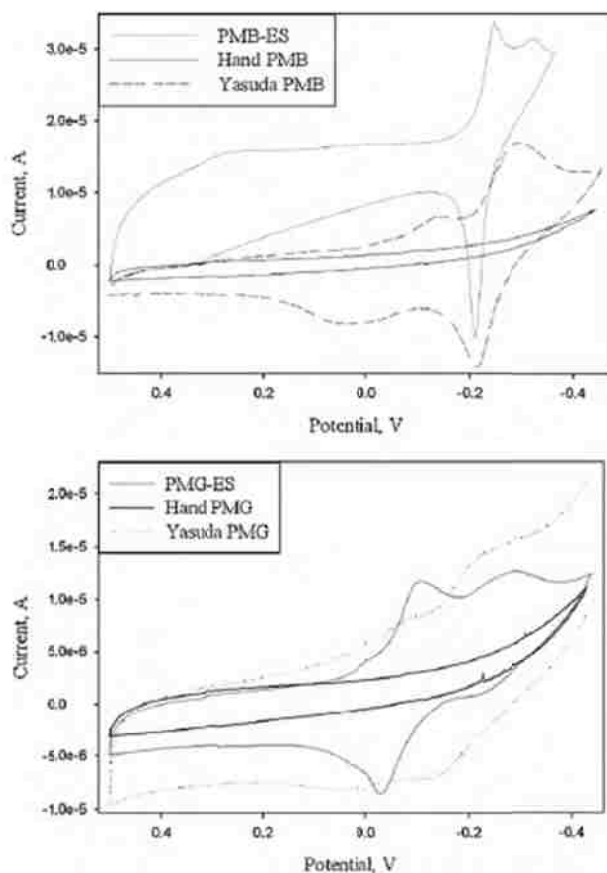
Figure B-2 Representative cyclic voltammograms showing the redox chemistry of (1) PMB-ES, Hand PMB and Yasuda PMB modified glassy carbon electrodes and (2) PMG-ES, Hand PMG and Yasuda PMG modified glassy carbon electrodes in buffer.

The six polymers were analyzed with UV–vis. These results can be seen for methylene blue and its polymers in Figure B-3(a) and for methylene green and its polymers in Figure B-3(b). The UV–vis absorbance spectra of the Yasuda products are strikingly similar to that of the monomers at lower energies. Additional peaks are seen for Yasuda PMB at 390 and 490 nm and at 315, 370 and 430 nm for Yasuda PMG.
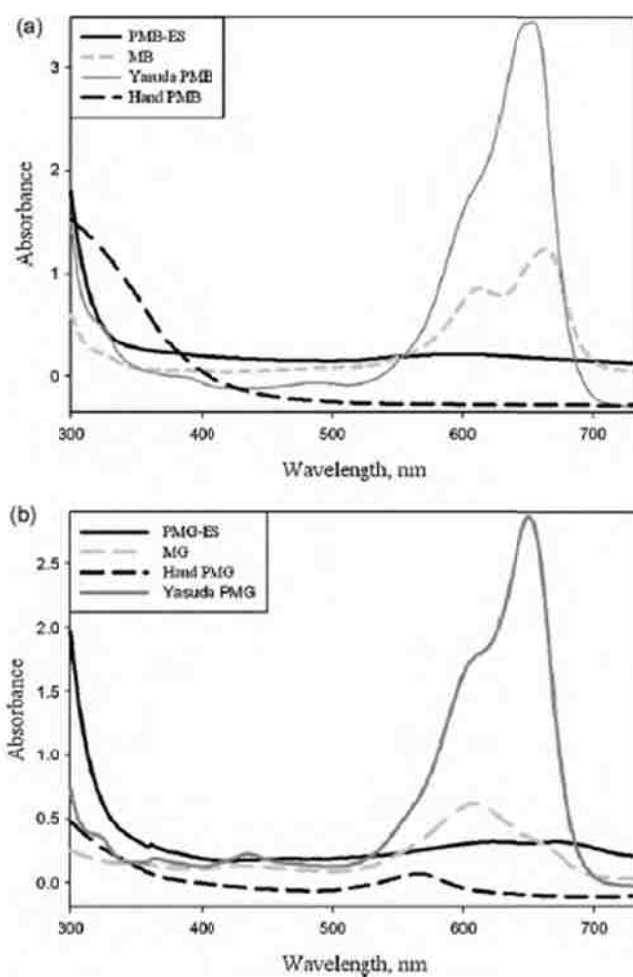
Figure B-3 UV-Vis spectra obtained for the (a) methylene blue and (b) methylene green and its polymers

We believe these are indicative of increased aromaticity, possibly from a double bond formed from a nitrogen to nitrogen linkage between monomer units. However, the polymers synthesized with the Hand and Nelson protocol had completely different UV–vis absorbance spectra. Hand PMB has a broad peak at 340 nm and Hand PMG has a peak at 575 nm. The uniqueness of the spectra for the materials formed from the synthesis by Hand and Nelson is more evident that this protocol results in material that is dramatically different in structure when compared to the monomers and all of the other polymers. The difference in the electronic transition of the material formed from the Hand and Nelson protocol may be partly due to the absence of methyl groups at the non-pyridinal nitrogens, but would not entirely account for such a large change indicating that a major backbone or functional group change(s) occurred.

As for NMR analyses, the chemical shifts observed in the NMR spectra of the monomers and the polymers are listed in Table B-1. Both chemically synthesized poly(methylene blue) products uniquely generated a peak at δ 2.8, which we believe is representative of a N–N bond. Yasuda PMB, uniquely, produced a peak at δ 1.3, which is indicative of the linkage between the two nitrogens along with the addition of a methyl group. Peaks at δ 3.8 and δ 4.5 are unique to the Hand PMB sample. ChemExper predicts that these peaks may be from the addition of a hydroxyl on the sulfur atom, indicating that the sulfur may have been converted to a sulfone group. The peaks from δ 6.5 to δ 8.7 in the ^{1}H NMR were used to analyze the aromatic portion of the tetradecalin backbone ring system. A doublet of doublets is a typical feature within this region for aromatic structures. This was seen at δ 7.4 for MB, δ 7.5 for MG, δ 7.5 for Yasuda PMB and δ 8.7 for PMB-ES. The fact that we did not see this with the PMG-ES, Hand PMG and Hand

PMB means that the protons in the aromatic region have very different chemical environments as compared to the monomers.

Table B-1 NMR shifts (δ) in ppm and coupling constants (J) in hertz for the polymers

Sample	δ (ppm)
MB	1.0 (s, NH), 3.5 (s, CH), 4.6 (s, CH), 4.9 (s), 7.3 (d, CH J 2.77), 7.4 (dd, CH J 9.61, 2.77), 7.9 (d, CH J 9.67)
MG	1.1 (s, NH), 1.2 (s, NH), 2.6 (s, NH), 3.4 (s, CH), 7.3 (d, CH J 2.85), 7.5 (dd, CH J 9.69, 2.76), 7.9 (d, CH J 9.51), 8.0 (d, CH J 0.65)
Hand PMB	1.1 (t, NH), 1.3 (s, NH), 2.0 (s, NH), 2.1 (s, NH), 2.5 (s, NH), 2.7 (s, NH), 2.8 (s, NH), 3.4 (s, CH), 3.5 (s, CH), 3.5 (s, CH), 3.7 (s, CH), 3.7 (s, CH), 3.8 (s, CH), 4.1 (s, CH), 4.5 (s, OH), 4.6 (s, CH), 5.0 (p, CH), 7.3 (t, CH J 51.0, 0.13), 8.1 (s, CH)
Yasuda PMB	0.84 (s, NH), 1.1 (sextuplet, NH, 1.01), 1.2 (s, NH), 1.3 (s, NH), 2.8 (s, NH), 3.1 (p, CH J 1.68), 3.2 (s, CH), 3.4 (s, CH), 3.5 (s, NH), 7.4 (d, CH J 2.77), 7.5 (dd, CH J 9.64, 2.76), 8.0 (d, CH J 9.58)
Hand PMG	1.1 (s, NH), 1.2 (d, NH), 1.8 (s, NH), 1.9 (s, NH), 2.2 (s, NH), 3.1 (p, CH), 3.1 (s, CH), 3.4 (s, CH), 3.5 (s, CH), 3.7 (d, CH), 7.9 (s, CH)
PMB-ES	2.3 (s, NH), 2.4 (s, NH), 2.5 (s, NH), 4.5 (p, CH J 1.62), 4.7 (s, CH), 4.8 (s, CH), 5.1 (s, CH), 5.7 (s, CH), 6.0 (p, CH J 1.51), 6.3 (s, CH), 7.0 (s, CH), 8.5 (s, CH J 9.72), 8.7 (dd, CH J 2.73, 9.66), 9.1 (s, CH)
PMG-ES	0.9 (s, NH), 1.2 (m, NH), 1.3 (d, NH J 0.72), 1.4 (m, NH), 1.5 (s, NH), 1.6 (s, NH), 1.7 (s, NH), 2.0 (d, NH), 2.2 (s, NH), 2.5 (s, NH), 2.6 (d, NH J 0.92), 2.7 (s, NH), 3.0 (s, CH), 3.2 (s, CH), 3.4 (s, CH), 3.7 (t, CH J 5.6), 3.9 (d, CH J 5.16), 4.85 (s, CH), 8.1 (s, CH)

Abbreviations: s (single), d (doublet), dd (doublet of a doublet), t (triplet), p (pentet), o (octet) and m (multilet).

As for the XPS analyses, Table B-2 shows elemental analysis results for MB and MG powders and some of the polymers. Table B-3 shows the high resolution spectra for these same materials. When compared to the monomer, the Hand PMB and Hand PMG polymers uniquely have a smaller percentage of carbon and at least twice as much oxygen and sulfur than the monomer. The largest increase in functional groups according to the deconvolution data belongs to the S–O linkages for these polymers. These observations may correspond to the loss of methyl groups and the addition of a hydroxyl group(s) to the structures during polymerization. From this observation, it can be inferred

that the sulfur gets oxidized to a sulfone for the Hand polymers. Also, there is evidence in literature that it is possible that the Hand and Nelson reaction oxidatively cleaves one sulfur carbon linkage, so that the two rings are only linked by the nitrogen in the center of the ring system,[286] which would also be consistent with the UV–vis spectra. The power of cerium as an oxidant is demonstrated in a reaction described by He and Horiuchi[286] in which cerium is used as a reactant to break an oxygen to carbon bond thus breaking open a ring, which is accompanied by further oxidation. In the case of the Hand PMB and PMG synthesis, the thiazine's sulfur to carbon bond (which is even weaker of a bond than that studied by He and Horiuchi[286]) may break open upon addition of the cerium followed by further oxidation. Thus, we believe that the strength of the oxidants in the Hand synthesis caused the resulting polymer structures to vary dramatically from that of the monomer or any other polymer studied in this paper.

Table B-2 Elemental quantification of the polymers and their monomers

	C 1s (%)	N 1s (%)	O 1 (%)	S 2p (%)
MB	80.7	5.0	12.8	1.5
PMB-ES	65.0	13.1	18.2	3.7
Hand PMB	50.2	4.8	38.0	7.0
Yasuda PMB	75.9	9.7	11.8	2.7
MG	75.3	13.4	8.2	3.1
PMG-ES	67.8	12.2	16.8	3.2
Hand PMG	65.7	3.2	27.5	3.5

As for the nitrogen percentage results in the XPS, the composition of nitrogen in the PMB-ES is more than double the monomer indicating nitrogen linkage with the removal of another functional group such as a proton or methyl. There is an increase in the representation of the pyridinic N for the electrochemically synthesized polymers only indicating more of an aromatic polymer than the monomers. This determination led Rincón and colleagues to establish that one of the possible links for polymer formation is

at ring–N(CH$_3$)–ring.[70, 73] Both polymers synthesized electrochemically show a significant increase in most other types of nitrogen, except nitro nitrogens, as well. Thus, the nitro group must not play a role in the polymer formation. This is expected due to the fact that the electrochemistry of methylene green and methylene blue as electrochemically synthesized polymers are similar. It is noteworthy that the nitro group is not affected for any of the polymers, nor does any other analysis in our laboratory thus far indicate this. Thus, the data from the deconvolution data also shows that the Hand and Yasuda polymers are joining by the non-pyridinal nitrogens.

Table B-3 High resultion XPS spectra of the polymers and monomers

	C-C	C*,C-S	C-N-C (pyridinic)CH$_3$-N	C-O	C-O/N-C-O	C-N-C	N-R$_3$, NH(CO)O, NH(R)$_2$	Pyridine+, N(R$_3$)+, NH$_3$+/NCH$_3$+	NO$_2$	S-O	S-O, O-C-O*	O*-C-O	C-S	C$_2$-S-O$_2$ (sulfone)
	284.6	285.3	286.1	287.0	288.7	399.6	400.4	401.9	405.9	531.5	532.2	533.6	164.1	168.1
MB	25.9	33.9	9.2	6.2	5.7	4.2			0.5	1.2	6.5	5.1	0.9	0.6
PMB-ES	19.3	14.6	19.4	4.3	7.9	4.4	6.1		1.8	7.8	8.7	1.9	2.4	1.4
Hand PMB	15.2	21.1	5.9	4.0	4.0	0.9		3.4	0.4	8.7	22.7	6.5		7.1
Yasuda PMB	18.1	25.0	22.6	5.1	5.1	7.1		1.2	1.4	3.3	6.4	2.0	2.2	0.5
MG	20.9	37.8	6.3	5.6	4.8	8.5		1.4	4.0	0.7	4.8	1.0	2.0	1.1
PMG-ES	24.1	18.4	12.3	4.5	8.4	0.5	4.7	0.5	4.2	6.2	7.7	1.1	2.2	1.0
Hand PMG			19.4	15.5	1.7					100	50.1			

The binding energy (eV) for each peak is represented by the italicized numbers.

Now that we have thoroughly characterized the chemically synthesized polymers and briefly studied their redox chemistry, we studied their activity as an electrocatalyst for NADH oxidation. The kinetics of the ES and Yasuda polymers are compared in Figure B-4. The same experiments were performed with a blank glassy carbon electrode and these are shown in Figure B-4 as well. The error, in large part, is due to the difference in the surface of the GCEs[124] and the non-uniformity of each polymer film.[85] The moles of catalytic sites for the GCEs were compared by integrating the area under the redox peaks of the cyclic voltammograms. For the electrodes with PMB-ES, PMG-ES, Yasuda PMB

and Yasuda PMG as the electrocatalyst, the number of picomoles of catalytic active sites are listed in Table B-4.
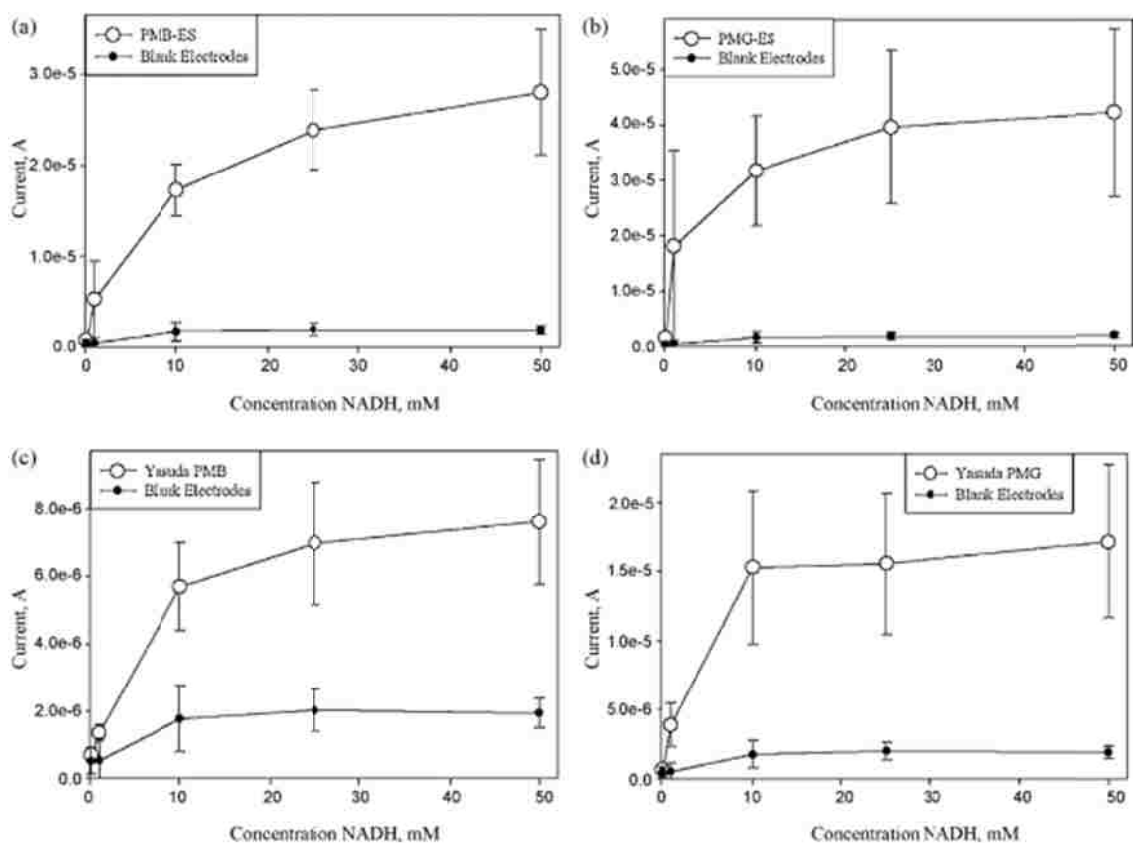
Figure B-4 Amperometric current measured from the electrocatalysis of NADH by (a) PMB-ES, (b) PMG-ES, (c) Yasuda PMB and (d) Yasuda PMG modified glassy carbon electrodes by varying NADH concentration in pH 7.4 phosphate buffer with 1 M NaNO₃

Whereas it has already been established in the past that PMG-ES is a better electrocatalyst for the oxidation of NADH than PMB-ES,[88] here we present the k_{cat} for comparison of the Yasuda polymers as well. These values are listed in Table B-4. Since Yasuda PMG's rate of catalysis is three times more than any other polymer studied—including the electrochemically synthesized polymers, this makes it a more attractive electrocatalyst for biofuel cells and other nicotinamide-based systems.

Table B-4 k_{cat} values for chemically and electrochemically synthesized polymers

Polymer	Number of picomoles of catalytic active sites	k_{cat} (s^{-1})
PMB-ES	143 ± 19	1.05 ± 0.40
Yasuda PMB	49.4 ± 1.5	1.52 ± 0.66
PMG-ES	39.4 ± 11.6	6.16 ± 3.16
Yasuda PMG	29.2 ± 14.8	19.0 ± 6.8

After evaluating the NADH electrocatalysis of the chemically synthesized polymers and comparing them to the electropolymerized polymers, the chemically synthesized polymers were employed in a methanol/air biofuel cell, which shows the utility of the chemically synthesized polymers in this application. The methanol/air biofuel cell data is shown in Table B-5. The Yasuda PMG catalyst produced the highest maximum power density, but there is no statistical difference between the power density of the Yasuda PMG and the PMG-ES. This shows that a chemically synthesized form of poly(methylene green) can be used for NAD-based biofuel cell systems and although it does not improve performance, it provide comparable performance to an electropolymerized poly(methylene green). The differences in the current and power densities that were generated from the varied polymers in the methanol/air biofuel cell were not as significant as the differences in current generated from the varied polymers in the NADH amperometric studies described in the above paragraph. It is likely that the PMG polymers are not performing to their full potential due to limits from a more complicated system that has significant transport and extraction limitations.

Table B-5 Maximum current densities and maximum power densities measured from the various electrocatalytic polymers in a methanol/air biofuel cell

Polymer	Maximum current ($\mu A/cm^2$)	Maximum power density ($\mu W/cm^2$)
PMB-ES	258 ± 49	87.1 ± 35.4
Yasuda PMB	440 ± 231	125 ± 14
PMG-ES [24]	544 ± 82	136 ± 27
Yasuda PMG	491 ± 63	157 ± 37

B.4. Conclusions

Overall, this research is the first evidence of the chemical synthesis of poly(methylene green) and poly(methylene blue). Two syntheses are described using cerium and iron as oxidants. The half wave potentials and the activity of the polymers as electrocatalysts vary for the chemically synthesized polymers in comparison to the electrochemically polymerized analogs, which is consistent with analytical evidence that the structure of the chemically synthesized polymers vary from those electrochemically synthesized. Kinetic studies show that the chemically synthesized Yasuda PMG has three times higher kcat than any other polymer studied—including the electrochemically synthesized polymers. However, the chemically synthesized polymers show only comparable performance to the electrochemically synthesized polymers when used as electrocatalysts in a methanol biofuel cell due to other bioanode limitations.

Acknowledgements

Appendix C.   Electropolymerization of Methylene Green on Nanostructured Materials for NADH Oxidation

Claudia W. Narváez V.[1], Rosalba A. Rincón[1], Vinod K. Radhakrishnan[2], Virginia Davis[2], Plamen Atanassov[1]

[1]*Department of Chemical and Nuclear Engineering, University of New Mexico, Albuquerque, NM 87106, USA.*
[2]*Department of Chemical Engineering, Auburn University. Auburn, AL 36849*
To be submitted to Langmuir

Abstract

Electropolymerization of MG on nanostructured materials based on single-walled carbon nanotubes (SWNTs) was investigated and is presented on this paper. The motivation behind this exploratory research is based on the comparable size of SWNTs (diameter ~1 nm) and enzymes, which opens the possibility of creating "smart" materials that provide catalytic effects in the proximity of the enzymes. Since the focus of this work is on NAD^+-dependent enzymes and NADH oxidation needs to be catalyzed, the presence of poly-(MG) is necessary in anode design based on those enzymes. Thus, in order to utilize SNWTs to wire the enzymes to the electrode and catalyzing the NADH oxidation reaction, a question is raised on whether SWNTs can be modified with poly-(MG). A novel material called "bucky paper" which is made with SWNTs was chosen as electrode material for electropolymerization of MG. If SWNTs can be directly modified with poly-(MG) they would provide an electrocatalyst for NADH oxidation that can be placed in close proximity to the enzyme, increasing the efficiency of the catalysis and therefore of the anode.

156

C.1. Experimental

All experiments were performed in VersaSTAT 3 (Princeton Applied Research). The material characterization was performed using Scanning Electron Microscope (Hitachi S-5200).

HiPco SWNTs were obtained from Unidym Inc. (Menlo Park, CA) and had a length to diameter (aspect) ratio of ~ 600 and a purity of ~ 90%. Isopropanol (purity > 99%), methylene green (Fluka Cat. 66870), lyophilized malate dehydrogenase (MDH) (2700 units/mg) from porcine heart (USB products from Affymetrix Cat. 18665), L-(-)-malic acid (Sigma Cat. M1000), NADH (Sigma Cat. N6005), and NAD$^+$ (Fluka Cat. 43407) were used without further purification. Phosphate buffer pH 7 and TRIS buffer pH 7.4 were prepared from analytical grade reagents.

Bucky papers preparation

Two types of SWNTs bucky papers were fabricated for and employed in this work. BP1 bucky paper was fabricated by magnetically stirring 60 mg of purified HiPCo SWNTs in isopropanol (1 mg/ml) for three days to produce a uniform dispersion of small bundles. Then, the dispersion was filtered through a 0.2 μm PTFE filter paper. BP2 bucky paper was fabricated by stirring 60 mg SWNTs and 13 mg MG in isopropanol (1 mg/ml) followed by filtering the suspension through a 0.2 μm PTFE filter paper. The bucky papers were dried at room temperature for 15 minutes, peeled off the filter paper, and vacuum dried overnight at 80 °C. The thickness of the bucky papers was measured to be approximately 350 μm.

In order to maintain the SWNTs' pristine properties, no sonication or functionalization was performed. The SWNTs were stirred in isopropanol to break up

large nanotube aggregates while still retaining large ropes of nanotubes. The presence of nanotube ropes in the bucky paper increase the porosity of the bucky paper, thus facilitating enhanced transport of materials while still preserving a network for electrical conductivity. The MG and SWNTs were stirred together, prior to filtration, in order to distribute MG evenly though the nanotubes and to maximize interfacial contact between the SWNTs and MG.

Electrode construction

A cavity electrode was chosen for this study since it can be filled with any powder material for electrochemical analysis. 50% teflonized carbon powder (XC50) was used as gluing material and compacted into the cavity of the electrode. Then, a piece of bucky paper of the same diameter as the cavity was placed and pressed on top of the compressed XC50. The bucky paper's surface was then modified by poly-(MG) deposition.

Poly-(MG) was deposited on the surface of the bucky papers by cyclic voltammetry in a similar fashion to what has been described in the previous chapters. The standard three-electrode cell used Ag/AgCl and Pt wire as the reference and counter electrodes respectively, and the bucky paper-cavity electrode as the working electrode. The electrodeposition was performed by 10 CVs at a scan rate of 0.005 V/s in a range of -0.5 to 1.3 V in de-aerated 0.5 mM MG, 0.1 M KNO_3, 50 mM PBS at pH 7. Similar steps were used, also, for the rotating disk electrode (RDE) at 1600 rpm. By following this procedure, the BP1-MG and BP2-MG electrodes were built.

Hydrodynamic polarization curves

Hydrodynamic polarization curves were developed in order to find the ideal potential at which poly-(MG) on the electrodes oxidizes NADH for both BPl-MG and BP2-MG

electrodes. They were developed in quiescent mode as well in RDE experiment at 1600 rpm. The steady state currents were measured by applying constant potentials that ranged from -0.05 V to 0.35 V vs. Ag/AgCl. For NADH, the current was measured in 1 mM NADH, 10 mM NADH and a blank of PBS solutions for both BP1-MG and BP2-MG. A similar process was performed for the RDE at 1600 rpm.

NADH oxidation

For this step, the concentration of NADH stock solution was found experimentally by measuring its absorbance using UV-VIS spectrophotometer. Then, chronoamperometric curves were obtained by monitoring the steady-state current generated by periodic addition of aliquots from 58 mM NADH stock solution to the cell containing PBS pH 7. The applied potential was 0.3 V vs. Ag/AgCl, determined from the hydrodynamic polarization curves. The steady-state currents were then plotted against NADH concentration.

Evaluation of poly-(MG) modified bucky papers in an enzymatic system

Chronoamperometric measurements were also performed to evaluate the behavior of BP1-MG and BP2-MG in the presence of a NAD^+-dependent enzyme (malate dehydrogenase, MDH). The electrolyte (KNO_3 PBS pH 7) contained free enzyme in solution (0.05 mg/mL buffer) and 10 mM NAD^+ diffusive cofactor. For the evaluation of the performance of the electrodes as NADH electrocatalysts, the steady-state currents were monitored after consecutive additions of 1 M L-malate substrate at an applied potential of 0.1 V vs. Ag/AgCl. The steady-state currents were then plotted against substrate concentration to study the kinetics of the system.

C.2. Results and discussion

Characterization of bucky papers

SWNTs provide high electrical conductivity to the bucky papers. BP1 showed a resistivity of 14.7 mΩ/mg and BP2 47.2 mΩ/mg. As expected, both bucky papers show low resistivity demonstrating their quality as conducting material which is highly desirable for the electrode design. Additionally, SWNTs enhance the porosity of the electrode material which helps providing a higher surface area and would facilitate the mass transport through the electrode. The combination of porosity provided by the SWNTs and hydrophilicity provided by the isopropanol (IPA) conferred wettability to the bucky papers. The SEM images show how the strains of SWNTs effectively conferred high porosity (Figure C-1), due to the bundles formed by the nanotubes. Moreover, BP2 showed better wettability than BP1 due to the presence of MG which is highly hydrophilic. Thus the combination of IPA and MG in BP2 conferred the material with a higher hydrophilicity than BP1 (IPA + SWNTs). Due to their porosity and their hydrophilicity, both materials are quite brittle. Despite their fragility, the cavity electrode design provided easiness in the construction of the electrodes.
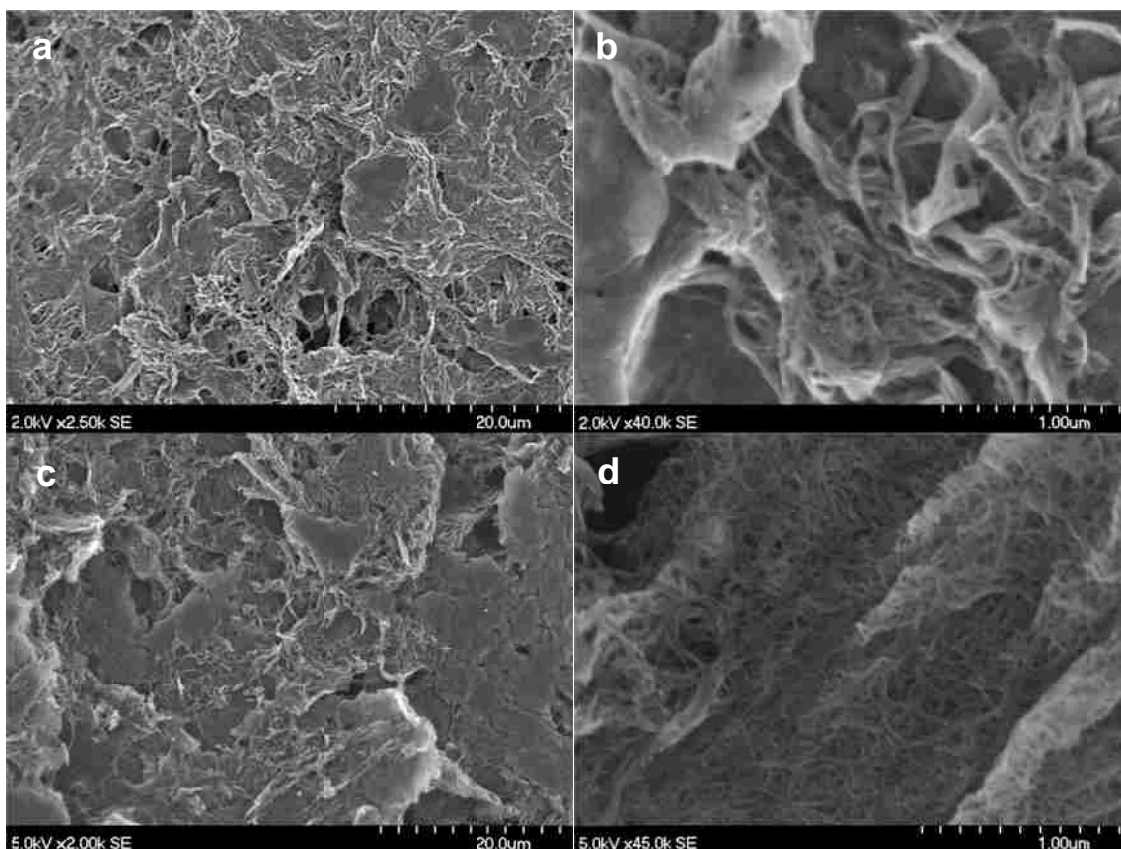
Figure C-1 SEM micrographs of unmodified bucky papers: a) and b) BP1, and c) and d) BP2

Electropolymerization of MG

MG polymerization on the bucky papers was successfully performed by cyclic voltammetry. As mentioned above, poly-(MG) was deposited on the surface of the bucky papers via CV from -0.5 and 1.3 V vs. Ag/AgCl at 5 mV/s of scan rate. The oxidative peak of MG is observed around 0.2 V vs. Ag/AgCl on both BP1 and BP2 papers (Figure C-2). The voltammograms obtained for electropolymerization on bucky papers differs from those obtained on conventional glassy carbon electrodes (Figure 5-2) due to the complete different structure of the supporting material.
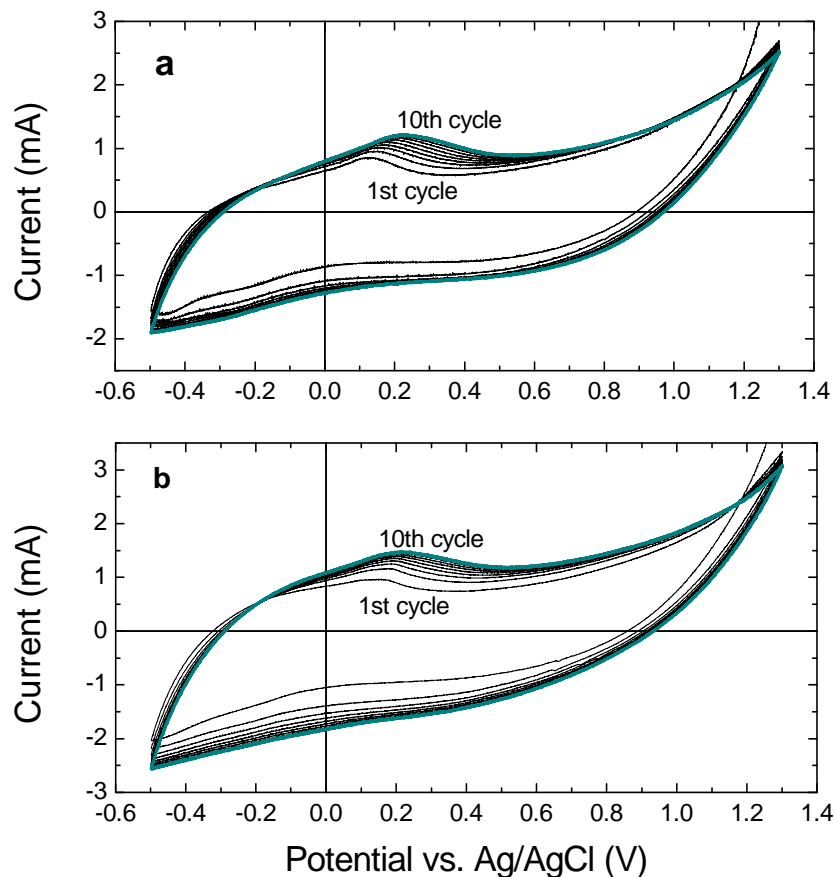
Figure C-2 Electropolymerization of MG on: a) BP1 and b) BP2. Scan rate: 5 mV/s

The resulting materials were examined by SEM and the micrographs are shown in Figure C-3. A clear difference is observed when comparing these images to those of the unmodified bucky papers (Figure C-1). It is observed that the electropolymerization of MG onto nanostructured bucky paper materials yields different structure of poly-(MG). The appearance of particles and clusters of particles within the surface of the carbon nanotubes is observed. It can be hypothesized that this type of formation is due to several factors such as length-scale, roughness, porosity and partial hydrophobicity of the underlying surface of the bucky papers, which avoids the formation of a uniform film as

it has been observed on GC electrodes (Figure 5-4). The particle size of the deposits ranges between 50-200 nm as depicted in Figure C-3b and Figure C-3d.
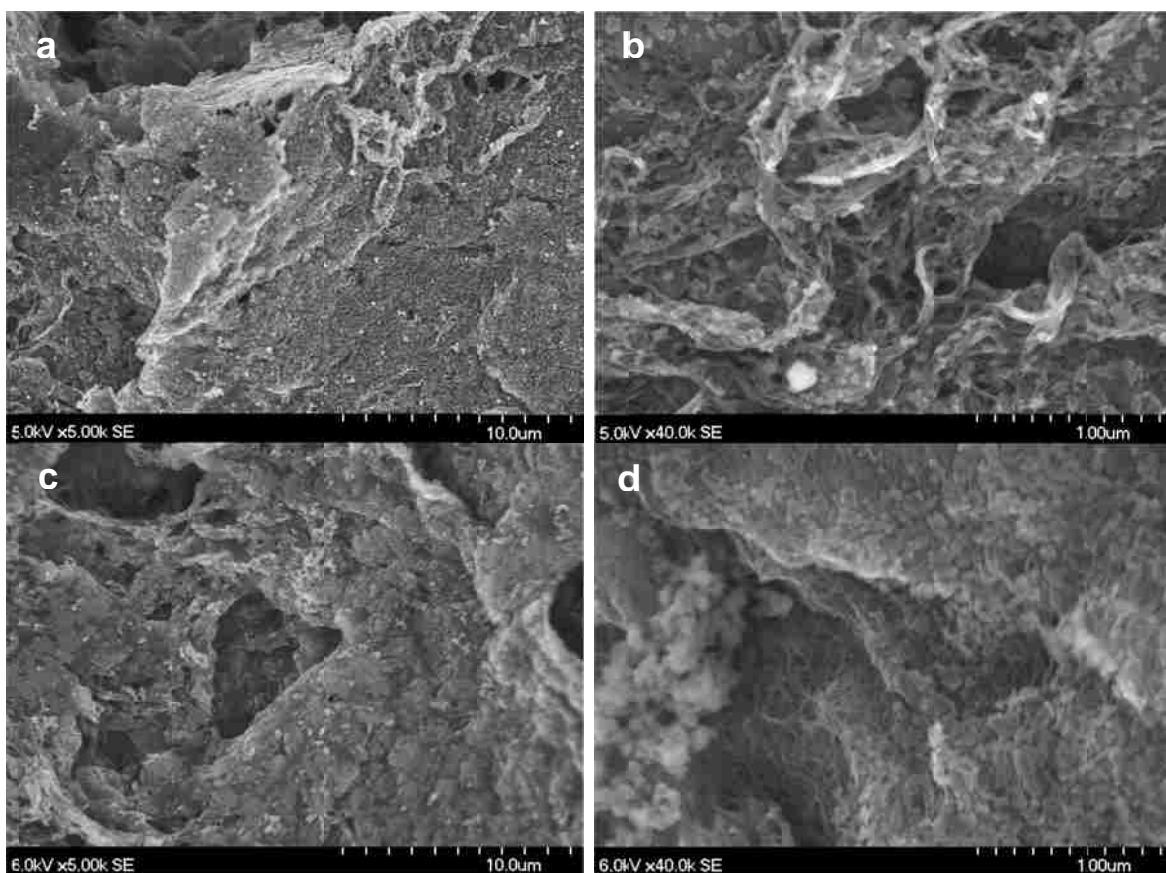
Figure C-3 SEM micrographs of bucky papers after poly-(MG) deposition: a) and b) BP1 and, c) and d) BP2

Hydrodynamic polarization curves

By building a hydrodynamic polarization curves (Figure C-4), the ideal working potential for NADH was determined for both poly-(MG) modified BP1 and BP2 electrodes.
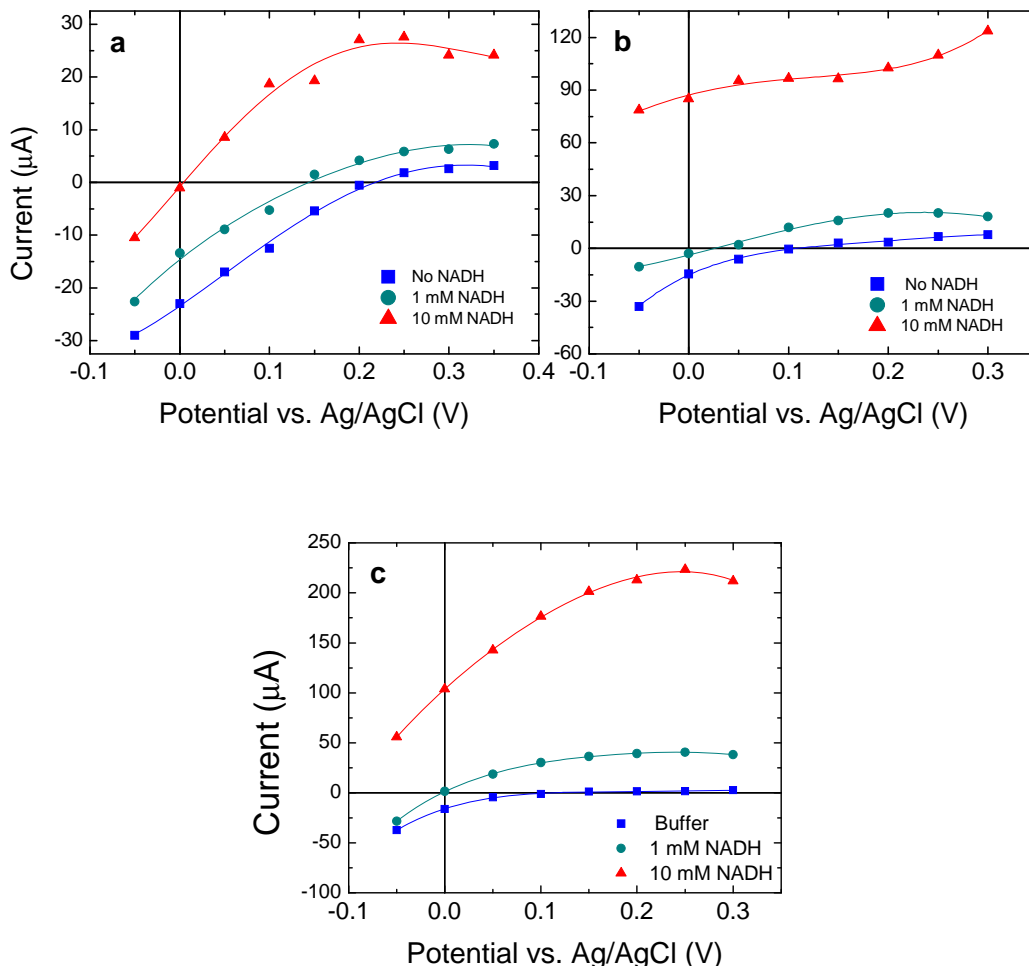
Figure C-4 Hydrodynamic polarization curves at different concentration of NADH for a) poly-(MG)-BP1 (stirred), b) poly-(MG)-BP2 (stirred), and c) poly-(MG)-BP2 (RDE at 1600 rpm)

For the poly-(MG)-BP1 electrode, the working potential found was 0.3 V vs. Ag/AgCl. It is observed that the current response to applied potentials increases as NADH concentration. When comparing Figure C-4a to b at the same concentrations and applied potentials, it is observed that a higher current response is produced by poly-(MG)-BP2 which can be attributed to the presence of MG in the compositional material of the bucky paper, enhancing the catalytic effect of the electrode. The steady-state current measured at 0.2 V was of approximately 25 µA for 10 mM NADH on poly-

(MG)-BP1 (Figure C-4a) while its value under at the same potential and concentration of NADH was close to 100 μA for poly-(MG)-BP2 (Figure C-4b), resulting in a 4-fold increase.

Since poly-(MG)-BP2 resulted in a higher current increase therefore indicating better catalytic activity towards NADH oxidation, the electrode was further studied in RDE experiments. Figure C-4c shows a hydrodynamic polarization curve obtained for poly-(MG)-BP2 in RDE setup with rotating speed of 1600 rpm. When comparing both curves with the poly-(MG)-BP2 (Figure C-4a and c) a 2-fold increase is observed in the steady-state current response at 0.2 V and 10 mM of NADH. This observation suggests that BP2 exhibits some mass transport dependance in the oxidation process of NADH. The increment of the current response in poly-(MG)-BP2 demostrates that the initial amount of MG in this material induces a larger number of NADH oxidative reactions per unit time, although it does not enhances the conductivity of the material compared to poly-(MG)-BP1.

NADH oxidation

Chronoamperometric experiments were performed in order to evaluate the kinetics of NADH oxidation at poly-(MG) modified bucky paper electrodes. The oxidation of NADH to NAD^+ is electrochemically observed by the increase of current measured with each addition of NADH aliquots. The applied potential was of 0.3 V for both electrodes and the current was recorded when it reached steady-state conditions. These curves were used to study the relationship between the current generated with respect to the concentration of the substrate (NADH). It is observed in Figure C-5 that oxidative current is generated by poly-(MG)-modified bucky paper electrodes as a consequence of adding

NADH, which demonstrates again the electrocatalytic activity of the bucky paper electrodes that were prepared. The concentration dependence data was then fitted to a linear relationship (Fickian behavior), but a deviation from this behavior can be observed for the highest concentration values. This observation is in agreement with previously reported results for poly-(MG)-modified electrodes (Chapter 5). Moreover, once again it is observed that poly-(MG)-BP2 yields higher catalytic currents than poly-(MG)-BP1.
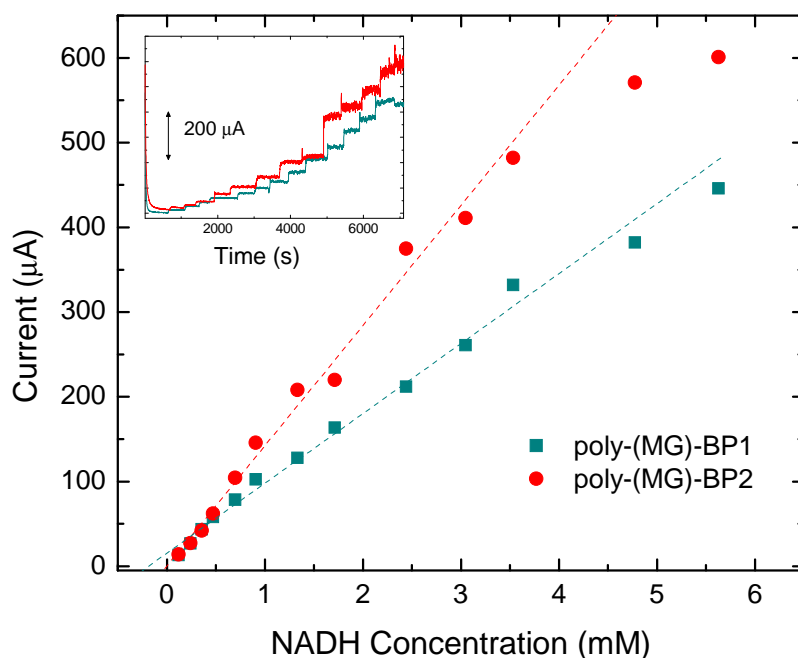
Figure C-5 Steady-state current dependence with respect to NADH concentration for poly-(MG)-BP1 and poly-(MG)-BP2. Applied potential: 0.3 V vs. Ag/AgCl. Inset: Chronoamperometric curves

Electrodes evaluation in the presence of NAD^+-dependent enzyme

The oxidation of L-malate catalyzed by NAD^+-dependent MDH was observed due in the presence of both poly-(MG)-modified BP1 and BP2, catalyzing the enzymatic cofactor's re-oxidation. Michaelis-Menten kinetics behavior was observed for both electrodes and is represented in Figure C-6. In order to perform chronoamperometric measurements the

cofactor NAD$^+$ was added in excess to the electrolyte, and the enzyme was free in solution. The applied potential was 0.1 V as previously studied for poly-(MG)-modified GC electrodes. The current was also allowed to reach steady-state conditions after each addition of L-malate aliquots, before being recorded.
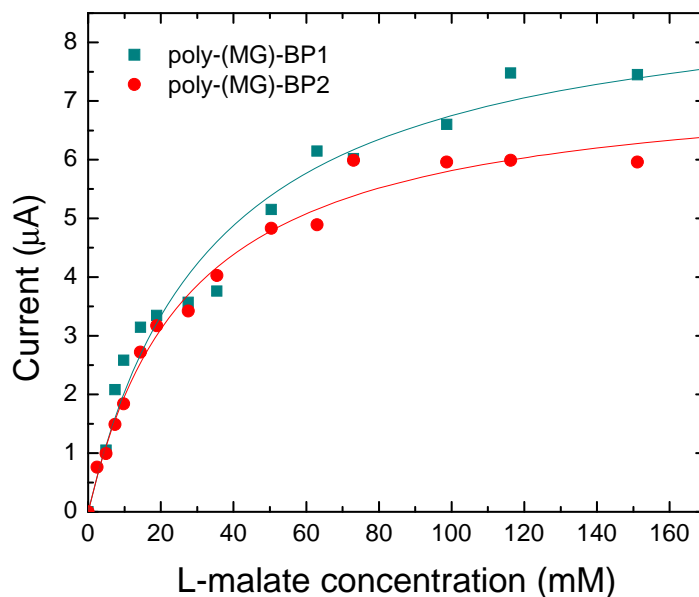
Figure C-6 Michaelis-Menten kinetics of MDH for the oxidation of L-malate for poly-(MG)-BP1 and poly-(MG)-BP2

The MDH enzyme was found to have an apparent Michaelis-Menten constant K_M^{app} of 34 ± 5 mM for poly-(MG)-BP1 electrode with a maximum current i_{max} of 9.1 ± 0.5 μA. For poly-(MG)-BP2 electrode the value of K_M^{app} was found to be 28 ± 3 mM with a maximum current i_{max} of 7.4 ± 0.3 μA. Even though poly-(MG)-BP2 shows a lower maximum current (unlike the previous results) in comparison with poly-(MG)-BP1, it does have a lower K_M^{app} value, suggesting better reaction rates.

C.3. Conclusion

An exploratory study was made to electropolymerize MG onto new nanostructured SWNTs-based materials (bucky papers). Poly-(MG) was effectively deposited onto two types of bucky papers (BP1 prepared with SWNTs and isopropanol and, BP2 prepared with SWNTs, isopropanol and MG) and both demonstrated to be catalytically active with respect to NADH oxidation. The oxidation of NADH was further exhibited when adding a NAD^+-dependent enzyme (MDH) and testing it towards its substrate (L-malate) oxidation. Catalytic activity following Michaelis-Menten behavior was observed for each electrode and was only possible due to the electrocatalytic effect of poly-(MG) bucky papers. Chronoamperometry was used for evaluation of the electrodes towards NADH oxidation and later for L-malate oxidation with MDH. The NADH oxidation deviated from Fick's law behavior at high concentrations of NADH, as previously observed for poly-(MG) deposited on GC (Chapter 5). The catalytic activity of PMG was observed during chronoamperometric measurements of oxidation at 0.3 V for NADH and 0.1 V for L-malate oxidation by MDH. The use of SWNTs enhanced the surface area of the electrode material and provided sufficient conductivity. The nanostructure of the bucky papers allowed for growth of poly-(MG) in the form of particles, resulting in a high number of catalytic active sites per unit area for the enzyme to react. BP2 modified electrode presented in general better catalytic behavior, expressed in higher oxidative currents for NADH suggesting that the presence of MG monomer in the bucky paper material improves the electrode design. Despite the favorable results, due to the mechanical properties of the bucky paper materials, integration in 3-D bioanode design

becomes complicated. This research however demonstrates the versatility of SWNTs and

opens the door for many potential applications of SWNTs as electrode materials.

References

1.   Potter, M. C., Electrical Effects Accompanying the Decomposition of Organic Compounds. *Proc. R. Soc. B* **1911,** *84* (571), 260-276.

2.   Yahiro, A. T.; Lee, S. M.; Kimble, D. O., Bioelectrochemistry .I. Enzyme utilizing bio-fuel cells studies. *Biochim. Biophys. Acta* **1964,** *88* (2), 375-&.

3.   Drake, R. F.; Kusserow, B. K.; Messinge.S; Matsuda, S., A tissue implantable fuel cell power supply. *T. Am. Soc. Art. Int. Org.* **1970,** *16*, 199-&.

4.   Davis, G.; Hill, H. A. O.; Aston, W. J.; Higgins, I. J.; Turner, A. P. F., Bioelectrochemical fuel-cell vased on a quinoprotein, alcohol-dehydrogenase. *Enzyme Microb. Technol.* **1983,** *5* (5), 383-388.

5.   Barton, S. C.; Gallaway, J.; Atanassov, P., Enzymatic biofuel cells for Implantable and microscale devices. *Chem. Rev.* **2004,** *104* (10), 4867-4886.

6.   Sokic-Lazic, D.; Minteer, S. D., Citric acid cycle biomimic on a carbon electrode. *Biosens. Bioelectron.* **2008,** *24* (4), 939-944.

7.   Sokic-Lazic, D.; Minteer, S. D., Pyruvate/air enzymatic biofuel cell capable of complete oxidation. *Electrochem. Solid-State Lett.* **2009,** *12* (9), F26-F28.

8.   Sokic-Lazic, D.; Arechederra, R. L.; Treu, B. L.; Minteer, S. D., Oxidation of biofuels: fuel diversity and effectiveness of fuel oxidation through multiple enzyme cascades. *Electroanal.* **2010,** *22* (7-8), 757-764.

9.   Gorton, L.; Hale, P. D.; Persson, B.; Boguslavsky, L. I.; Karan, H. I.; Lee, H. S.; Skotheim, T. A.; Lan, H. L.; Okamoto, Y., Electrocatalytic oxidation of nicotinamide adenine-dinucleotide cofactor at chemically modified electrodes. *ACS Symp. Ser.* **1992,** *487*, 56-83.

10.   Underwood, A. L.; Burnett, R. W., Electrochemistry of biological compounds. In *Electroanalytical Chemistry: A Series of Advances*, Bard, A. J., Ed. Marcel Dekker: New York, 1973; Vol. 6, pp 1-85.

11.   Schmakel, C. O.; Santhanam, K. S. V.; Elving, P. J., Nicotinamide adenine-dinucleotide (NAD+) and related compounds - Electrochemical redox pattern and and allied chemical behavior. *J. Am. Chem. Soc.* **1975,** *97* (18), 5083-5092.

12.   Bresnahan, W. T.; Elving, P. J., The role of adsorption in the initial one-electron electrochemical reduction of nicotinamide adenine-dinucleotide (NAD+). *J. Am. Chem. Soc.* **1981,** *103* (9), 2379-2386.

13.   Jensen, M. A.; Bresnahan, W. T.; Elving, P. J., Comparative adsorption of adenine and nicotinamide adenine-dinuleotide (NAD+) at an aqueous-solution mercury interface. *Bioelectrochem. Bioenerg.* **1983,** *11* (4-6), 299-306.

14.   Moiroux, J.; Deycard, S.; Malinski, T., Electrochemical reduction of NAD+ and pyridinium cations adsorbed at the mercury water interface - Electrochemical-behavior of adsrobed pyridinyl radicals. *J. Electroanal. Chem.* **1985,** *194* (1), 99-108.

15.   Blankespoor, R. L.; Miller, L. L., Electrochemical oxidation of NADH - Kinetic control by product inhibition and surface coating. *J. Electroanal. Chem.* **1984,** *171* (1-2), 231-241.

16.   Blaedel, W. J.; Haas, R. G., Electrochemical oxidation of NADH analogs. *Anal. Chem.* **1970,** *42* (8), 918-&.

17.   Leduc, P.; Thévenot, D., Chemical and electrochemical oxidation of aqueous solutions of NADH and model compounds. *Bioelectrochem. Bioenerg.* **1974,** *1* (1-2), 96-107.

18.   Moiroux, J.; Elving, P. J., Mechanistic aspects of the electrochemical oxidation of dihydronicotinamide adenine-dinucleotide (NADH). *J. Am. Chem. Soc.* **1980,** *102* (21), 6533-6538.

19.   Jaegfeldt, H., Adsorption and electrochemical oxidation behavior of NADH at a clean platinum-electrode. *J. Electroanal. Chem.* **1980,** *110* (1-3), 295-302.

20.   Elving, P. J.; Bresnahan, W. T.; Moiroux, J.; Samec, Z., NAD NADH as a model redox system - Mechanism, mediation, modification by the environment. *Bioelectrochem. Bioenerg.* **1982,** *9* (3), 365-378.

21.   Ludvik, J.; Volke, J., Evidence for a radical intermediate in the anodic-oxidation of reduced nicotinamide adenine dinucleotides obtained by electrogenerated chemi-luminescence. *Anal. Chim. Acta* **1988,** *209* (1-2), 69-78.

22.   Gorton, L.; Bartlett, P. N., NAD(P)-Based Biosensors. In *Bioelectrochemistry: fundamentals, experimental techniques, and applications*, Bartlett, P. N., Ed. John Wiley & Sons, Inc. : West Sussex, 2008; pp 157-198.

23.   Blaedel, W. J.; Jenkins, R. A., Study of Electrochemical Oxidation of Reduced Nicotinamide Adenine-Dinucleotide. *Anal. Chem.* **1975,** *47* (8), 1337-1343.

24.   Chenault, H. K.; Whitesides, G. M., Regeneration of nicotinamide cofactors for use in organic-synthesis. *Appl. Biochem. Biotechnol.* **1987,** *14* (2), 147-197.

25.   Karyakin, A. A.; Ivanova, Y. N.; Revunova, K. V.; Karyakina, E. E., Electropolymerized flavin adenine dinucleotide as an advanced NADH transducer. *Analytical Chemistry* **2004,** *76* (7), 2004-2009.

26.   Gorton, L., Chemically modified electrodes for the electrocatalytic oxidation of nicotinamide coenzymes. *J. Chem. Soc., Faraday Trans. 1 F* **1986,** *82* (4), 1245-1258.

27.   Gorton, L.; Csöregi, E.; Domínguez, E.; Emnéus, J.; Jönsson-Pettersson, G.; Marko-Varga, G.; Persson, B., Selective detection in flow analysis based on the combination of immobilized enzymes and chemically modified electrodes. *Anal. Chim. Acta* **1991,** *250*, 203-248.

28.   Bartlett, P. N.; Tebbutt, P.; Whitaker, R. G., Kinetic aspects of the use of modified electrodes and mediators in bioelectrochemistry. *Prog. React. Kinet.* **1991,** *16* (2), 55-155.

29.   Schuhmann, W.; Schmidt, H. L., Amperometric biosensors for substrates of oxidases and dehydrogenases. In *Advances in Biosensors*, Turner, A. P. F.; Renneberg, R., Eds. JAI Press: London, 1992 Vol. 1, pp 79-130.

30.   Schuhmann, W.; Huber, J.; Wohlschläger, H.; Strehlitz, B.; Gründig, B., Electrocatalytic oxidation of NADH at mediator-modified electrode surfaces. *J. Biotechnol.* **1993,** *27* (2), 129-142.

31.   Katakis, I.; Domínguez, E., Catalytic electrooxidation of NADH for dehydrogenase amperometric biosensors. *Microchim. Acta* **1997,** *126* (1), 11-32.

32.   Lobo, M. J.; Miranda, A. J.; Tuñón, P., Amperometric biosensors based on NAD(P)-dependent dehydrogenase enzymes. *Electroanal.* **1997,** *9* (3), 191-202.

33.   Lorenzo, E.; Pariente, F.; Hernàndez, L.; Tobalina, F.; Darder, M.; Wu, Q.; Maskus, M.; Abruña, H. D., Analytical strategies for amperometric biosensors based on chemically modified electrodes. *Biosens. Bioelectron.* **1998,** *13* (3-4), 319-332.

34.   Armstrong, F. A.; Wilson, G. S., Recent developments in faradaic bioelectrochemistry. *Electrochim. Acta* **2000,** *45* (15-16), 2623-2645.

35.   Habermuller, L.; Mosbach, M.; Schuhmann, W., Electron-transfer mechanisms in amperometric biosensors. *Fresenius J. Anal. Chem.* **2000,** *366* (6-7), 560-568.

36.   Gorton, L.; Domínguez, E., Electrocatalytic oxidation of NAD(P)H at mediator-modified electrodes. *Rev. Mol. Biotechnol.* **2002,** *82* (4), 371-392.

37.   Gorton, L.; Domínguez, E., Electrochemistry of NAD(P)+/NAD(P)H. In *Bioelectrochemistry*, Bard, A. J.; Stratmann, M.; Wilson, G. S., Eds. Wiley-VHC: Weinheim, 2002; Vol. 9, pp 67-143.

38.   Palmore, G. T. R.; Bertschy, H.; Bergens, S. H.; Whitesides, G. M., A methanol/dioxygen biofuel cell that uses NAD(+)-dependent dehydrogenases as catalysts: application of an electro-enzymatic method to regenerate nicotinamide adenine dinucleotide at low overpotentials. *J. Electroanal. Chem.* **1998,** *443* (1), 155-161.

39.   Kuwana, T.; Tse, D. C. S., Electrocatalysis of NADH using quinones and modified quinone electrodes. *Abstr. Pap. Am. Chem. Soc.* **1978,** *176* (SEP), 31-31.

40.   Tse, D. C. S.; Kuwana, T., Electrocatalysis of dihydronicotunamide adenosine-diphosphate with quinones and modified quinones electrodes. *Anal. Chem.* **1978,** *50* (9), 1315-1318.

41.   Degrand, C.; Miller, L. L., An electrode modified with polymer-bound dopamine which catalyzes NADH oxidation. *J. Am. Chem. Soc.* **1980,** *102* (18), 5728-5732.

42.   Jaegfeldt, H.; Torstensson, A. B. C.; Gorton, L. G. O.; Johansson, G., Catalytic-oxidation of reduced nicotinamide adenine-dinuleotide by graphite-electrodes modified with adsorbed aromatics containing catechol functionalities. *Anal. Chem.* **1981,** *53* (13), 1979-1982.

43.   Ueda, C.; Tse, D. C. S.; Kuwana, T., Stability of catechol modified carbon electrodes for electrocatalysis of dihydronicotinamide adenine-dinucleotide and ascorbic-acid. *Anal. Chem.* **1982,** *54* (6), 850-856.

44.   Fukui, M.; Kitani, A.; Degrand, C.; Miller, L. L., Propagation of a redox reaction through a quinoid polymer film on an electrode. *J. Am. Chem. Soc.* **1982,** *104* (1), 28-33.

45.   Lau, A. N. K.; Miller, L. L., Electrochemical-behavior of dopamine polymer - dopamine release as a primitive analog of a synapse. *J. Am. Chem. Soc.* **1983,** *105* (16), 5271-5277.

46.   Jaegfeldt, H.; Kuwana, T.; Johansson, G., Electrochemical stability of catechols with a pyrene side-chain strongly adsorbed on graphite-electrodes for catalytic-oxidation of dihydronicotinamide adenine-dinucleotide. *J. Am. Chem. Soc.* **1983,** *105* (7), 1805-1814.

47.   Gorton, L.; Torstensson, A.; Jaegfeldt, H.; Johansson, G., Electrocatalytic oxidation of reduced nicotinamide coenzymes by graphite-electrodes modified with an adsorbed phenoxazinium salt, meldola blue. *J. Electroanal. Chem.* **1984,** *161* (1), 103-120.

48.   Gorton, L.; Johansson, G.; Torstensson, A., A kinetic-study of the reaction between dihydronicotinamide adenine-dinucleotide (NADH) and electrode modified by adsorption of 1,2-Benzophenoxazine-7-one. *J. Electroanal. Chem.* **1985,** *196* (1), 81-92.

49.   Persson, B.; Gorton, L., A comparative-study of some 3,7-diaminophenoxazine derivatives and related-compounds for electrocatalytic oxidation of NADH. *J. Electroanal. Chem.* **1990,** *292* (1-2), 115-138.

50.   Persson, B., A chemically modified graphite electrode for electrocatalytic oxidation of reduced nicotinamide adenine-dinucleotide based on a phenothiazine derivative, 3-beta-naphthoyl-toluidine blue-O. *J. Electroanal. Chem.* **1990,** *287* (1), 61-80.

51.   Polasek, M.; Gorton, L.; Appelqvist, R.; Markovarga, G.; Johansson, G., Amperometric glucose sensor amperometric glucose-dehydrogenase immobilized on a graphite electrode modified with an N, N'-bis(benzophenoxazinyl) derivative of benzene-1,4-dicarboxamide. *Anal. Chim. Acta* **1991,** *246* (2), 283-292.

52.   Torstensson, A.; Gorton, L., Catalytic-oxidation of NADH by surface-modified graphite-electrodes. *J. Electroanal. Chem.* **1981,** *130* (1-3), 199-207.

53.   Huck, H., Catalytic-oxidation of NADH on graphite-electrodes with adsorbed phenoxazine derivatives. *Fresen. Z. Anal. Chem.* **1982,** *313* (7), 548-552.

54.   Kimura, Y.; Niki, K., Electrochemical oxidation of nicotineamide-adenine dinucleotide (NADH) by modified pyrolytic graphite. *Anal. Sci.* **1985,** *1* (3), 271-274.

55.   Appelqvist, R.; Markovarga, G.; Gorton, L.; Torstensson, A.; Johansson, G., Enzymatic determination of glucose in a flow system by catalytic-oxidation of the nicotinamide coenzyme at a modified electrode. *Anal. Chim. Acta* **1985,** *169* (MAR), 237-247.

56.   Munteanu, F. D.; Kubota, L. T.; Gorton, L., Effect of pH on the catalytic electro oxidation of NADH using different two-electron mediators immobilised on zirconium phosphate. *J. Electroanal. Chem.* **2001,** *509* (1), 2-10.

57.   Munteanu, F. D.; Mano, N.; Kuhn, A.; Gorton, L., Mediator-modified electrodes for catalytic NADH oxidation: high rate constants at interesting overpotentials. *Bioelectrochemistry* **2002,** *56* (1-2), 67-72.

58.   de Lucca, A. R.; de S. Santos, A.; Pereira, A. C.; Kubota, L. T., Electrochemical behavior and electrocatalytic study of the methylene green coated on modified silica gel. *J. Colloid Interface Sci.* **2002,** *254* (1), 113-119.

59.   Gligor, D.; Muresan, L. M.; Dumitru, A.; Popescu, I. C., Electrochemical behavior of carbon paste electrodes modified with methylene green immobilized on two different X type zeolites. *J. Appl. Electrochem.* **2007,** *37* (2), 261-267.

60.   Miyawaki, O.; Wingard, L. B., Electrochemical and glucose-oxidase coenzyme activity of flavin adenine-dinucleotide covalently attached to glassy-carbon at the adenine amino group. *Biochim. Biophys. Acta* **1985,** *838* (1), 60-68.

61.   Lawrence, N. S.; Wang, J., Chemical adsorption of phenothiazine dyes onto carbon nanotubes: Toward the low potential detection of NADH. *Electrochem. Commun.* **2006,** *8* (1), 71-76.

62.   Sakai, H.; Nakagawa, T.; Tokita, Y.; Hatazawa, T.; Ikeda, T.; Tsujimura, S.; Kano, K., A high-power glucose/oxygen biofuel cell operating under quiescent conditions. *Energy Environ. Sci.* **2009,** *2* (1), 133-138.

63.   Mengoli, G.; Musiani, M. M.; Zotti, G., Electrode modification by insitu electropolymerization of phenothiazine. *J. Electroanal. Chem.* **1984,** *175* (1-2), 93-104.

64.   Schuhmann, W.; Huber, J.; Mirlach, A.; Daub, J., Polyazulenes .5. Covalent binding of glucose-oxidase to functionalized polyazulenes - The 1st application of polyazulenes in amperometric biosensors. *Adv. Mater.* **1993,** *5* (2), 124-126.

65.   Karyakin, A. A.; Strakhova, A. K.; Karyakina, E. E.; Varfolomeyev, S. D.; Yatsimirsky, A. K., The electrochemical polymerization of methylene-blue and

bioelectrochemical activity of the resulting film. *Bioelectrochem. Bioenerg.* **1993,** *32* (1), 35-43.

66.   Karyakin, A. A.; Karyakina, E. E.; Schuhmann, W.; Schmidt, H. L.; Varfolomeyev, S. D., New amperometric dehydrogenase electrodes based on electrocatalytic NADH-oxidation at poly(methylene blue)-modified electrodes. *Electroanal.* **1994,** *6* (10), 821-829.

67.   Schlereth, D. D.; Schuhmann, W.; Schmidt, H. L., Spectroelectrochemical chracterization of ultra-thin films formed by electropolymerization of phenothiazine-derivatives on transparent gold electrodes. *J. Electroanal. Chem.* **1995,** *381* (1-2), 63-70.

68.   Silber, A.; Hampp, N.; Schuhmann, W., Poly(methylene blue)-modified thick-film gold electrodes for the electrocatalytic oxidation of NADH and their application in glucose biosensors. *Biosens. Bioelectron.* **1996,** *11* (3), 215-223.

69.   Yang, R.; Ruan, C.; Deng, J., A H2O2 biosensor based on immobilization of horseradish peroxidase in electropolymerized methylene green film on GCE. *J. Appl. Electrochem.* **1998,** *28* (11), 1269-1275.

70.   Karyakin, A. A.; Karyakina, E. E.; Schmidt, H. L., Electropolymerized azines: A new group of electroactive polymers. *Electroanal.* **1999,** *11* (3), 149-155.

71.   Karyakin, A. A.; Karyakina, E. E.; Schuhmann, W.; Schmidt, H. L., Electropolymerized azines: Part II. In a search of the best electrocatalyst of NADH oxidation. *Electroanal.* **1999,** *11* (8), 553-557.

72.   Mao, L. Q.; Yamamoto, K., Glucose and choline on-line biosensors based on electropolymerized Meldola's blue. *Talanta* **2000,** *51* (1), 187-195.

73.   Kertesz, V.; Van Berkel, G. J., Electropolymerization of methylene blue investigated using on-line electrochemistry/electrospray mass spectrometry. *Electroanal.* **2001,** *13* (17), 1425-1430.

74.   Shan, D.; Mu, S. L.; Mao, B. W., Detection of intermediate during the electrochemical polymerization of azure B and growth of poly(azure B) film. *Electroanal.* **2001,** *13* (6), 493-498.

75.   Shan, D.; Mousty, C.; Cosnier, S.; Mu, S. L., A composite poly azure B-clay-enzyme sensor for the mediated electrochemical determination of phenols. *J. Electroanal. Chem.* **2002,** *537* (1-2), 103-109.

76.   Vasilescu, A.; Andreescu, S.; Bala, C.; Litescu, S. C.; Noguer, T.; Marty, J. L., Screen-printed electrodes with electropolymerized Meldola Blue as versatile detectors in biosensors. *Biosens. Bioelectron.* **2003,** *18* (5-6), 781-790.

77.   Li, N. B.; Duan, J. P.; Chen, G. N., Electrochemical polymerization of azure blue II and its electrocatalytic activity toward NADH oxidation. *Chin. J. Chem.* **2003,** *21* (9), 1191-1197.

78.   Chen, C. X.; Mu, S. L., Electrochemical polymerization of azure A and properties of poly(azure A). *J. Appl. Polym. Sci.* **2003,** *88* (5), 1218-1224.

79.   Karyakin, A. A.; Ivanova, Y. N.; Karyakina, E. E., Equilibrium (NAD(+)/NADH) potential on poly(Neutral Red) modified electrode. *Electrochem. Commun.* **2003,** *5* (8), 677-680.

80.   Sha, Y. F.; Gao, Q.; Qi, B.; Yang, X. R., Electropolymerization of azure B on a screen-printed carbon electrode and its application to the determination of NADH in a flow injection analysis system. *Microchim. Acta* **2004,** *148* (3-4), 335-341.

81.   Gao, Q.; Wang, W. D.; Ma, Y.; Yang, X. R., Electrooxidative polymerization of phenothiazine derivatives on screen-printed carbon electrode and its application to determine NADH in flow injection analysis system. *Talanta* **2004,** *62* (3), 477-482.

82.   Broncova, G.; Shishkanova, T. V.; Matejka, P.; Volf, R.; Kral, V., Citrate selectivity of poly(neutral red) electropolymerized films. *Anal. Chim. Acta* **2004,** *511* (2), 197-205.

83.   Damos, F. S.; Luz, R. C. S.; Kubota, L. T., Study of poly(methylene blue) ultrathin films and its properties by electrochemical surface plasmon resonance. *J. Electroanal. Chem.* **2005,** *581* (2), 231-240.

84.   Mariotti, M. P.; Riccardi, C. D. S.; Fertonani, F. L.; Yamanaka, H., Strategies for developing NADH detector based on meldola blue in different immobilization methods: A comparative study. *J. Braz. Chem. Soc.* **2006,** *17* (4), 689-696.

85.   Ulyanova, Y. V.; Blackwell, A. E.; Minteer, S. D., Poly(methylene green) employed as molecularly imprinted polymer matrix for electrochemical sensing. *Analyst* **2006,** *131* (2), 257-261.

86.   Chen, C.; Gao, Y., Monitoring formation of poly(neutral red) film by EQCM. *Russ. J. Electrochem.* **2007,** *43* (3), 267-272.

87.   Evtitgyn, G. A.; Porfireva, A. V.; Hianik, T.; Cheburova, M. S.; Budnikov, H. C., Potentiometric DNA sensor based on electropolymerized phenothiazines for protein detection. *Electroanal.* **2008,** *20* (12), 1300-1308.

88.   Blackwell, A. E.; Moehlenbrock, M. J.; Worsham, J. R.; Minteer, S. D., Comparison of electropolymerized thiazine dyes as an electrocatalyst in enzymatic biofuel cells and self powered sensors. *J. Nanosci. Nanotechnol.* **2009,** *9* (3), 1714-1721.

89.   Evtugyn, G.; Porfireva, A.; Ivanov, A.; Konovalova, O.; Hianik, T., Molecularly Imprinted Polymerized Methylene Green as a Platform for Electrochemical Sensing of Aptamer-Thrombin Interactions. *Electroanal.* **2009,** *21* (11), 1272-1277.

90.   Zhao, R. J.; Jiang, Q.; Sun, W.; Jiao, K., Electropolymerization of methylene blue on carbon ionic liquid electrode and its electrocatalysis to 3,4-dihydroxybenzoic acid. *J. Chin. Chem. Soc.* **2009,** *56* (1), 158-163.

91.   Gligor, D.; Dilgin, Y.; Popescu, I. C.; Gorton, L., Poly-phenothiazine derivative-modified glassy carbon electrode for NADH electrocatalytic oxidation. *Electrochim. Acta* **2009,** *54* (11), 3124-3128.

92.   Prieto-Simon, B.; Fabregas, E., Comparative study of electron mediators used in the electrochemical oxidation of NADH. *Biosens. Bioelectron.* **2004,** *19* (10), 1131-1138.

93.   Schuhmann, W.; Lammert, R.; Hammerle, M.; Schmidt, H. L., Electrocatalytic properties of polypyrrole in amperometric electrodes. *Biosens. Bioelectron.* **1991,** *6* (8), 689-697.

94.   Schuhmann, W., Conducting polymers and their application in amperometric biosensors. In *Diagnostic Biosensor Polymers*, Usmani, A. M.; Akmal, N., Eds. Amer Chemical Soc: Washington, 1994; Vol. 556, pp 110-123.

95.   Narasaiah, D., An enzyme electrode for hydrogen-peroxide detection based on peroxidase immobilized on a glassy-carbon electrode. *Biosens. Bioelectron.* **1994,** *9* (6), 415-422.

96.   Guiseppielie, A.; Wilson, A. M.; Tour, J. M.; Brockmann, T. W.; Zhang, P.; Allara, D. L., Specific immobilization of electropolymerized polypyrrole thin-films onto interdigitated microsensor electrode arrays. *Langmuir* **1995,** *11* (5), 1768-1776.

97.   Yamato, H.; Ohwa, M.; Wernet, W., Stability of polypyrrole and poly(3,4-ethylenedioxythiophene) for biosensor application. *J. Electroanal. Chem.* **1995,** *397* (1-2), 163-170.

98.   Hiller, M.; Kranz, C.; Huber, J.; Bauerle, P.; Schuhmann, W., Amperometric biosensors produced by immobilization of redox enzymes at polythiophene-modified electrode surfaces. *Adv. Mater.* **1996,** *8* (3), 219-&.

99.   Popescu, I. C.; Cosnier, S.; Labbe, P., Peroxidase-glucose oxidase-poly(amphiphilic pyrrole) bioelectrode for selectively mediated amperometric detection of glucose. *Electroanal.* **1997,** *9* (13), 998-1004.

100.   Situmorang, M.; Gooding, J. J.; Hibbert, D. B.; Barnett, D., Electrodeposited polytyramine as an immobilisation matrix for enzyme biosensors. *Biosens. Bioelectron.* **1998,** *13* (9), 953-962.

101.   Garjonyte, R.; Malinauskas, A., Amperometric glucose biosensors based on Prussian Blue- and polyaniline-glucose oxidase modified electrodes. *Biosens. Bioelectron.* **2000,** *15* (9-10), 445-451.

102.   Chen, J.; Burrell, A. K.; Collis, G. E.; Officer, D. L.; Swiegers, G. F.; Too, C. O.; Wallace, G. G., Preparation, characterisation and biosensor application of conducting polymers based on ferrocene substituted thiophene and terthiophene. *Electrochim. Acta* **2002,** *47* (17), 2715-2724.

103.   Marx, K. A.; Zhou, T., Comparative study of electropolymerization versus adsorption of tyrosine and the decyl ester of tyrosine on platinum electrodes. *J. Electroanal. Chem.* **2002,** *521* (1-2), 53-60.

104.   Pandey, P. C.; Singh, G., Electrochemical polymerization of aniline in proton-free nonaqueous media - Dependence of microstructure and electrochemical properties of polyaniline on solvent and dopant. *J. Electrochem. Soc.* **2002,** *149* (4), D51-D56.

105.   Gao, Q. A.; Yang, F.; Ma, Y.; Yang, X. R., The modification of screen-printed carbon electrodes with amino group and its application to construct a H2O2 biosensor. *Electroanal.* **2004,** *16* (9), 730-735.

106.   Wang, J.; Musameh, M., Carbon-nanotubes doped polypyrrole glucose biosensor. *Anal. Chim. Acta* **2005,** *539* (1-2), 209-213.

107.   Xu, Y.; Ye, X. Y.; Yang, L.; He, P. A.; Fang, Y. Z., Impedance DNA biosensor using electropolymerized polypyrrole/multiwalled carbon nanotubes modified electrode. *Electroanal.* **2006,** *18* (15), 1471-1478.

108.   Dai, Z. H.; Liu, F. X.; Lu, G. F.; Bao, J. C., Electrocatalytic detection of NADH and ethanol at glassy carbon electrode modified with electropolymerized films from methylene green. *J. Solid State Electrochem.* **2008,** *12* (2), 175-180.

109.   Marx, K. A.; Zhou, T. A.; McIntosh, D.; Braunhut, S. J., Electropolymerized tyrosine-based thin films: Selective cell binding via peptide recognition to novel electropolymerized biomimetic tyrosine RGDY films. *Anal. Biochem.* **2009,** *384* (1), 86-95.

110.   Muhammet, S. M.; Cete, S.; Arslan, F.; Yasar, A., Amperometric cholesterol biosensors based on the electropolymerization of pyrrole and aniline in sulphuric acid for the determination of cholesterol in serum. *Artif. Cells Blood Substit. Biotechnol.* **2009,** *37* (6), 273-278.

111. Sassolas, A.; Blum, L. J.; Leca-Bouvier, B. D., New electrochemiluminescent biosensors combining polyluminol and an enzymatic matrix. *Anal. Bioanal. Chem.* **2009,** *394* (4), 971-980.

112. Sen, S., Amperometric glucose sensor based on the entrapment of glucose oxidase in electrochemically synthesized pyrrole/N,N-dimethylaminopyrrole (Py/DMAPy) copolymer film. *Asian J. Chem.* **2009,** *21* (5), 4063-4076.

113. Ates, M.; Sarac, A. S., Conducting polymer coated carbon surfaces and biosensor applications. *Prog. Org. Coat.* **2009,** *66* (4), 337-358.

114. Liu, X. Y., A novel sensor based on electropolymerization poly(safranine) film electrode for voltammetric determination of 4-nitrophenol. *Bull. Korean Chem. Soc.* **2010,** *31* (5), 1182-1186.

115. Sanchez, C. O.; Isla, A.; Bustos, C.; Diaz, F.; Gatica, N., Biosensors' preparation to be used for entrapment method with copolymers polyaniline derivatives. *J. Chil. Chem. Soc.* **2010,** *55* (2), 233-235.

116. Raitman, O. A.; Katz, E.; Buckmann, A. F.; Willner, I., Integration of polyaniline/poly(acrylic acid) films and redox enzymes on electrode supports: An in situ electrochemical/surface plasmon resonance study of the bioelectrocatalyzed oxidation of glucose or lactate in the integrated bioelectrocatalytic systems. *J. Am. Chem. Soc.* **2002,** *124* (22), 6487-6496.

117. Lee, S.; Choi, B.; Tsutsumi, A., Electrochemical properties of polyaniline/carboxydextran (PANI/carDEX) composite films for biofuel cells in neutral aqueous solutions. *Biotechnol. Lett.* **2009,** *31* (6), 851-855.

118. Lee, S.; Choi, B.; Tsutsumi, A., Polyaniline/carboxydextran-gold hybrid nanomaterials as a biofuel cell electrode platform. *J. Chem. Eng. Jpn.* **2009,** *42* (8), 596-599.

119. Yang, D. W.; Liu, H. H., Poly(brilliant cresyl blue)-carbonnanotube modified electrodes for determination of NADH and fabrication of ethanol dehydrogenase-based biosensor. *Biosens. Bioelectron.* **2009,** *25* (4), 733-738.

120. Wen, D.; Deng, L.; Zhou, M.; Guo, S. J.; Shang, L.; Xu, G. B.; Dong, S. J., A biofuel cell with a single-walled carbon nanohorn-based bioanode operating at physiological condition. *Biosens. Bioelectron.* **2010,** *25* (6), 1544-1547.

121. Tuncagil, S.; Odaci, D.; Varis, S.; Timur, S.; Toppare, L., Electrochemical polymerization of 1-(4-nitrophenyl)-2,5-di(2-thienyl)-1 H-pyrrole as a novel immobilization platform for microbial sensing. *Bioelectrochemistry* **2009,** *76* (1-2), 169-174.

122. Sadki, S.; Schottland, P.; Brodie, N.; Sabouraud, G., The mechanisms of pyrrole electropolymerization. *Chem. Soc. Rev.* **2000,** *29* (5), 283-293.

123. Inzelt, G., *Conducting Polymers A New Era in Electrochemistry*. 1st ed.; Springer: Budapest, 2008; p 282.

124. Svoboda, V.; Cooney, M.; Liaw, B. Y.; Minteer, S.; Piles, E.; Lehnert, D.; Barton, S. C.; Rincon, R.; Atanassov, P., Standardized characterization of electrocatalytic electrodes. *Electroanal.* **2008,** *20* (10), 1099-1109.

125. Arai, G.; Matsushita, M.; Yasumori, I., Electrochemical oxidation of nicotinamide-adenine dinucleotide (NADH) with quinonoid polymer modified electrode. *Nippon Kagaku Kaishi* **1985,** (5), 894-897.

126.   Deinhammer, R. S.; Ho, M.; Anderegg, J. W.; Porter, M. D., Electrochemical oxidation of amine-containing compounds: a route to the surface modification of glassy carbon electrodes. *Langmuir* **1994,** *10* (4), 1306-1313.

127.   Pariente, F.; Lorenzo, E.; Abruna, H. D., Electrocatalysis of NADH Oxidation with Electropolymerized Films of 3,4-Dihydroxybenzaldehyde. *Anal. Chem.* **1994,** *66* (23), 4337-4344.

128.   Pariente, F.; Lorenzo, E.; Tobalina, F.; Abruna, H. D., Aldehyde Biosensor Based on the Determination of NADH Enzymically Generated by Aldehyde Dehydrogenase. *Anal. Chem.* **1995,** *67* (21), 3936-3944.

129.   Pariente, F.; Tobalina, F.; Darder, M.; Lorenzo, E.; AbruÃ±a, H. D., Electrodeposition of redox-active films of dihydroxybenzaldehydes and related analogs and their electrocatalytic activity toward NADH oxidation. *Anal. Chem.* **1996,** *68* (18), 3135-3142.

130.   Pariente, F.; Tobalina, F.; Moreno, G.; HernÃ¡ndez, L.; Lorenzo, E.; AbruÃ±a, H. D., Mechanistic studies of the electrocatalytic oxidation of NADH and ascorbate at glassy carbon electrodes modified with electrodeposited films derived from 3,4-dihydroxybenzaldehyde. *Anal. Chem.* **1997,** *69* (19), 4065-4075.

131.   Tobalina, F.; Pariente, F.; Hernández, L.; Abruña, H. D.; Lorenzo, E., Carbon felt composite electrodes and their use in electrochemical sensing: a biosensor based on alcohol dehydrogenase. *Anal. Chim. Acta* **1998,** *358* (1), 15-25.

132.   Zare, H. R.; Golabi, S. M., Electrocatalytic oxidation of reduced nicotinamide adenine dinucleotide (NADH) at a chlorogenic acid modified glassy carbon electrode. *J. Electroanal. Chem.* **1999,** *464* (1), 14-23.

133.   Ikariyama, Y.; Ishizuka, T.; Sinohara, H.; Aizawa, M., A unique biosensing system for pyruvate and lactate using a mediator-coexisted lactate dehydrogenase-NAD conductive membrane *Denki Kagaku* **1990,** *58* (12), 1097-1102.

134.   Yabuki, S.; Shinohara, H.; Ikariyama, Y.; Aizawa, M., Electrical activity controlling system for a mediator-coexisting alcohol dehydrogenase-NAD conductive membrane. *J. Electroanal. Chem.* **1990,** *277* (1-2), 179-187.

135.   Dong-mei, Z.; Hui-Qun, F.; Hong-yuan, C.; Huang-xian, J.; Yun, W., The electrochemical polymerization of methylene green and its electrocatalysis for the oxidation of NADH. *Analytica Chimica Acta* **1996,** *329* (1-2), 41-48.

136.   Cai, C. X.; Xue, K. H., Electrocatalysis of NADH oxidation with electropolymerized films of nile blue A. *Anal. Chim. Acta* **1997,** *343* (1-2), 69-77.

137.   Cai, C.-X.; Xue, K.-H., Electrocatalysis of NADH oxidation with electropolymerized films of azure I. *J. Electroanal. Chem.* **1997,** *427* (1-2), 147-153.

138.   Cai, C.-X.; Xue, K.-H., Electrochemical polymerization of toluidine blue o and its electrocatalytic activity toward NADH oxidation. *Talanta* **1998,** *47* (5), 1107-1119.

139.   Cai, C.-X.; Xue, K.-H., The effects of concentration and solution pH on the kinetic parameters for the electrocatalytic oxidation of dihydronicotiamide adenine dinucleotide (NADH) at glassy carbon electrode modified with electropolymerized film of toluidine blue o. *Microchem. J.* **2000,** *64* (2), 131-139.

140.   Malinauskas, A.; Niaura, G.; Bloxham, S.; Ruzgas, T.; Gorton, L., Electropolymerization of preadsorbed layers of some azine redox dyes on graphite. *J. Colloid Interface Sci.* **2000,** *230* (1), 122-127.

141.   Svoboda, V.; Cooney, M. J.; Rippolz, C.; Liaw, B. Y., In situ characterization of electrochemical polymerization of methylene green on platinum electrodes. *J. Electrochem. Soc.* **2007,** *154* (3), D113-D116.

142.   Klotzbach, T.; Minteer, S. D., Effects of hydrophobic modification of chitosan on transport properties, ion exchange capacities, and enzyme immobilization. *Abstr. Pap. Am. Chem. Soc.* **2006,** *231*, 355.

143.   Cooney, M. J.; Petermann, J.; Lau, C.; Minteer, S. D., Characterization and evaluation of hydrophobically modified chitosan scaffolds: Towards design of enzyme immobilized flow-through electrodes. *Carbohydr. Polym.* **2009,** *75* (3), 428-435.

144.   Lau, C.; Martin, G.; Minteer, S. D.; Cooney, M. J., Development of a chitosan scaffold electrode for fuel cell applications. *Electroanal.* **2010,** *22* (7-8), 793-798.

145.   Addo, P. K.; Arechederra, R. L.; Minteer, S. D., Evaluating Enzyme Cascades for Methanol/Air Biofuel Cells Based on NAD(+)-Dependent Enzymes. *Electroanal.* **2010,** *22* (7-8), 807-812.

146.   Monsan, P.; Combes, D., Enzyme stabilization by immobilization. In *Immobilized Enzymes and Cells*, Mosbach, K., Ed. Academic Press: San Diego, 1988; Vol. 137, pp 584-598.

147.   Mitchell, D. J.; Baker, J. O.; Og, K. K.; Grohmann, K.; Himmel, M. E., Enhanced utility of polysaccharidases through chemical cross-linking and immobilization. In *Enzymes in Biomass Conversion*, Leatham, G. F.; Himmel, M. E., Eds. American Chemical Society Boston, Massachusetts, 1991; pp 137-151.

148.   Krajewska, B., Chitin abd its derivatives as supports for immobilization of enzymes. *Acta Biotechnol.* **1991,** *11* (3), 269-277.

149.   Haacker, J. Immobilized Enzymes. http://www.rpi.edu/dept/chem-eng/Biotech-Environ/IMMOB/Immob.htm (accessed July 28th, 2010).

150.   Skjak-Braek, G.; Anthonsen, T.; Sandfor, P., *Chitin and chitosan: Sources, chemistry, biochemistry, physical properties, and applications* Elsevier Science *&* Technology Books: London, 1988; p 842.

151.   Rinaudo, M., Chitin and chitosan: Properties and applications. *Prog. Polym. Sci.* **2006,** *31* (7), 603-632.

152.   Batrakova, E. V.; Han, H. Y.; Alakhov, V. Y.; Miller, D. W.; Kabanov, A. V., Effects of pluronic block copolymers on drug absorption in Caco-2 cell monolayers. *Pharm. Res.* **1998,** *15* (6), 850-855.

153.   Esquenet, C.; Buhler, E., Phase behavior of associating polyelectrolyte polysaccharides. 1. Aggregation process in dilute solution. *Macromolecules* **2001,** *34* (15), 5287-5294.

154.   Zhou, Q. M.; Xie, Q. J.; Fu, Y. C.; Su, Z. H.; Jia, X.; Yao, S. Z., Electrodeposition of carbon nanotubes-chitosan-glucose oxidase biosensing composite films triggered by reduction of p-benzoquinone or H2O2. *J. Phys. Chem. B* **2007,** *111* (38), 11276-11284.

155.   Madihally, S. V.; Matthew, H. W. T., Porous chitosan scaffolds for tissue engineering. *Biomaterials* **1999,** *20* (12), 1133-1142.

156.   Roh, I. J.; Kwon, I. C., Fabrication of a pure porous chitosan bead matrix: influences of phase separation on the microstructure. *J. Biomater. Sci., Polym. Ed.* **2002,** *13* (7), 769-782.

157.   Zhao, L.; Chang, J., Preparation and characterization of macroporous chitosan/wollastonite composite scaffolds for tissue engineering. *J. Mater. Sci.-Mater. Med.* **2004,** *15* (5), 625-629.

158.   Wan, Y.; Wu, H.; Wen, D. J., Porous-conductive chitosan scaffolds for tissue engineering, 1 - Preparation and characterization. *Macromol. Biosci.* **2004,** *4* (9), 882-890.

159.   Ho, M. H.; Kuo, P. Y.; Hsieh, H. J.; Hsien, T. Y.; Hou, L. T.; Lai, J. Y.; Wang, D. M., Preparation of porous scaffolds by using freeze-extraction and freeze-gelation methods. *Biomaterials* **2004,** *25* (1), 129-138.

160.   Li, Z. S.; Ramay, H. R.; Hauch, K. D.; Xiao, D. M.; Zhang, M. Q., Chitosan-alginate hybrid scaffolds for bone tissue engineering. *Biomaterials* **2005,** *26* (18), 3919-3928.

161.   Karageorgiou, V.; Kaplan, D., Porosity of 3D biornaterial scaffolds and osteogenesis. *Biomaterials* **2005,** *26* (27), 5474-5491.

162.   Adekogbe, I.; Ghanem, A., Fabrication and characterization of DTBP-crosslinked chitosan scaffolds for skin tissue engineering. *Biomaterials* **2005,** *26* (35), 7241-7250.

163.   Huang, Y.; Onyeri, S.; Siewe, M.; Moshfeghian, A.; Madihally, S. V., In vitro characterization of chitosan-gelatin scaffolds for tissue engineering. *Biomaterials* **2005,** *26* (36), 7616-7627.

164.   Nakamatsu, J.; Torres, F. G.; Troncoso, O. P.; Yuan, M. L.; Boccaccini, A. R., Processing and characterization of porous structures from chitosan and starch for tissue engineering scaffolds. *Biomacromolecules* **2006,** *7* (12), 3345-3355.

165.   Hsieh, C. Y.; Hsieh, H. J.; Liu, H. C.; Wang, D. M.; Hou, L. T., Fabrication and release behavior of a novel freeze-gelled chitosan/gamma-PGA scaffold as a carrier for rhBMP-2. *Dent. Mater.* **2006,** *22* (7), 622-629.

166.   Hsieh, C. Y.; Tsai, S. P.; Ho, M. H.; Wang, D. M.; Liu, C. E.; Hsieh, C. H.; Tseng, H. C.; Hsieh, H. J., Analysis of freeze-gelation and cross-linking processes for preparing porous chitosan scaffolds. *Carbohydr. Polym.* **2007,** *67* (1), 124-132.

167.   Hsieh, W. C.; Chang, C. P.; Lin, S. M., Morphology and characterization of 3D micro-porous structured chitosan scaffolds for tissue engineering. *Colloids Surf., B* **2007,** *57* (2), 250-255.

168.   Hirano, S., Chitin and chitosan as novel biotechnological materials. *Polym. Int.* **1999,** *48* (8), 732-734.

169.   Lai, H. L.; Abu'Khalil, A.; Craig, D. Q. M., The preparation and characterisation of drug-loaded alginate and chitosan sponges. *Int. J. Pharm.* **2003,** *251* (1-2), 175-181.

170.   Berger, J.; Reist, M.; Mayer, J. M.; Felt, O.; Gurny, R., Structure and interactions in chitosan hydrogels formed by complexation or aggregation for biomedical applications. *Eur. J. Pharm. Biopharm.* **2004,** *57* (1), 35-52.

171.   Berger, J.; Reist, M.; Mayer, J. M.; Felt, O.; Peppas, N. A.; Gurny, R., Structure and interactions in covalently and ionically crosslinked chitosan hydrogels for biomedical applications. *Eur. J. Pharm. Biopharm.* **2004,** *57* (1), 19-34.

172.   Jayakumar, R.; Nwe, N.; Tokura, S.; Tamura, H., Sulfated chitin and chitosan as novel biomaterials. *Int. J. Biol. Macromol.* **2007,** *40* (3), 175-181.

173.   Liu, Q.; Rauth, A. M.; Wu, X. Y., Immobilization and bioactivity of glucose oxidase in hydrogel microspheres formulated by an emulsification-internal gelation-adsorption-polyelectrolyte coating method. *Int. J. Pharm.* **2007,** *339* (1-2), 148-156.

References

174.	Zhitomirsky, I.; Hashambhoy, A., Chitosan-mediated electrosynthesis of orgarlic-inorganic nanocomposites. *J. Mater. Process. Technol.* **2007,** *191* (1-3), 68-72.
175.	Baek, S. H.; Kim, B.; Suh, K. D., Chitosan particle/multiwall carbon nanotube composites by electrostatic interactions. *Colloids Surf., A* **2008,** *316* (1-3), 292-296.
176.	Chen, L.; Gorski, W., Bioinorganic composites for enzyme electrodes. *Anal. Chem.* **2001,** *73* (13), 2862-2868.
177.	Huang, H.; Hu, N. F.; Zeng, Y. H.; Zhou, G., Electrochemistry and electrocatalysis with heme proteins in chitosan biopolymer films. *Anal. Biochem.* **2002,** *308* (1), 141-151.
178.	Bindhu, L. V.; Abraham, E. T., Immobilization of horseradish peroxidase on chitosan for use in nonaqueous media. *J. Appl. Polym. Sci.* **2003,** *88* (6), 1456-1464.
179.	Wang, G.; Xu, J. J.; Chen, H. Y.; Lu, Z. H., Amperometric hydrogen peroxide biosensor with sol-gel/chitosan network-like film as immobilization matrix. *Biosens. Bioelectron.* **2003,** *18* (4), 335-343.
180.	Wang, Y. T.; Zhu, J. Z.; Zhu, R. J.; Zhu, Z. Q.; Lai, Z. S.; Chen, Z. Y., Chitosan/Prussian blue-based biosensors. *Meas. Sci. Technol.* **2003,** *14* (6), 831-836.
181.	Chen, X.; Jia, J. B.; Dong, S. J., Organically modified sol-gel/chitosan composite based glucose biosensor. *Electroanal.* **2003,** *15* (7), 608-612.
182.	Ghanem, A.; Ghaly, A., Immobilization of glucose oxidase in chitosan gel beads. *J. Appl. Polym. Sci.* **2004,** *91* (2), 861-866.
183.	Zhang, M. G.; Smith, A.; Gorski, W., Carbon nanotube-chitosan system for electrochemical sensing based on dehydrogenase enzymes. *Anal. Chem.* **2004,** *76* (17), 5045-5050.
184.	Tan, X. C.; Ll, M. J.; Cai, P. X.; Luo, L. J.; Zou, X. Y., An amperometric cholesterol biosensor based on multiwalled carbon nanotubes and organically modified sol-gel/chitosan hybrid composite film. *Anal. Biochem.* **2005,** *337* (1), 111-120.
185.	Li, J.; Liu, Q.; Liu, Y. J.; Liu, S. C.; Yao, S. Z., DNA biosensor based on chitosan film doped with carbon nanotubes. *Anal. Biochem.* **2005,** *346* (1), 107-114.
186.	Zhang, M. G.; Gorski, W., Electrochemical sensing platform based on the carbon nanotubes/redox mediators-biopolymer system. *J. Am. Chem. Soc.* **2005,** *127* (7), 2058-2059.
187.	Liu, Y.; Wang, M. K.; Zhao, F.; Xu, Z. A.; Dong, S. J., The direct electron transfer of glucose oxidase and glucose biosensor based on carbon nanotubes/chitosan matrix. *Biosens. Bioelectron.* **2005,** *21* (6), 984-988.
188.	Liu, Y. Y.; Tang, J.; Chen, X. Q.; Xin, J. H., Decoration of carbon nanotubes with chitosan. *Carbon* **2005,** *43* (15), 3178-3180.
189.	Xu, Z. A.; Gao, N.; Chen, H. J.; Dong, S. J., Biopolymer and carbon nanotubes interface prepared by self-assembly for studying the electrochemistry of microperoxidase-11. *Langmuir* **2005,** *21* (23), 10808-10813.
190.	Zhang, M. G.; Gorski, W., Electrochemical sensing based on redox mediation at carbon nanotubes. *Anal. Chem.* **2005,** *77* (13), 3960-3965.
191.	Liu, Y.; Qu, X. H.; Guo, H. W.; Chen, H. J.; Liu, B. F.; Dong, S. J., Facile preparation of amperometric laccase biosensor with multifunction based on the matrix of carbon nanotubes-chitosan composite. *Biosens. Bioelectron.* **2006,** *21* (12), 2195-2201.

192.   Lu, X. B.; Hu, J. Q.; Yao, X.; Wang, Z. P.; Li, J. H., Composite system based on chitosan and room-temperature ionic liquid: Direct electrochemistry and electrocatalysis of hemoglobin. *Biomacromolecules* **2006,** *7* (3), 975-980.

193.   Luo, X. L.; Killard, A. J.; Smyth, M. R., Reagentless glucose biosensor based on the direct electrochemistry of glucose oxidase on carbon nanotube-modified electrodes. *Electroanal.* **2006,** *18* (11), 1131-1134.

194.   Qian, L.; Yang, X. R., Composite film of carbon nanotubes and chitosan for preparation of amperometric hydrogen peroxide biosensor. *Talanta* **2006,** *68* (3), 721-727.

195.   Tkac, J.; Ruzgas, T., Dispersion of single walled. carbon nanotubes. Comparison of different dispersing strategies for preparation of modified electrodes toward hydrogen peroxide detection. *Electrochem. Commun.* **2006,** *8* (5), 899-903.

196.   Yang, M. H.; Jiang, J. H.; Yang, Y. H.; Chen, X. H.; Shen, G. L.; Yu, R. Q., Carbon nanotube/cobalt hexacyanoferrate nanoparticle-biopolymer system for the fabrication of biosensors. *Biosens. Bioelectron.* **2006,** *21* (9), 1791-1797.

197.   Shieh, Y. T.; Yang, Y. F., Significant improvements in mechanical property and water stability of chitosan by carbon nanotubes. *Eur. Polym. J.* **2006,** *42* (12), 3162-3170.

198.   Pumera, M.; Sanchez, S.; Ichinose, I.; Tang, J., Electrochemical nanobiosensors. *Sens. Actuator B-Chem.* **2007,** *123* (2), 1195-1205.

199.   Qu, F. L.; Yang, M. H.; Shen, G. L.; Yu, R. Q., Electrochemical biosensing utilizing synergic action of carbon nanotubes and platinum nanowires prepared by template synthesis. *Biosens. Bioelectron.* **2007,** *22* (8), 1749-1755.

200.   Wu, Y. H.; Hu, S. S., Biosensors based on direct electron transfer in redox proteins. *Microchim. Acta* **2007,** *159* (1-2), 1-17.

201.   Wu, Z. G.; Feng, W.; Feng, Y. Y.; Liu, Q.; Xu, X. H.; Sekino, T.; Fujii, A.; Ozaki, M., Preparation and characterization of chitosan-grafted multiwalled carbon nanotubes and their electrochemical properties. *Carbon* **2007,** *45* (6), 1212-1218.

202.   Tkac, J.; Whittaker, J. W.; Ruzgas, T., The use of single walled carbon nanotubes dispersed in a chitosan matrix for preparation of a galactose biosensor. *Biosens. Bioelectron.* **2007,** *22* (8), 1820-1824.

203.   Casagrande, T.; Lawson, G.; Li, H.; Wei, J.; Adronov, A.; Zhitomirsky, I., Electrodeposition of composite materials containing functionalized carbon nanotubes. *Mater. Chem. Phys.* **2008,** *111* (1), 42-49.

204.   Benavidez, T. E.; Capra, R. H.; Alvarez, C. I.; Baruzzi, A. M., Amperometric biosensor based on immobilization of oxalate oxidase in a mucin/chitosan matrix. *Electroanal.* **2009,** *21* (7), 837-843.

205.   Sadik, O. A.; Aluoch, A. O.; Zhou, A. L., Status of biomolecular recognition using electrochemical techniques. *Biosens. Bioelectron.* **2009,** *24* (9), 2749-2765.

206.   Zhou, H. J.; Zhang, Z. P.; Yu, P.; Su, L.; Ohsaka, T.; Mao, L. Q., Noncovalent attachment of NAD(+) cofactor onto carbon nanotubes for preparation of integrated dehydrogenase-based electrochemical biosensors. *Langmuir* **2010,** *26* (8), 6028-6032.

207.   Liu, Y.; Wang, M. K.; Zhao, F.; Liu, B. F.; Dong, S. J., A low-cost biofuel cell with pH-dependent power output based on porous carbon as matrix. *Chem. Eur. J.* **2005,** *11* (17), 4970-4974.

References

208.   Klotzbach, T.; Watt, M.; Ansari, Y.; Minteer, S. D., Effects of hydrophobic modification of chitosan and Nafion on transport properties, ion-exchange capacities, and enzyme immobilization. *J. Membr. Sci.* **2006,** *282* (1-2), 276-283.

209.   Minteer, S. D.; Liaw, B. Y.; Cooney, M. J., Enzyme-based biofuel cells. *Curr. Opin. Biotechnol.* **2007,** *18* (3), 228-234.

210.   Moehlenbrock, M. J.; Minteer, S. D., Extended lifetime biofuel cells. *Chem. Soc. Rev.* **2008,** *37* (6), 1188-1196.

211.   Tan, Y. M.; Deng, W. F.; Ge, B.; Xie, Q. J.; Huang, J. H.; Yao, S. Z., Biofuel cell and phenolic biosensor based on acid-resistant laccase-glutaraldehyde functionalized chitosan-multiwalled carbon nanotubes nanocomposite film. *Biosens. Bioelectron.* **2009,** *24* (7), 2225-2231.

212.   Cooney, M. J.; Lau, C.; Windmeisser, M.; Liaw, B. Y.; Klotzbach, T.; Minteer, S. D., Design of chitosan gel pore structure: towards enzyme catalyzed flow-through electrodes. *J. Mater. Chem.* **2008,** *18* (6), 667-674.

213.   Cooney, M. J.; Svoboda, V.; Lau, C.; Martin, G.; Minteer, S. D., Enzyme catalysed biofuel cells. *Energy Environ. Sci.* **2008,** *1* (3), 320-337.

214.   Klotzbach, T. L.; Watt, M.; Ansari, Y.; Minteer, S. D., Improving the microenvironment for enzyme immobilization at electrodes by hydrophobically modifying chitosan and Nafion (R) polymers. *J. Membr. Sci.* **2008,** *311* (1-2), 81-88.

215.   Lau, C.; Cooney, M. J.; Atanassov, P., Conductive macroporous composite chitosan-carbon nanotube scaffolds. *Langmuir* **2008,** *24* (13), 7004-7010.

216.   Kim, J.; Parkey, J.; Rhodes, C.; Gonzalez-Martin, A., Development of a biofuel cell using glucose-oxidase- and bilirubin-oxidase-based electrodes. *J. Solid State Electrochem.* **2009,** *13* (7), 1043-1050.

217.   Liu, C. G.; Chen, X. G.; Park, H. J., Self-assembled nanoparticles based on linoleic-acid modified chitosan: Stability and adsorption of trypsin. *Carbohydr. Polym.* **2005,** *62* (3), 293-298.

218.   Spinks, G. M.; Shin, S. R.; Wallace, G. G.; Whitten, P. G.; Kim, S. I.; Kim, S. J., Mechanical properties of chitosan/CNT microfibers obtained with improved dispersion. *Sens. Actuator B-Chem.* **2006,** *115* (2), 678-684.

219.   Xu, Z.; Chen, X.; Dong, S. J., Electrochemical biosensors based on advanced bioimmobilization matrices. *Trac-Trend. Anal. Chem.* **2006,** *25* (9), 899-908.

220.   Ke, G.; Guan, W. C.; Tang, C. Y.; Guan, W. J.; Deng, F., Covalent functionalization of multiwalled carbon nanotubes with a low molecular weight chitosan. *Biomacromolecules* **2007,** *8* (2), 322-326.

221.   Spinks, G. A.; Shin, S. R.; Wallace, G. G.; Whitten, P. G.; Kim, I. Y.; Kim, S. I.; Kim, S. J., A novel "dual mode" actuation in chitosan/polyaniline/carbon nanotube fibers. *Sens. Actuator B-Chem.* **2007,** *121* (2), 616-621.

222.   Balasubramanian, K.; Burghard, M., Electrochemically functionalized carbon nanotubes for device applications. *J. Mater. Chem.* **2008,** *18* (26), 3071-3083.

223.   Esquenet, C.; Terech, P.; Boue, F.; Buhler, E., Structural and rheological properties of hydrophobically modified polysaccharide associative networks. *Langmuir* **2004,** *20* (9), 3583-3592.

224.   Jiang, G. B.; Quan, D. P.; Liao, K. R.; Wang, H. H., Preparation of polymeric micelles based on chitosan bearing a small amount of highly hydrophobic groups. *Carbohydr. Polym.* **2006,** *66* (4), 514-520.

225.   Bard, A. J.; Faulkner, L. R., *Electrochemical Methods: Fundamentals and Applications*. 2nd ed.; John Wiley & Sons, Inc. : New York, 2000; p 833.

226.   Wang, J., *Analytical Electrochemistry*. 3rd ed.; John Wiley & Sons, Inc.: Hoboken, 2006; p 250.

227.   Akkermans, R. P.; Roberts, S. L.; Marken, F.; Coles, B. A.; Wilkins, S. J.; Cooper, J. A.; Woodhouse, K. E.; Compton, R. G., Methylene green voltammetry in aqueous solution: Studies using thermal, microwave, laser, or ultrasonic activation at platinum electrodes. *J. Phys. Chem. B* **1999,** *103* (45), 9987-9995.

228.   Zhou, D. M.; Fang, H. Q.; Chen, H. Y.; Ju, H. X.; Wang, Y., The electrochemical polymerization of methylene green and its electrocatalysis for the oxidation of NADH. *Anal. Chim. Acta* **1996,** *329* (1-2), 41-48.

229.   Akers, N. L.; Moore, C. M.; Minteer, S. D., Development of alcohol/O-2 biofuel cells using salt-extracted tetrabutylammonium bromide/Nafion membranes to immobilize dehydrogenase enzymes. *Electrochim. Acta* **2005,** *50* (12), 2521-2525.

230.   Inzelt, G., *Conducting Polymers - A New Era in Electrochemistry*. 1 ed.; Springer Berlin Heidelberg: 2008; p 282.

231.   Munteanu, F. D.; Kubota, L. T.; Gorton, L. In *Effect of pH on the catalytic electro oxidation of NADH using different two-electron mediators immobilised on zirconium phosphate*, 2001; pp 2-10.

232.   Rincón, R. A.; Artyushkova, K.; Mojica, M.; Germain, M. N.; Minteer, S. D.; Atanassov, P., Structure and electrochemical properties of electrocatalysts for NADH oxidation. *Electroanal.* **2010,** *22* (7-8), 799-806.

233.   Friedrich, J. M.; Ponce-De-Leon, C.; Reade, G. W.; Walsh, F. C., Reticulated vitreous carbon as an electrode material. *J. Electroanal. Chem.* **2004,** *561* (1-2), 203-217.

234.   Sjoholm, K. H.; Cooney, M.; Minteer, S. D., Effects of degree of deacetylation on enzyme immobilization in hydrophobically modified chitosan. *Carbohydr. Polym.* **2009,** *77* (2), 420-424.

235.   Penner, R. M., Mesoscopic metal particles and wires by electrodeposition. *J. Phys. Chem. B* **2002,** *106* (13), 3339-3353.

236.   Olson, T. S.; Rincon, R. A.; Brevnov, D. A.; Atanassov, P., Gold-decorated flow-through electrodes: Effect of electrochemical time constant on electrodeposition of Au particles on reticulated vitreous carbon. *Electrochem. Solid-State Lett.* **2010,** *13* (3), D11-D14.

237.   de los Santos Álvarez, N.; Ortea, P. M.; Pañeda, A. M.; Castañón, M. J. L.; Ordieres, A. J. M.; Blanco, P. T., A comparative study of different adenine derivatives for the electrocatalytic oxidation of [beta]-nicotinamide adenine dinucleotide. *J. Electroanal. Chem.* **2001,** *502* (1-2), 109-117.

238.   Palmore, G. T. R., Biofuel Cells. In *Bioelectrochemistry: fundamentals, experimental techniques, and applications*, Bartlett, P. N., Ed. John Wiley & Sons, Inc. : West Sussex, 2008; pp 359-375.

239.   Yan, Y. M.; Tel-Vered, R.; Yehezkeli, O.; Cheglakov, Z.; Willner, I., Biocatalytic growth of Au nanoparticles immobilized on glucose oxidase enhances the ferrocene-mediated bioelectrocatalytic oxidation of glucose. *Adv. Mater.* **2008,** *20* (12), 2365-+.

240.   Stoica, L.; Dimcheva, N.; Ackermann, Y.; Karnicka, K.; Guschin, D. A.; Kulesza, P. J.; Rogalski, J.; Haltrich, D.; Ludwig, R.; Gorton, L.; Schuhmann, W., Membrane-less

biofuel cell based on cellobiose dehydrogenase (anode)/laccase (aathode) wired via specific Os-redox polymers. *Fuel Cells* **2009,** *9* (1), 53-62.

241.   Kar, P.; Wen, H.; Li, H.; Minteer, S. D.; Barton, S. C., Simulation of multi-step enzyme-catalyzed methanol oxidation with electrocatalytic cofactor regenearation for biofuel cells. *J. Electrochem. Soc* **2010**.

242.   Bird, R. B.; Stewart, W. E.; Lightfoot, E. N., *Transport Phenomena*. Second ed.; John Wiley & Sons, Inc: New York, 2002; p 895.

243.   Marangoni, A. G., *Enzyme kinetics : a modern approach*. Wiley-Interscience: Hoboken, N.J., 2003; p xiv, 229.

244.   Iwuoha, E. I.; de Villaverde, D. S.; Garcia, N. P.; Smyth, M. R.; Pingarron, J. M., Reactivities of organic phase biosensors. 2. The amperometric behaviour of horseradish peroxidase immobilised on a platinum electrode modified with an electrosynthetic polyaniline film. *Biosens. Bioelectron.* **1997,** *12* (8), 749-761.

245.   Ghindilis, A. L.; Atanasov, P.; Wilkins, E., Enzyme-catalyzed direct electron transfer: Fundamentals and analytical applications. *Electroanal.* **1997,** *9* (9), 661-674.

246.   Katz, E.; Shipway, A. N.; Willner, I., Biomaterial-nanoparticle hybrid systems: Synthesis, properties and applications. In *Nanoparticles - From Theory to Applications*, Schmid, G., Ed. Wiley-VCH: Weinheim, 2003; pp 368-421.

247.   Kano, K.; Ikeda, T., Bioelectrocatalysis, powerful means of connecting electrochemistry to biochemistry and biotechnology. *Electrochemistry* **2003,** *71* (2), 86-99.

248.   Sayler, G. S.; Simpson, M. L.; Cox, C. D., Emerging foundations: nano-engineering and bio-microelectronics for environmental biotechnology. *Curr. Opin. Microbiol.* **2004,** *7* (3), 267-273.

249.   *Defense against bioterror: Detection technologies, implementation strategies and commercial opportunities*. Springer: Berlin, 2005; p 340.

250.   Katz, E.; Shipway, A. N.; Willner, I., Biofuel cells: Functional design and operation. In *Handbook of Fuel Cells - Fundamentals, Technology and Applications*, Vielstich, W.; Gasteiger, H.; Lamm, A., Eds. John Wiley & Sons Inc: London, 2003; Vol. 1, pp 355-381.

251.   Lim, J.; Cirigliano, N.; Wang, J.; Dunn, B., Direct electron transfer in nanostructured sol-gel electrodes containing bilirubin oxidase. *Phys. Chem. Chem. Phys.* **2007,** *9* (15), 1809-1814.

252.   Wilson, R.; Turner, A. P. F., Glucose-oxidase - An ideal enzyme. *Biosens. Bioelectron.* **1992,** *7* (3), 165-185.

253.   Guiseppi-Elie, A.; Lei, C. H.; Baughman, R. H., Direct electron transfer of glucose oxidase on carbon nanotubes. *Nanotechnology* **2002,** *13* (5), 559-564.

254.   Ramanavicius, A.; Kausaite, A.; Ramanaviciene, A., Biofuel cell based on direct bioelectrocatalysis. *Biosens. Bioelectron.* **2005,** *20* (10), 1962-1967.

255.   Liang, W.; Yuan, Z. B., Direct electrochemistry of glucose oxidase at a gold electrode modified with single-wall carbon nanotubes. *Sensors* **2003,** *3* (12), 544-554.

256.   Cai, C. X.; Chen, J., Direct electron transfer of glucose oxidase promoted by carbon nanotubes. *Anal. Biochem.* **2004,** *332* (1), 75-83.

257.   Soukharev, V.; Mano, N.; Heller, A., A four-electron O-2-electroreduction biocatalyst superior to platinum and a biofuel cell operating at 0.88 V. *J. Am. Chem. Soc.* **2004,** *126* (27), 8368-8369.

258.   Ivnitski, D.; Branch, B.; Atanassov, P.; Apblett, C., Glucose oxidase anode for biofuel cell based on direct electron transfer. *Electrochem. Commun.* **2006,** *8* (8), 1204-1210.

259.   Luckarift, H. R.; Spain, J. C.; Naik, R. R.; Stone, M. O., Enzyme immobilization in a biomimetic silica support. *Nat. Biotechnol.* **2004,** *22* (2), 211-213.

260.   Naik, R. R.; Tomczak, M. M.; Luckarift, H. R.; Spain, J. C.; Stone, M. O., Entrapment of enzymes and nanoparticles using biomimetically synthesized silica. *Chem. Commun.* **2004,** (15), 1684-1685.

261.   Cha, J. N.; Shimizu, K.; Zhou, Y.; Christiansen, S. C.; Chmelka, B. F.; Stucky, G. D.; Morse, D. E., Silicatein filaments and subunits from a marine sponge direct the polymerization of silica and silicones in vitro. *Proc. Natl. Acad. Sci. U. S. A.* **1999,** *96* (2), 361-365.

262.   Kroger, N.; Deutzmann, R.; Sumper, M., Polycationic peptides from diatom biosilica that direct silica nanosphere formation. *Science* **1999,** *286* (5442), 1129-1132.

263.   Cha, J. N.; Stucky, G. D.; Morse, D. E.; Deming, T. J., Biomimetic synthesis of ordered silica structures mediated by block copolypeptides. *Nature* **2000,** *403* (6767), 289-292.

264.   Kroger, N.; Deutzmann, R.; Bergsdorf, C.; Sumper, M., Species-specific polyamines from diatoms control silica morphology. *Proc. Natl. Acad. Sci. U. S. A.* **2000,** *97* (26), 14133-14138.

265.   Luckarift, H. R.; Dickerson, M. B.; Sandhage, K. H.; Spain, J. C., Rapid, room-temperature synthesis of antibacterial bionanocomposites of lysozyme with amorphous silica or titania. *Small* **2006,** *2* (5), 640-643.

266.   Luckarift, H. R.; Balasubramanian, S.; Paliwal, S.; Johnson, G. R.; Simonian, A. L., Enzyme-encapsulated silica monolayers for rapid functionalization of a gold surface. *Colloids Surf., B* **2007,** *58* (1), 28-33.

267.   Rusling, J. F.; Forster, R. J., Electrochemical catalysis with redox polymer and polyion-protein films. *J. Colloid Interface Sci.* **2003,** *262* (1), 1-15.

268.   Laviron, E., General expression of the linear potential sweep voltammogram in the case of diffusionless electrochemical systems. *J. Electroanal. Chem.* **1979,** *101* (1), 19-28.

269.   Blomberg, E.; Claesson, P. M.; Froberg, J. C., Surfaces coated with protein layers: a surface force and ESCA study. *Biomaterials* **1998,** *19* (4-5), 371-386.

270.   Tangpasuthadol, V.; Pongchaisirikul, N.; Hoven, V. P., Surface modification of chitosan films. Effects of hydrophobicity on protein adsorption. *Carbohydr. Res.* **2003,** *338* (9), 937-942.

271.   Curulli, A.; Cusma, A.; Kaciulis, S.; Padeletti, G.; Pandolfi, L.; Valentini, F.; Viticoli, M., Immobilization of GOD and HRP enzymes on nanostructured substrates. *Surf. Interface Anal.* **2006,** *38* (4), 478-481.

272.   Longo, L.; Vasapollo, G.; Guascito, M. R.; Malitesta, C., New insights from X-ray photoelectron spectroscopy into the chemistry of covalent enzyme immobilization, with glutamate dehydrogenase (GDH) on silicon dioxide as an example. *Anal. Bioanal. Chem.* **2006,** *385* (1), 146-152.

273.   Wang, J.; Carlisle, J. A., Covalent immobilization of glucose oxidase on conducting ultrananocrystalline diamond thin films. *Diam. Relat. Mat.* **2006,** *15* (2-3), 279-284.

274. Hoven, V. P.; Tangpasuthadol, V.; Angkitpaiboon, Y.; Vallapa, N.; Kiatkamjornwong, S., Surface-charged chitosan: Preparation and protein adsorption. *Carbohydr. Polym.* **2007,** *68* (1), 44-53.

275. Jiang, L.; McNeil, C. J.; Cooper, J. M., Direct electron-transfer reaction of glucose-oxidase immobilized at a self-assembled monolayer. *J. Chem. Soc.-Chem. Commun.* **1995,** (12), 1293-1295.

276. Zhao, Y. D.; Zhang, W. D.; Chen, H.; Luo, Q. M., Direct electron transfer of glucose oxidase molecules adsorbed onto carbon nanotube powder microelectrode. *Anal. Sci.* **2002,** *18* (8), 939-941.

277. Liu, H. Y.; Hu, N. F., Study on direct electrochemistry of glucose oxidase stabilized by cross-linking and immobilized in silica nanoparticle films. *Electroanal.* **2007,** *19* (7-8), 884-892.

278. Zhang, J.; Feng, M.; Tachikawa, H., Layer-by-layer fabrication and direct electrochemistry of glucose oxidase on single wall carbon nanotubes. *Biosens. Bioelectron.* **2007,** *22* (12), 3036-3041.

279. Moore, C. M.; Minteer, S. D.; Martin, R. S., Microchip-based ethanol/oxygen biofuel cell. *Lab Chip* **2005,** *5* (2), 218-225.

280. Barsan, M. M.; Pinto, E. M.; Brett, C. M. A., Electrosynthesis and electrochemical characterisation of phenazine polymers for application in biosensors. *Electrochim. Acta* **2008,** *53* (11), 3973-3982.

281. Karyakin, A. A.; Bobrova, O. A.; Karyakina, E. E., Electroreduction of NAD(+) to enzymatically active NADH at poly(neutral red) modified electrodes. *J. Electroanal. Chem.* **1995,** *399* (1-2), 179-184.

282. Atamna, H.; Nguyen, A.; Schultz, C.; Boyle, K.; Newberry, J.; Kato, H.; Ames, B. N., Methylene blue delays cellular senescence and enhances key mitochondrial biochemical pathways. *Faseb J.* **2008,** *22* (3), 703-712.

283. Hand, R. L.; Nelson, R. F., Anodic decomposition pathways of ortho-substituted and meta-substituted anilines. *J. Electrochem. Soc.* **1978,** *125* (7), 1059-1069.

284. Yasuda, A.; Shimidzu, T., Chemical oxidative polymerization of aniline with ferric-chloride. *Polym. J.* **1993,** *25* (4), 329-338.

285. Arechederra, R. L.; Treu, B. L.; Minteer, S. D., Development of glycerol/O-2 biofuel cell. *J. Power Sources* **2007,** *173* (1), 156-161.

286. He, L. Y.; Horiuchi, A., Oxidation of 2-substituted cycloalkanones with cerium(IV) sulfate tetrahydrate in alcohols and acetic acid. *Bull. Chem. Soc. Jpn.* **1999,** *72* (11), 2515-2521.